PEOPLE'S DEMOCRATIC REPUBLIC OF ALGERIA
MINISTRY OF HIGHER EDUCATION AND SCIENTIFICRESEARCH
UNIVERSITY OF Abbés LAGHROUR" KHENCHELA
FACULTY OF SCIENCE AND TECHNOLOGY

Department of Mechanical Engineering

End-of-Studies Thesis

For the Award of the Master's Degree (L.M.D)

Specialization: Mechanical Engineering

Option: Mechanical Design

Thème

CFD simulation of a solar dryer used for agrifood applications

Presented by

- **Zegada Mondir**
- **Taibi Chems Eddine**

Membresdejury:

Pr.Mouna Maache	***P.R: University of Khenchela - President***
Dr. Zaamouche Radia	***M.C.B: University of Khenchela – Examiner***
Dr. Chehhat Abdelmadjid	***M.C.A :University of Khenchela - Supervisor***

2024/2025

Acknowledgements

First of all, we would like to sincerely thank our supervisor Dr Chehhat Abdelmadjid and

Professeur Boulahrouz Salim for his guidance, support and constructive feedback throughout the research for this dissertation. His experience and encouragement have been key factors in helping to complete this work.

We would like to thank the teaching staff of the Department of Mechanical Engineering of Université Abbès Laghrour Khenchela for the knowledge and help throughout our Master studies. We would like to sincerely thank the members of the jury for spending time evaluating this work and providing useful recommendations.

Our families deserve a special acknowledgement for their love, compassion and moral support throughout this process. Without their ongoing push, it would have made this experience much harder.

Lastly, we would like to thank our friends and classmates for being a continual source of motivation and entertainment throughout our studies.

Dedication

This work is dedicated to our families, who have provided us with unwavering love, support, and confidence as our sole strength along the way. In particular, we dedicate this work to our parents who have made sacrifices for us, believed in us, and provided us with guidance and insight to help shape us into the humans we are today.

We also want to dedicate this work to our friends, who we have shared both the difficulties and victories during this academic journey; your friendship and support made this path enjoyable and memorable.

Abstract

In this study, a numerical model of an indirect solar dryer was developed to analyze its performance in terms of pressure, temperature, and velocity distribution within the system. The simulation was conducted using Navier-Stokes and energy equations coupled with the turbulence model to simulate natural convection phenomena. The focus was placed on the impact of key design variables, including the chimney position (center, far left, far right), the absorber plate angle ($0^{\circ}, 30^{\circ}, 45^{\circ}$), and the heat flux values (100, 150, 200, 250, 300 [W/m²]) Results were extracted from three key locations (at the absorber surface, in the plenum chamber, and at the outlet). The findings revealed variations in pressure, temperature, and velocity distributions, highlighting the importance of optimized design in enhancing natural ventilation, achieving balanced heat distribution, and improving system efficiency.

Keywords: Indirect solar dryer, natural convection, numerical model, absorber plate angle, natural ventilation, thermal efficiency, chimney position.

الملخص

في هذه الدراسة، تم تطوير نموذج عددي لمجفف شمسي غير مباشر يعتمد على الحرارة المستمدة من الطاقة الشمسية لتحليل أداء المجفف من حيث توزيع الضغط، الحرارة، والسرعة داخل النظام، وذلك باستخدام معادلات نافير-ستوكس ومعادلات الطاقة مقترنة بنموذج الاضطراب لمحاكاة ظاهرة الحمل الحراري الطبيعي، مع التركيز على تأثير المتغيرات التصميمية كموضع المدخنة (المركز، أقصى اليسار، أقصى اليمين)، زاوية صفيحة الامتصاص($\mathbf{0^{\circ}30^{\circ}45^{\circ}}$)، والتدفق الحراري (100، 150، 200، 250، 300 [W/m²]) ، حيث تم استخراج النتائج من ثلاث محطات رئيسية (عند سطح جهاز الامتصاص، في منطقة المجمع، وعند المخرج)، وأظهرت النتائج تباينًا في توزيع الضغط والحرارة والسرعة، مؤكدةً دور التصميم الأمثل في تحسين التهوية الطبيعية، تحقيق توزيع حراري متوازن، وزيادة كفاءة النظام.

الكلمات المفتاحية : مجفف شمسي غير مباشر، الحمل الحراري الطبيعي ، نموذج عددي، زاوية صفيحة الامتصاص، التهوية الطبيعية، الكفاءة الحرارية ،موضع المدخنة.

Table of content

Chapter I: General information about drying

Chapter II. Overview of Dry Matter

Chapter III. Numerical Study

List of figures

Chapter I: General information about drying

Chapter II . Overview of Dry Matter

Chapter III. Numerical Study

List of tables

Chapter I.

Chapter III.

Nomenclature

Q: Volumetric flow rate.

v: Air velocity.

Asolar chimney: Cross-sectional vector area of the solar chimney.

ACH: Air change per hour.

Vroom: Volume of the room where the solar chimney is connected.

Mi: Thermal inertia of component *i*.

Ci: Heat capacity of component *i*.

dT/dt: Time rate of temperature change.

Qin/Qout: Energy received/lost by component *i*.

Mg, Cg: Mass and heat capacity of the glass cover.

Am: Area of the solar chimney components.

αg: Absorptivity of the glass cover.

G: Solar irradiance.

hr, hv: Radiative and convective heat transfer coefficients.

Tsky, Tg, Tp, Tf, Ta: Temperatures of the sky, glass cover, absorber plate, fluid, and ambient air.

σ: Stefan-Boltzmann constant.

εg: Emissivity of the glass cover.

Ra: Rayleigh number.

Gr: Grashof number.

Pr: Prandtl number.

g: Acceleration due to gravity.

β: Thermal expansion coefficient.

L: Characteristic length.

νf: Kinematic viscosity.

λi: Thermal conductivity of material *i*.

Cd: Discharge coefficient.

Ar: Area ratio.

Ain, Ao: Inlet and outlet areas of the solar chimney.

Mp, Cp: Mass and heat capacity of the absorber plate.

Min, Cin: Mass and heat capacity of the thermal insulator.

HRa: Relative humidity of the air.

Pv: Partial pressure of vapor in the mixture.

Ps: Saturation pressure at the same temperature.

Ms: Mass of dry product.

dX: Variation in the moisture content of the product to be dried.

Ss: Drying surface area.

Xe: Moisture content of the product at the inlet.

Xs: Moisture content of the product at the outlet.

Me: Mass of water.

Ms (dry air): Mass of dry air.

HT: Hygrometric degree.

General introduction

Drying is one of the best strategies to preserve food, as solar dryers are a powerful innovation that promotes economic advancement. Drying was likely one of the earliest food preservation techniques used by humans, possibly predating cooking in some instances. Reducing the moisture content in agricultural products minimizes spoilage and allows for the provision of safe and long-lasting products. Known as "sun drying," it is the oldest known method for drying crops and involves placing agricultural products on mats, rooftops, or open drying floors exposed to sunlight.

However, this method has some drawbacks. Exposed crops are vulnerable to unfavorable weather conditions, such as humidity, dust, wind, and rain. Pests, including birds, insects, and rodents, may also increase the likelihood of crop loss. This approach relies entirely on favorable weather, has a very slow drying rate, and increases the risk of mold growth, which damages and spoils crops. Sun drying also requires large areas of land, is time-consuming, and demands significant physical labor.

Mechanical drying techniques were developed alongside industrial and social advancements. However, these technologies consume significant energy and are costly, increasing the product's price. Recent advancements in "sun drying," driven by efforts to improve it, have led to the development of "solar drying."

Specialized solar dryers in solar drying help control the drying process and protect agricultural products from damage caused by dust, insects, and rain. They significantly reduce damage during the drying process by generating higher temperatures, lower relative humidity, and lower moisture content in the products compared to traditional "sun drying." Additionally, solar dryers are more cost-effective than mechanical drying methods, require less space, and take less time. Thus, solar drying presents a superior alternative to both mechanical and natural drying methods.[1]

Evaluating the efficiency of solar energy use in my region, Bouhmama, Khenchela Province, Algeria—where apples are abundantly cultivated—provides an ideal case study. This area offers a unique opportunity to examine the effects of solar drying as one of the modern techniques that combine production efficiency with environmental sustainability. By utilizing renewable natural resources like sunlight, this method transforms fresh fruit into long-lasting

products, such as crispy apple chips. Since this method preserves the nutritional value of apples and enhances their natural flavor, it is a healthy choice that meets the growing demand for preservative-free food.(Appel Bouhmama)[2]

Apples are among the most consumed fruits worldwide, available throughout all seasons. According to the Food and Agriculture Organization (FAO) Corporate Statistical Database, global apple consumption and production amounts to approximately 81 million metric tons [1]. This significant consumption leads to a substantial generation of apple waste, particularly from juice and soda industries.

Apple peel, a major co-product of apple processing, is an excellent source of nutrients. It is rich in various vitamins, notably vitamins A and C, which are present in higher concentrations compared to other vitamins . Additionally, apple peel is a valuable source of minerals, being particularly high in calcium and phosphorus .

In this paper, we aim to experimentally investigate the drying kinetics of apple slices under controlled conditions of temperature and airflow rate using an indirect solar dryer. Additionally, it seeks to evaluate the impact of thermally-aerated drying parameters on the drying kinetics as well as the bioactive properties of the apple slices.

Furthermore, the use of solar drying, especially in agricultural areas primarily dependent on farming output, helps reduce food waste and adds economic value. This technology lowers production costs and supports environmental sustainability by reducing dependence on conventional energy sources. Consequently, solar drying offers an excellent opportunity to produce high-quality, healthy, and environmentally friendly products, thereby supporting the local economy and promoting sustainable development.[3]

Chapter I

General information about drying

Chapter I. General information about drying

I.1 Definition of Drying

Drying has been characterized as the method whereby dampness is vaporized from a fabric and is cleared absent from the surface, some of the time beneath vacuum, but regularly by implies of carrier gas which passes through or over the fabric . Commonly, drying is conceived as the evacuation of water into a hot airstream, but drying may include the expulsion of any unstable fluid into any warmed gas. For drying, so characterized, to require put, the wet fabric must get warm from its environment by convection, radiation or conduction, or by inside era such as dielectric or inductive warming; the dampness within the body dissipates and the vapor is gotten by a carrier gas. This drying handle is portrayed in Figure I.1[4]

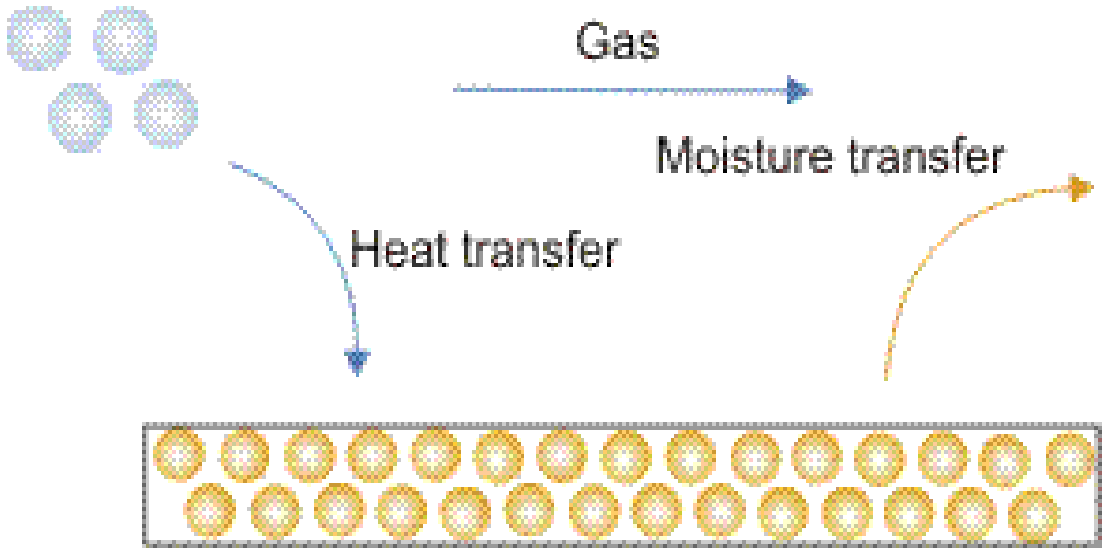

Figure I.1.Convective drying process.

We can distinguish different drying processes:

- Mechanical processes (decantation, filtration and centrifugal compression).
- Thermal processes by increasing the temperature and decreasing the vapor pressure in the gas phase, where the moisture is extracted by evaporation and diffusion .
- Chemical process (using dehydrating agents such as calcium chloride to extract water).

Drying has a number of close synonyms[5]:

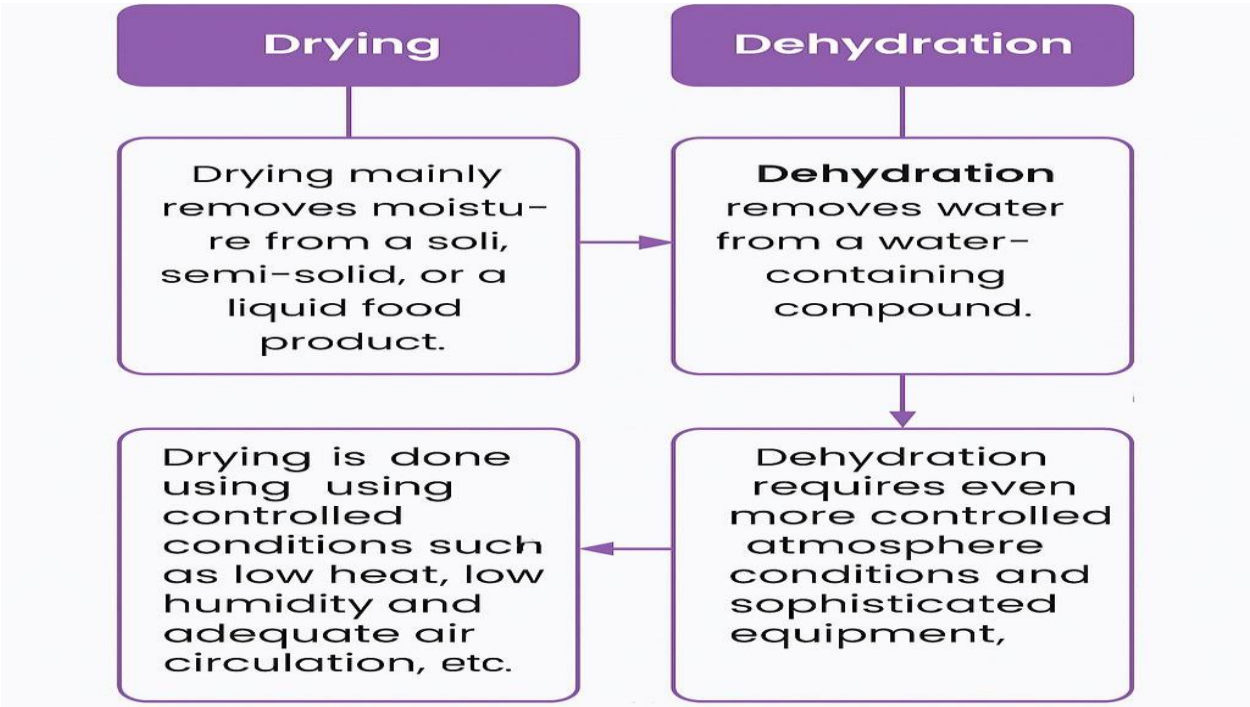

Figure I.2.Comparison Between Drying and Dehydration

I.2 Types of solar dryer

A sun based dryer could be a gadget that produces utilize of the sun's vitality to dry and protect natural products and other items. In expansion to being prudent, utilizing sun oriented vitality for drying purposes diminishes the natural impact caused by nourishment conservation. it makes strides the conservation handle and has critical environmental benefits. A few strategies of developing a sun powered dryer can be connected which by and large can be partitioned into three distinctive categories;

coordinate-, backhanded- and half breed sun powered dryers which in turn can be either passive or dynamic utilizing assistant vitality to make strides the drying prepare. To assess the execution of a sun powered dryer, a few parameters ought to be taken into consideration. The most execution parameters are the drying rate, the drying air temperature and relative mugginess, the wind current rate, the conclusion item quality and the financial costs and benefits (Augustus et al., 2002). The foremost imperative parameter to consider when planning the sun powered collector is the drying temperature, as this will mostly decide the drying rate and the item quality in terms of wellbeing. Agreeing to the Orange Book by Tetra Pak (Tetra Pak, 1998), the drying temperature ought to be over 50 °C since microscopic organisms will halt duplicating at this temperature. Besides, it would be conceivable to pasteurise natural product juices at any temperature surpassing 50 °C, but the sanitization time will diminish logarithmically with expanding temperature. Asan case, expanding the temperature from 50 °C to 60 °C will diminish the drying time from 320 hoursto 12 hours, which would be more sensible for a sun oriented dryer. In any case, Vitamin C will begin corrupting at temperatures over 50 °C meaning that as well tall drying temperatures seem cause serious misfortunes of supplements. Agreeing to Randi Phinney, PhD understudy at the office of nourishment innovations at Lund College, it is suggested tokeep the drying temperature underneath 65 °C to protect supplements (Phinney et al., 2015).

I.2.1 Direct solar drying

A direct solar dryer is characterized by the product being directly exposed to solar irradiation, but there are several different variationsof the method that can be applied. One method has been illustrated in figure I.3,[6] where the foods are protected by a layer of glass.[7]

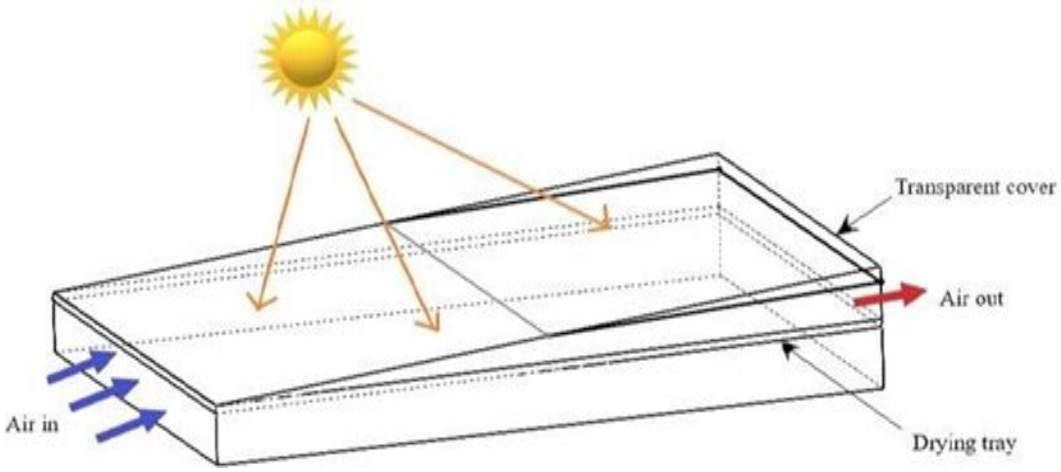

Figure I.3.Schematic of a direct solar dryer.

❖ **Passive Solar Dryers**

A drying box is what most people call this kind of dryer. The concept behind this sort of dryer is shown in Figure I.4.[8] The transparent cover reflects a portion of the incoming solar radiation, and the remainder is sent into the dryer. The solar radiation that enters the dryer is partially reflected by the drying goods, while the other half is absorbed by the materials that make up the dryer's walls and the products themselves.

The temperature of these components rises as a result, leading to the emission of long- wavelength heat radiation, which has a low transmissivity through the cover. The greenhouse effect is the name for this phenomenon. The transparent cover also helps to minimize heat losses due to convection with the environment around it (Aumporn, 2017).[9]

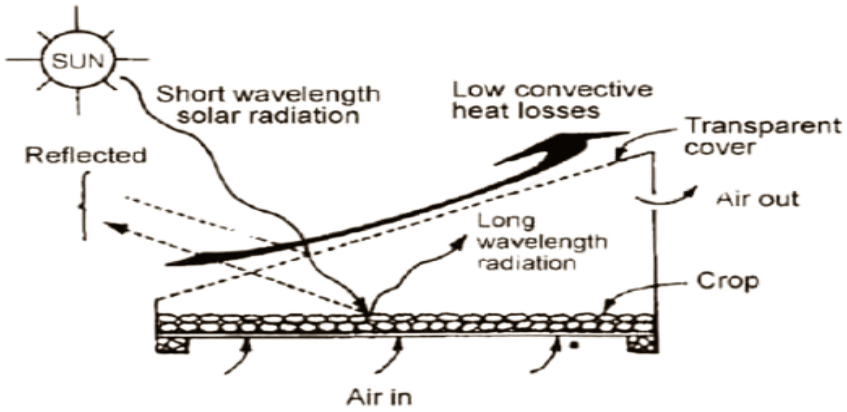

Figure I.4.Principle of a Solar Dryer Operating in Direct Mode with Natural Convection.

❖ **Active Solar Dryers**

In this kind of dryer, a fan is used to circulate the drying air inside the dryer. As a result, regulating the airflow rate helps to lower product overheating and shorten the drying process. This kind of dryer is demonstrated in Figure I.5.[10].[9]

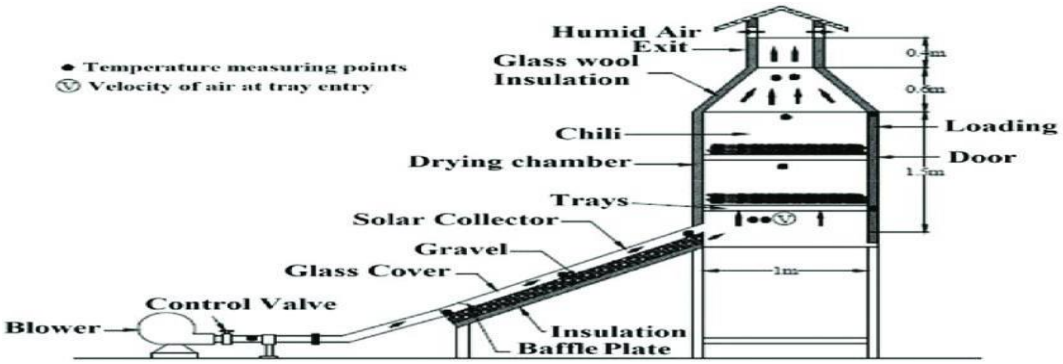

Figure I.5.Example of a Direct Solar Dryer with Forced Convection.

I.2.2 Indirect solar drying

Indirect solar dryers utilize pre-heated airfrom a heat source to dry the products ina separate drying chamber (see Figure I.6)[11],preventing the products from being directly exposed to sunlight. The air flow throughout the dryer is generally forced using fans, but could also be generated by natural convection which would be a more preferable alternative for a developing country (Kumar et al., 2015).[7]

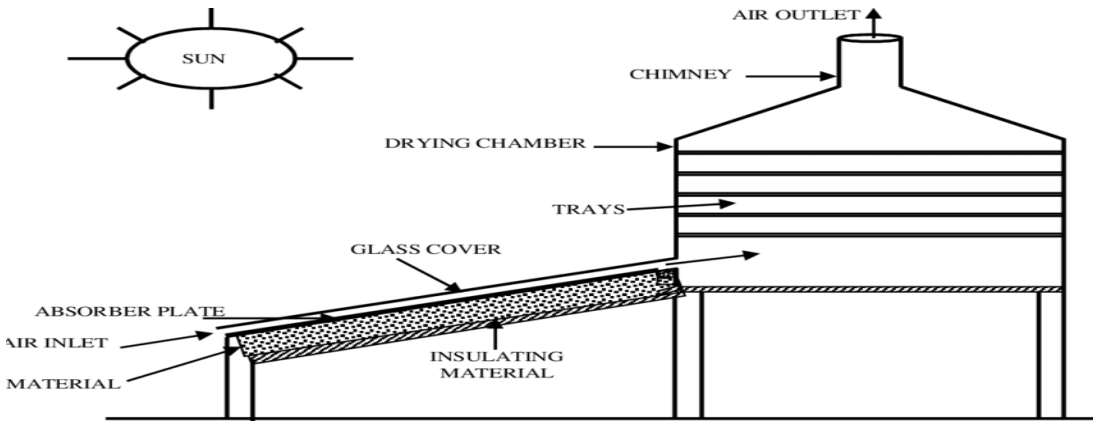

Figure I.6.Schematic of an Indirect Solar Dryer.

❖ **Passive Solar Dryers**

The air, which is drying, enters the drying room spontaneously after being preheated in the solar collector. By using the chimney effect of a duct positioned over the drying chamber, transfers between the solar collector and the drying chamber may be increased. [Aumporn, 2017] describes it as having a straightforward design, which makes it inexpensive.

❖ **Active Solar Dryers**

In general, they consist of a drying chamber, a fan to force the heated air into the drying chamber, and a solar collector to preheat the drying air [Aumporn, 2017].

In an indirect solar dryer, a comparative study between forced convection drying and natural convection drying of bananas revealed findings that were similar to those of Mohanraj and Chandrasekar (2007) and Bennamoun and Belhamri (2003) [Hassanain, 2009]. A schematic of direct and indirect solar dryers running with natural and forced convection is shown in Figure I.7.[9]

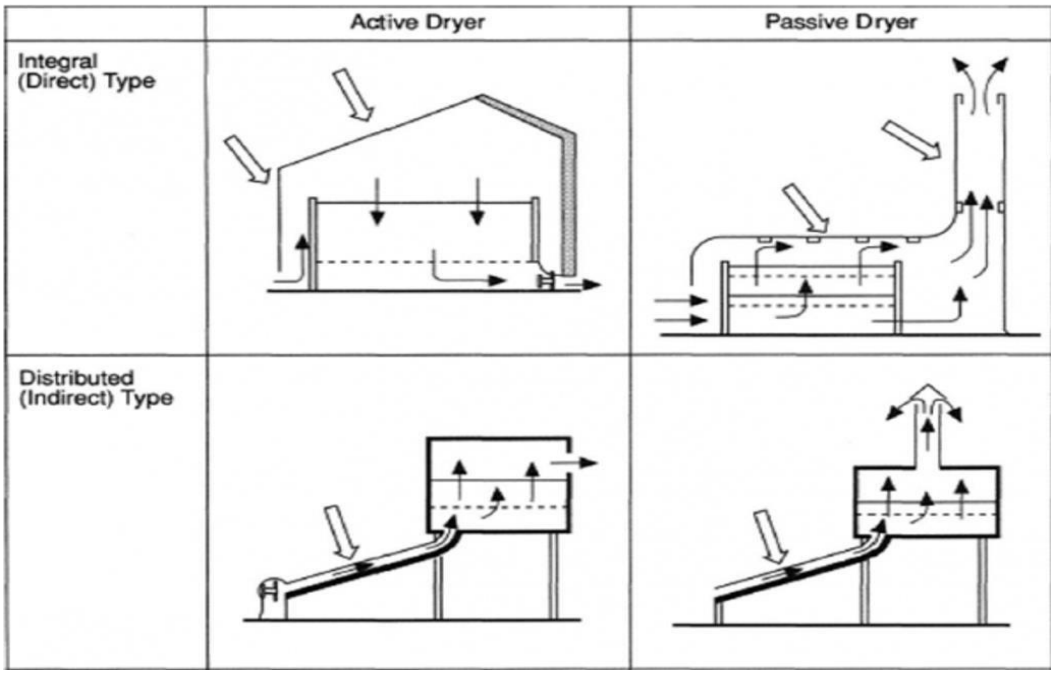

Figure I.7.Examples of direct and indirect solar dryers operating in natural convection mode and forced convection mode.

I.2.3 Hybrid solar drying

The direct and indirect drying methods are combined in a hybrid solar dryer, where a solar collector to preheat the air to a clear drying chamber, where the goods may be dried, a black absorber is used. according to Figure I.8,[12] be directly exposed to sunlight. The hybrid dryers may be paired with supplemental energy sources, like PV cells or biomass for backup energy. One of the best The advantage of a hybrid solar dryer is that the drying process is faster than any other option now available. while continuing to ensure a high standard of product quality (Kumar et al. , 2015). However, more Complex structures will probably need a higher degree of competence to run, making it a a less appealing option for Mozambique's rural regions (Augustus et al. , 2002). A passive hybrid solar dryer would be a more efficient design for a dryer that only uses natural convection. a good option, but it would still leave the possibility of case hardening occurring in the SAP pouches in the drying chamber.[7]

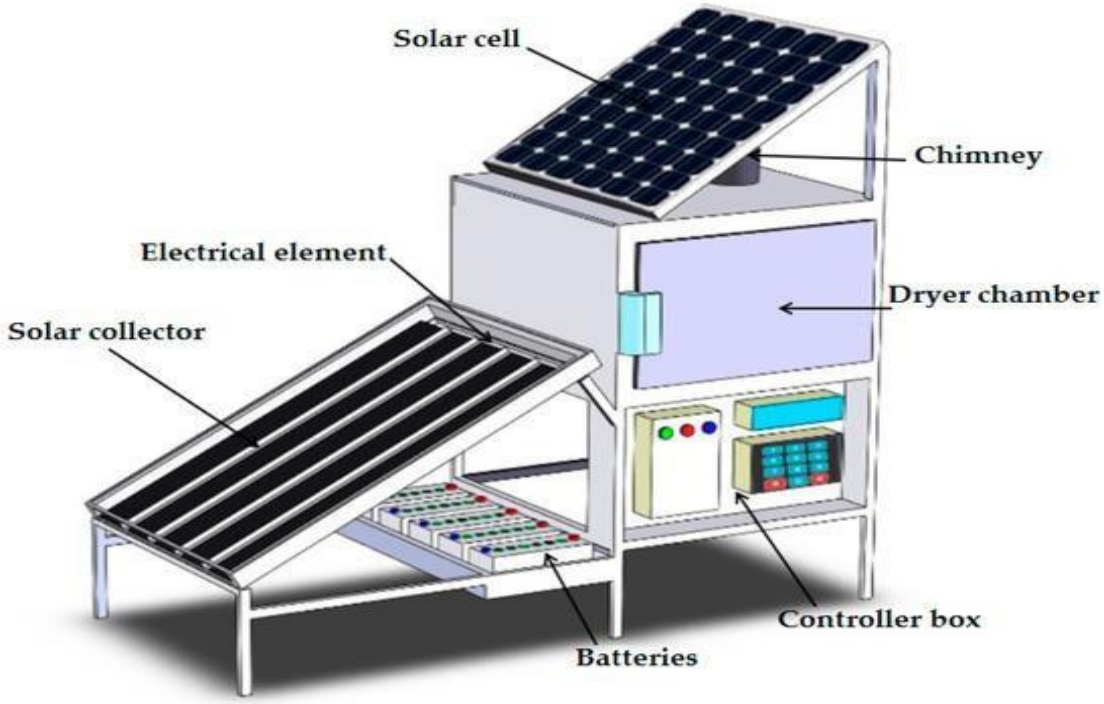

Figure I.8.hybrid solar dryer

I.2.4 Natural Dryers

They use sunlight and air directly, with products spread on racks, mats, in cribs, or even placed on the ground. (The principle of open-air drying is simple: solar radiation falls on the surface of the crop, and part of the energy is reflected back to the environment Figure I.9.[13]

These dryers are very inexpensive but require regular human intervention, such as protecting or collecting the product in case of rain, frequent stirring to prevent overheating of the upper layer, and ensuring the lower layer dries evenly.

This type of dryer is often traditional in farming communities to address temporary preservation challenges while awaiting sale or consumption.[9]

However, it has disadvantages, such as:

- Loss of poorly dried or spoiled products during stirring.
- Destruction of vitamins A and C due to direct sun exposure.
- Damage from weather conditions and pests (insects, rats, dust).

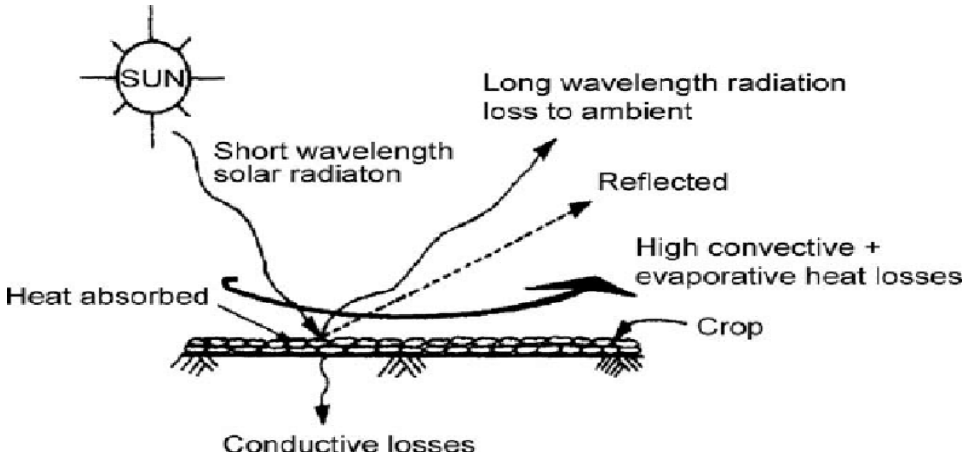

Figure I.9.Principle of Open-Air Drying

I.2.5 Mixed modes solar dryer

This solar dryer comprises three major components: a collector, a drying chamber, and a chimney, as depicted in Figure I.10,[14] The product absorbs heat energy both directly from the sun and indirectly from the solar air collector [12,44,45]. This technique incorporates the advantages of direct and indirect solar dryers.[9]

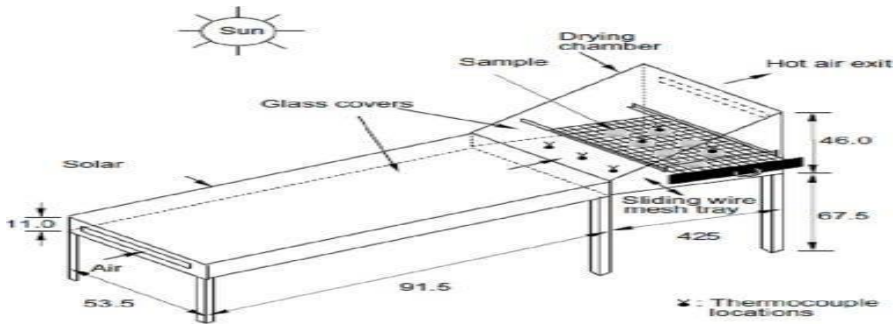

Figure I.10 The mixed modes solar dryer

I.3 Differences between Solar Drying Methods

Solar drying methods differ in their design, functionality, efficiency, and cost. Below are the primary types of solar drying methods and their differences[15]:

Table I.1.Differences between Solar Drying Methods.

	Direct Solar Drying	Indirect Solar Dryig	Hybrid Solar Dryig	Naturl Dryers	Mixed Mode Solar Dryers
Source of Heat/Energy	Direct sunligt	Indiret sunligt throuh collectors	Sun+additional energy sourcs	Sun and wind	Combinatin of direct and indirect
Protection from Environmental Factors	Unprotected	Protected	Protected	Unprotected	Protected
Efficiency and Quality	Moderate	High	Very high	Low	Very high
Cost	Very low	Moderate	High	Very low	High
Dependence on WeathrConditions	Fully dependet	Largely dependet	Flexible (not fulydependent)	Fully dependet	Flexible (not fully dependent)
Control Over Process	No control	Moderate control	High control	No control	High control
Drying Speed	Moderate	Moderate	Fast	Slow	Very fast

I.4 Table of Advantages and Disadvantages

Below is a concise summary of the advantages and disadvantages associated with

each solar drying method[15]:

Table I.2.Table of Advantages and Disadvantages.

Type	Advantages	Disadvantages
Direct Solar Drying	- Very low cost - Simple and easy to implement - Environmentally friendly	- Exposed to contamination (dust, insects) - Weather-dependent - Product quality loss
Indirect Solar Drying	- Protects products from contamination - Provides better Temperature control - Enhances product quality	- Higher cost than direct - Complex design - Slower drying speed
Hybrid Solar Drying	- Works in all weather conditions - High efficiency and quality - Faster drying speed	- High cost - Requires advanced design - Additional energy consumption
Natural Dryers	- No complex equipment needed - Very low cost - Environmentally friendly	- Slow drying process - Exposed to contamination - Inefficient in unfavorable weather
Mixed Mode Solar Dryers	- Combines direct and Indirect methods	- High cost - Complex design
	- Excellent efficiency and quality - Full control over	- Requires regular maintenance

I.5 The principle of indirect solar dryer

Working principle of indirect solar drying system In a passive solar dryer, air is heated and circulated naturally by buoyancy force or as a result of wind pressure or in combination of both. as depicted in Figure I.11,[16] Normal and reverse absorber cabinet dryer and greenhouse dryer operates in passive mode. The active solar dryers solar energy and motorized and fans/pumps for air circulation. All active solar dryer are,

thus, by their application, forced convection dryer. In a integral type active dryers, the solar collector forms an integral part of the roof/wall of the drying/storage chamber. a distributed type active solar dryer is one in which the solar collector and drying chamber are separate units. Mixed-mode type dryer are rather uncommon designs and it combines some features of the integral and distributed type. [17]

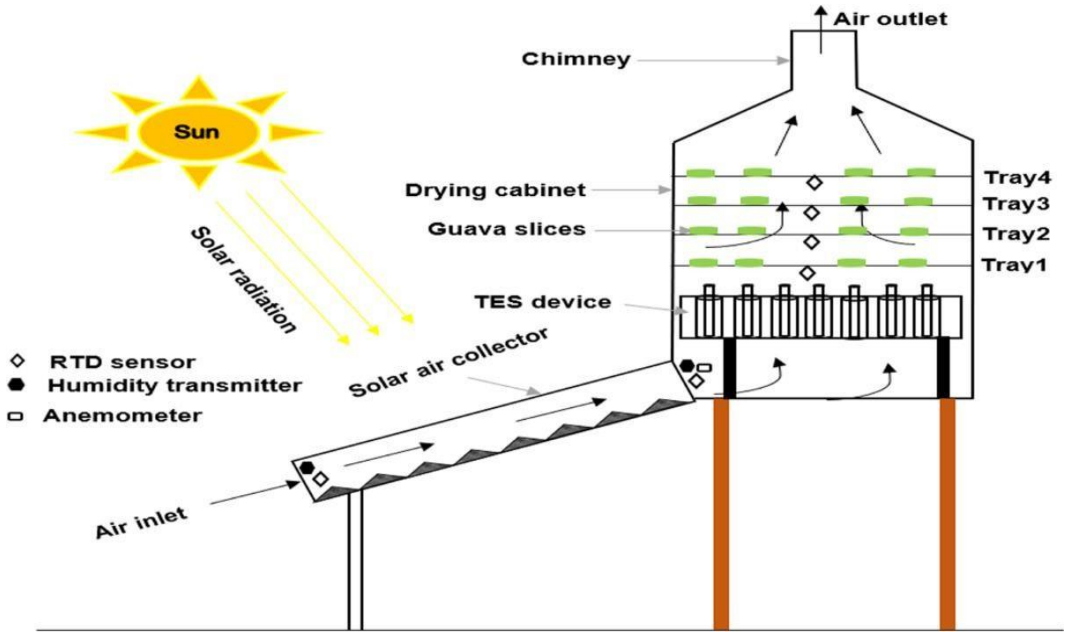

Figure I.11. the principle of indirect solar dryer

I.6 Different Modes of Drying

Drying can be performed in several ways, and the most commonly used classification criterion is based on the method of heat transfer between the product and the heat source.

❖ Drying by Conduction

The product to be dried is brought into direct contact with a hot solid surface, where heat transfer occurs through contact between the surface of the hot wall and the product. This drying method is widely used in the textile and paper industries.

❖ Drying by Convection

In this method, a flow of hot air is directed toward the product. A natural difference in temperature and partial water vapor pressure develops between the product and the air, leading to:

- Heat transfer from the air to the product due to the temperature difference.
- Water transfer in the opposite direction due to the difference in water concentration in the air.

This drying method accounts for more than 85% of industrial dryers and is extensively used in the agri-food sector.

❖ **Drying by Radiation**

Infrared radiation is applied to the product, enabling rapid heating of thin product layers (500 μm). The radiation is generated either by electronic devices (microwaves) or by heating an infrared emitter. This method is commonly applied in the paint and photographic film industries.

❖ **Microwave Drying**

Microwaves penetrate the materials and experience power attenuation due to transfer processes. Unlike infrared radiation, microwaves can dry thicker layers of materials.

❖ **Freeze Drying (Lyophilization)**

Freeze drying combines the effects of cold and vacuum to sublimate ice crystals, transitioning directly from the solid (ice) phase to the vapor phase. The vapor is then removed from the drying chamber using mechanical vacuum pumps or steam jet ejectors.

❖ **Solar Drying**

This involves heating the product using direct solar radiation (direct drying) or using a solar collector that captures and/or concentrates solar radiation to increase air temperature (indirect drying). This drying method is widely used in the agri-food sector.

❖ **Energy Considerations**

The drying methods mentioned above, except for solar drying, are significant energy consumers, accounting for 10–15% of global industrial energy consumption. Additionally, these processes are challenging to implement, particularly in rural areas where access to energy sources (electricity, gas, etc.) is often limited. Therefore,

utilizing free solar energy is beneficial and reduces process costs, especially in developing countries. [18]

I.7 Applications of solar technology

Solar energy refers primarily to the use of solar radiation for practical ends. All otherrenewable energies other than geothermal and tidal derive their energy from the sun.

Solar technologies are broadly characterized as either passive or active depending on the way they capture, convert and distribute sunlight. Active solar techniques use photovoltaic panels, pumps, and fans to convert sunlight into useful outputs. Passive solar technique sinclude selecting materials with favorable thermal properties, designing spaces that naturally circulate air, and referencing the position of a building to the Sun. Active solar technologies increase the supply of energy and are considered supply side technologies, while passive solar technologies reduce the need for alternate resources and are generally considered demand side technologies.

The applications of solar energy which are enjoying most success to-day are: Heating and cooling of residential building.

- ❖ Solar water heating.
- ❖ Solar drying of agricultural and animal products.
- ❖ Solar distillation on a small community scale.
- ❖ Salt production by evaporation of seawater or inland brines.
- ❖ Solar cookers.
- ❖ Solar engines for water pumping.
- ❖ Food refrigeration.
- ❖ Bio conversion and wind energy, which are indirect source of solar energy.

- ❖ Solar furnaces.
- ❖ Solar electric power generation by -(i) Solar ponds.(ii) Steam generators heated by rotating reflectors (heliostat mirrors), or by tow erconcept. (iii) Reflectors with lenses and pipes for fluid circulation (cylindrical par abolic reflectors).[19]

I.8 Influential Parameters on Drying Kinetics

- ❖ Drying Air Temperature (Ta)
- ❖ Relative Humidity of Drying Air (Hr)
- ❖ Drying Air Velocity (Va)
- ❖ Recycling Rate of Drying Air
- ❖ Size of the Product to be Dried
- ❖ Thickness of the Product to be Dried (Ep)

- **Influence of Drying Air Temperature (Ta)**

The temperature of the drying air significantly affects the drying rate. This influence is due to the heat transfer to the product, which increases as the air temperature rises. Additionally, the product's temperature increases more substantially at higher air temperatures. Consequently, the diffusion rates of water within the product become significant.[20]

- **Influence of Drying Air Humidity (Hr)**

The moisture content of the air plays a crucial role in the behavior of drying kinetics for certain products. This influence appears to be more pronounced at the beginning of the drying process and diminishes as the air temperature increases.[21]

- **Influence of Drying Air Velocity (Va)**

The air velocity positively affects the drying kinetics, especially at the start of the operation. However, for products where drying kinetics are controlled by the internal migration of water, the influence of air velocity on the drying rate becomes negligible.[22]

- **Influence of the Recycling Rate of Drying Air**

Recycling plays a significant role in drying operations. Although the air exiting the dryer is more humid, its temperature remains high[13].

- **The Size of the Product to Be Dried**

The dehydration rate also depends on the intracellular diffusion speed of water from the dilution of cellular sap, which is itself a function of the fruit's thickness. The drying behavior of dates depends on their morphological characteristics. Consequently, dates are used whole to simulate the real conditions of dates in the industry.

- **Influence of the Thickness of the Product to Be Dried (Ep)**

As this thickness increases, the water vapor must travel a longer path, largely explaining the slowing down of the drying process [14].

I.9 Drying Rate

$$V_s = \frac{-dM_v}{S_s . dt} = \frac{M_s . dx}{S_s . dt} \quad (1)$$

$$M_v = M_s . dX \quad (2)$$

$$dX = X_e - X_s \quad (3)$$

M_V: The mass of evaporated water.

Ms: The mass of dry product.

dX: The variation in the moisture content of the product to be dried.

Ss: The drying surface area.

Xe: The moisture content of the product at the inlet.

Xs: The moisture content of the product at the outlet.

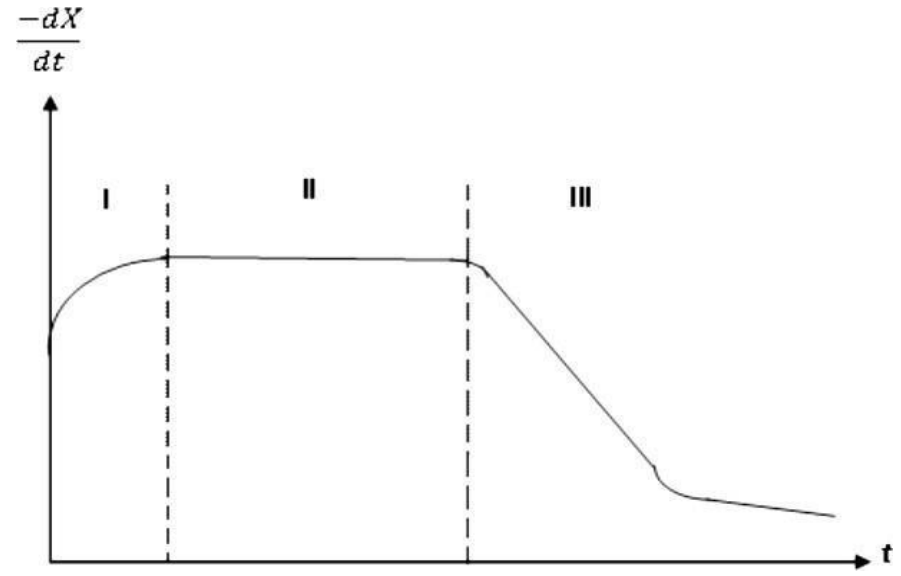

Figure I.12. Drying Rate as a Function of Time

The above curve illustrates the variation of the drying rate as a function of time. As observed, the drying operation occurs in three distinct phases:

1. The First Phase: Heating Phase (Region I)

This phase nearly disappears when the product is in the form of particles or leaves. It corresponds to the heating of the wet material until it reaches the wet-bulb temperature characteristic of the drying environment. This phase is generally very short compared to the overall drying time. During this phase, the product's moisture content changes slightly, and its temperature either increases or decreases until it stabilizes at the wet-bulb temperature.[20]

2. The Second Phase: Constant Rate Phase (Region II)

This phase occurs only when free water evaporates from the surface of the product. Evaporation takes place at the wet-bulb temperature, and the water activity (aw) at the product’s surface equals 1. Drying during this phase is described as isenthalpic. In this phase, the incoming heat flux is equal to the heat flux required for water evaporation from the product.[20]

3. The Third Phase: Falling Rate Phase (Region III)

This phase is characterized by a decrease in the drying rate.[20]

I.10 Drying Kinetics

The drying kinetics of various products are studied using curves that represent the evolution of the drying rate as a function of time. These curves are typically obtained under different experimental conditions (temperature, drying air velocity, humidity, etc.). They characterize the overall behavior of the product being dried over time.

In Figure I.13, we have plotted the variations of the solid's moisture content xx, the drying rate (dX /dT) and the solid's temperature (Solid) as a function of the operation time. All drying studies show that the drying rate curves as a function of time vary depending on the nature of the product. However, in general, the drying process can be observed to pass through three main phases:

- ❖ A phase of heating the solid.
- ❖ A constant-rate drying phase.
- ❖ A falling-rate drying phase.

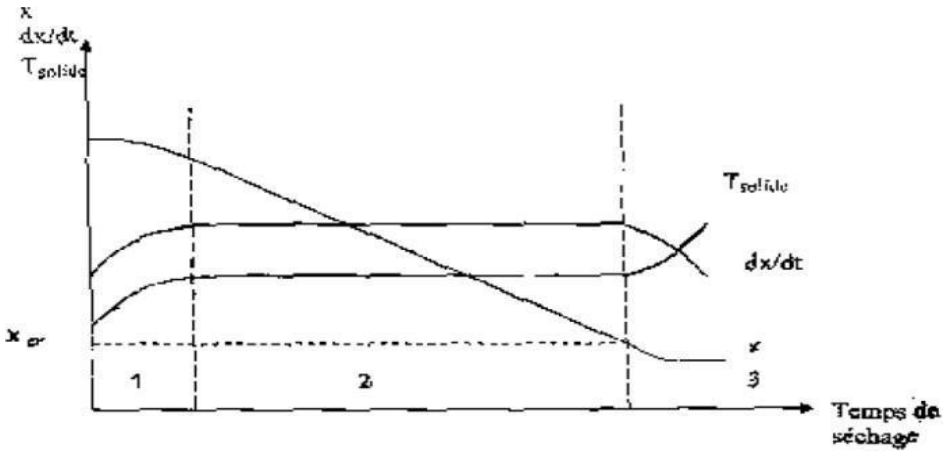

Figure I.13. Drying Kinetics

❖ A phase of temperature adjustment of the solid

During this period, the moisture content of the product varies but not significantly, and the temperature of the product changes (increases or decreases) until it reaches the wet-bulb temperature.[23]

❖ Constant-Rate Drying Phase

The study of the constant-rate phase shows that this phase is comparable to what the evaporation of water would be if no solid were present. This occurs when either there is a significant amount of water on the surface of the solid or the diffusion of water from the interior of the solid to the surface is sufficiently rapid.

During this phase, drying is considered to occur adiabatically, as there is no heat exchange with the surroundings. The latent heat of water vaporization is entirely supplied by the cooling of the hot air. Thus, the process takes place at constant enthalpy. On the psychrometric chart, the hot air evolves along an isenthalpic line (adiabatic saturation line): the heat lost due to cooling is entirely compensated by the enthalpy supplied by the water vapor. This includes a term from its formation by evaporation and a much smaller term from its heating (the heating of the solid is negligible in this phase if the air temperatures are not too high). During this period, the temperature of the solid remains constant and is equal to the wet-bulb temperature of the air.[23]

I.11 Drying of Agro-Food Products

There are several methods for dehydrating agro-food products. However, convective drying, also known as forced convection drying, remains the most common and widely used technique. It is also the method applied in this study.[24]

I.12 Key Properties of Drying Air

I.12.1 Absolute Humidity (Moisture Content on a Dry Basis):

Absolute or specific humidity, also referred to simply as the humidity of a gas, is the mass of moisture mixed with one kilogram of dry gas. This humidity, denoted as HH, is given by the following equation[25]:

$$H_{\propto} = \frac{M_e}{M_s} \qquad (4)$$

With:

M_e: Mass of water

M_s:Mass of dry air

If **P** is considered the total pressure of the gas and vapor mixture, it can be expressed for the case of humid air as:

$$\mathbf{H_{\propto} = 0.662\left[\frac{P}{p - p_v}\right]} \quad \textbf{(5)}$$

I.12.2 Relative Humidity

Water vapor is present in the air as vapor $P_V \leq (T)$ The relative humidity or hygrometric degree H_T of the air is defined by the following equation [26]:

$$\boldsymbol{H_T = \frac{P_V}{P_{S(T)}} .100} \quad \textbf{(6)}$$

Pv: The partial pressure of vapor in the mixture.

Ps: The saturation pressure in the same mixture, measured at the same temperature

I.12.3 Degree of Saturation

The degree of saturation is the ratio of the specific humidity of air to the specific humidity of saturated air at the same temperature [26]:

$$\boldsymbol{\varphi = \frac{H_a}{H_{as}}} \quad \textbf{(7)}$$

In cases where **P1** and **P** are both small compared to PP (such as in humid air at atmospheric pressure and relatively low temperatures), the equation can be expressed as[25]:

$$\boldsymbol{\varphi = \frac{H_a}{H_{as}} = \frac{P_V}{P_S}} \quad \textbf{(8)}$$

I.13 Water Activity and Sorption Isotherm

I.13.1 Water Activity in the Product

The water activity in a product is the ratio of the vapor pressure of water **PV**at the product's surface to the vapor pressure of pure water **Ps(T)** at the product's temperature**T**.

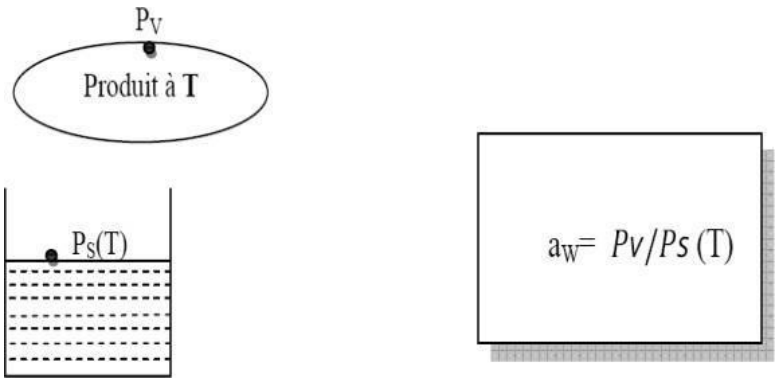

Figure I.14.Water activity in the product

Let us now consider a product and air in equilibrium with each other, where PV, T, PVa, and Ta represent, respectively, the water vapor pressures and the temperatures of the product and the air.

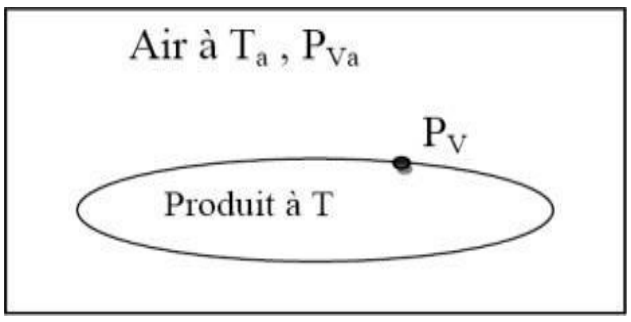

· Figure I.15.The product and air in equilibrium

he imposed equilibrium conditions are T = Ta (no heat transfer) and PV = Pva (no mass transfer). However, the relative humidity HRa of the air is expressed as:

$$HRa = Pva / Ps(Ta) \quad (9)$$

From which we deduce: **HRa = a_w**

Thus, the water activity in a product is also the relative humidity of air in equilibrium with the product. The significance of this value is that it varies only slightly with temperature, whereas the water vapor pressure PV varies significantly.

I.13.2 Sorption

Isotherms Definition

The water activity (aw) in a product mainly depends on its water content (Xéq) and its temperature (T).

The curve representing, for a given temperature, the water content (Xéq) of a product as a function of the water activity value (aw) or the relative humidity of the air in equilibrium (HRE) is called:

- Adsorption isotherms if it is experimentally determined starting from a dry product.
- Desorption isotherms if it is experimentally determined starting from a water-saturated product [27].

The (Figure I.16) shows that the two curves are generally different because drying a product (transition from aw = 1 to aw < 0.6) leads to irreversible structural and porosity changes. There is a phenomenon of hysteresis.

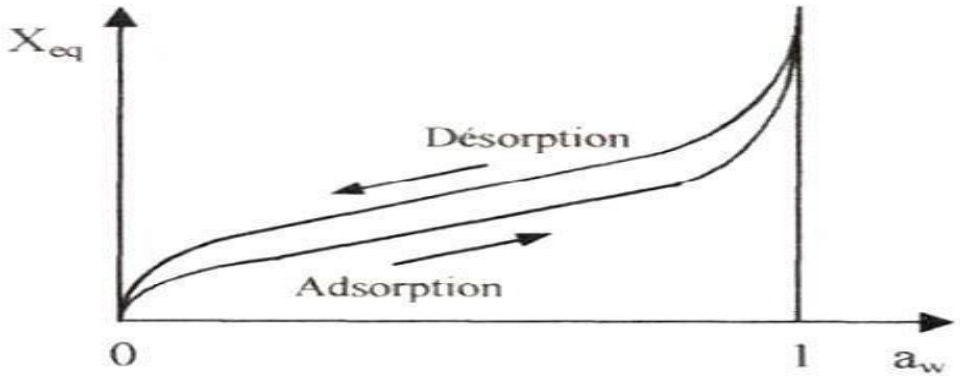

Figure I.16. Adsorption/desorption isotherms

Adsorption-desorption isotherms generally have three zones, each corresponding to a particular mode of water binding to the product:

- **Zone 1**: Formation of a molecular monolayer on the product's surface. This zone is characterized by the action of Van der Waals forces between hydrophilic groups and water molecules. Water molecules are adsorbed progressively until a monolayer covers the entire external surface and the pores of the product. Water is in a rigid state due to the strong bonding forces between water molecules and the surface. Transition to the next zone occurs when the entire surface is saturated.
- **Zone 2**: Adsorption of molecules onto the initial monolayer. In this zone, the isotherm is linear, and water is in an intermediate state between solid and liquid.
- **Zone 3**: Water present in liquid form in the pores of the material. The film thickness is sufficient for the water to exist in liquid form within the capillary structure of the material

Chapter II

Overview of Dry Matter

II.1 Apropos De Produit

The apple tree originally comes from Central Asia, but it has spread and gained popularity around the world, becoming the most widely cultivated fruit tree and one of the most beneficial for health and healing. Apples are generally round to slightly oval in shape, with smooth, shiny skin. Their color varies by variety—ranging from green to yellow to red. In terms of health benefits, apples are considered second only to oranges.

Apples are a nutritious fruit, rich in vitamins A and C, and potassium. They contain no sodium, cholesterol, or fat, and are a good source of pectin fiber—one apple contains about five grams of fiber.

This fruit is beneficial for nearly every illness and helps support the body's vital organs. Eating apples may help prevent strokes, lower cholesterol levels, and reduce the risk of liver, colon, and prostate cancers. Additionally, apples are effective in fighting obesity and excess weight. [II1].

Figure II.1.Apple

II.2 Apple Composition

The composition of an apple may vary slightly from one variety to another, but in general, a medium-sized apple (about 182 grams) contains the following elements:

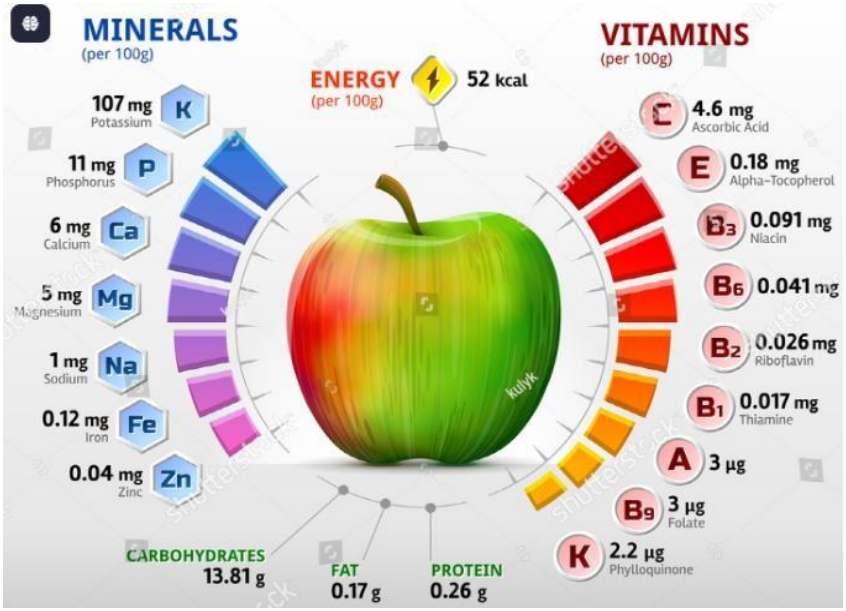

Figure II.2. Apple Composition

II. 2.1 Water

Apples are made up of mostly water, with more than 82% of their total composition being water.

II.2.2 Carbohydrates

They contain between 9 and 15 grams of carbohydrates per 100 grams of fresh fruit, mainly in the form of fructose, sucrose, and glucose. [II**2**]

II.2.3 Fiber

Apples are relatively high in dietary fiber, with 3 to 3.7 grams per 100 grams of whole fruit, and about 2.1 grams per 100 grams when peeled. [II**2**]

II.2.4 Proteins and Fats

Apples contain around 0.26 grams of protein and 0.17 grams of fat per 100 grams. The fats include saturated, monounsaturated, and polyunsaturated fatty acids. [II**2**]

II.2.5 Minerals and Trace Elements

They are a good source of potassium (0.145 g/100 g), and also provide calcium, magnesium, phosphorus, iron, zinc, copper, manganese, boron, and selenium. [II**2**]

II.2.6 Vitamins

Apples are fairly rich in vitamin C (0.01 g/100 g) and also provide B vitamins (B1, B2, B3, B5, B6, B9) along with fat-soluble vitamins like provitamin A (0.07 mg) and vitamin E (0.5 mg). [II**2**]

II.2.7 Phytochemicals

They contain phenolic acids (including cinnamic, gallic, ascorbic, p-coumaric, salicylic, and vanillic acids) as well as flavonoids such as quercetin, myricetin, catechin, epicatechin, kaempferol, rutin, naringenin, and resorcinol. [II**3**]

In short, apples are valued not just for their sweet taste and crisp texture, but also for their rich blend of essential nutrients and health-promoting bioactive compounds.

II.3 Dénomination des différents stades de maturation des pommes processus de séchage

Apple ripening is generally divided into stages based on how mature the apple is for use or consumption. The following are the main stages of apple ripening :

- **Growth Stage (Pre-Ripening Stage)**

The apple is still growing in size, with high starch and low sugar levels. The flesh remains firm, and taste develops profile is not yet developed. [II4]

- **Beginning of Physiological Ripening Stage**

Here, starch is beginning to convert to simple sugars (fructose, glucose, sucrose). Color will begin to change slowly with the development of the typical apple smell. [II4]

- **Full Ripening Stage (Optimal Harvest Stage)**

The fruit has achieved final color depending on variety (red, yellow, green). Sugar content is high and the acidity levels are low. Flesh is becoming softer and flavor is balanced. This is the stage to eat vs. store. [II4]

- **Post-Ripening Stage (Senescence or Aging)**

Flesh has begun to lose firmness. Sensory qualities (taste, aroma) are deteriorating and rotting risk is increasing. [II4]

II.3.1 Traitements post-récolte de pomme

It is critical to use postharvest treatments for apples to prolong storage life, protect quality, and inhibit disease. Key methods and practices that have application to postharvest handling of apples are listed below:

Figure II.3. Post-harvest treatments of apple

II.3.1.1 Sorting and Selection

Sorting aims to remove damaged, diseased, or otherwise lower quality fruit. It is critical to avoid spreading disease and to maintain quality of the batch, which often involves a careful inspection and, at times, testing for firmness or sugar content.

Figure II.4.Sorting and Selection

II.3.1.2 Cleaning and washing

The emphasis of this stage is to remove dirt, pesticide residue and other forms of microbial contamination. Cleaning can involve dry air, water rinsing or brushing. Disinfectant solutions (like chlorine) are mostly used in this activity because they help to lower microbial counts. [II5]

II.3.1.3 Drying

After washing, the fruit should be dried well to remove moisture that may support mold growth. Drying can be a key component prior to packaging or storage.

Figure II.5.Cleaning and Washing

II.3.1.4 Waxing

A wax coating on apples can aid in the loss of water as well as firmness and especially on visual appeal. This method is highly utilized in most apple producing countries. [II6]

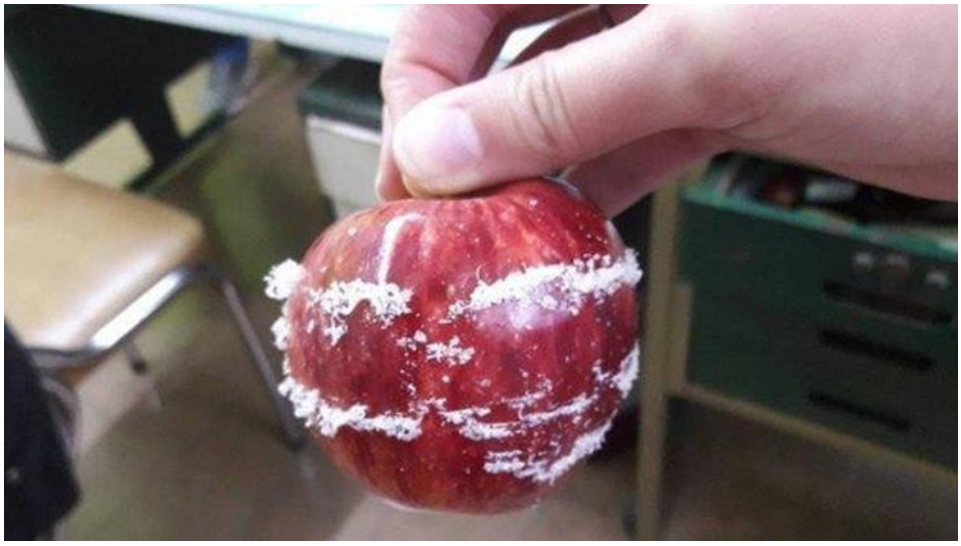

Figure II.6.Waxing

II.3.1.5 Refrigeration and Storage

To reduce ripening rates, apples should be stored at optimal cold storage temperature. Proper refrigeration is important for prolonging storage life. [II 7]

Figure II.7. Refrigeration and Storage

II.3.2.6 Controlled Atmosphere Storage

Regulating the storage environment – especially the gas concentrations of oxygen and carbon dioxide – can slow the respiration of apples and preserve apples longer. [II7]

II.3.1.7 Disease Monitoring and Control

Preventing post-harvest diseases includes proactive measures such as removing rotten fruit, cleaning equipment and storage areas, routinely checking stored apples and applying antifungal treatments when appropriate.

These post-harvest processing practices help maintain the quality of apples throughout the supply chain from the moment they are harvested until they reach a supermarket's shelf or your kitchen. They are important in keeping apples fresh, flavorful, and nutritious up until the moment they are consumed.

II.3.2 Temperature and Storage Duration

Temperature and Storage Duration: Two Important Factors in Maintaining Apple Quality.

Temperature and duration of storage are two key factors affecting the quality of apples (specifically, their freshness, crispness, and flavor). If they are not managed properly, apples can accelerate softening and flavor loss or spoil prematurely. [II8]

II.3.2.1 Storage Temperature:

- Refrigerated

Apples will hold best at a storage temperature of between 32°F and 39°F (0°C to 4°C). By keeping apples at low temperatures, the ripening process can be slowed down to prolong the shelf life of the product and maintain its taste, texture and quality [II9]. By using standard cold storage rooms, including those with controlled atmospheric conditions, apples can be kept for months in the industry [II10]

- Room temperature

Apples will ripen much faster at room temperatures of approximately 68°F (20°C).

As a result, room temperature storage is not ideal and is only practical for short-term storage of apples (a few days to a week). For above and beyond that time period, it would be ideal to keep apples in cool space [II11]

II.3.2.2 Storage Duration

- Refrigeration:

When stored properly in a refrigerator—above freezing and less than 39 °F (4 °C)—apples can last anywhere from a few weeks to a few months. In this case, the length of time that apples will last is highly variable and dependent on the apple variety, initial ripeness, and storage conditions [II11]

- Room temperature:

At room temperature (about 68 °F or 20 °C), apples generally remain fresh for only a few days to about a week. Then they started to lose their firmness, become increasingly susceptible to microbial spoilage, dehydration, and rot This means that apples stored at room temperature should ideally be consumed shortly after purchasing. [II9]

II.3.2.3Long-Term Storage

For long-term storage, such as in warehouses or controlled commercial environments, apples are placed in cold rooms where the temperature (usually 32°F to 34°F (0°C to 1°C)), and most importantly, the relative humidity (90-95% humidity) is strictly controlled [II9]. Under such ideal conditions, storage of months to even 1 year is possible using long-term storage technologies such as Controlled Atmosphere (CA) and Modified Atmosphere (MA) [II11].

It should also be emphasized that different apple varieties have different long-term storage capabilities based on biochemical composition and ethylene sensitivity. For example, Granny Smith apples tend to store longer than McIntosh apples [II8].

Gaseous management is essential in delaying fruit ripening but specifically in lowering ethylene levels and increasing carbon-dioxide levels [II12].

A combination of refrigeration, low temperature, and careful humidity and gas management is the best way to elongate shelf-life after harvest while keeping apple flavor, texture, and nutritional quality intact. Prudent management of temperature, relative humidity, and gases will ensure flavor and freshness of apples when eaten well after harvest.

II.3.3 Solar Drying of Rehydrated Apples

Solar drying of rehydrated apples is a low-cost, traditional, and sustainable way of preserving apples, while enhancing the concentration of flavor and retaining most of the nutrients [II13]. This method is especially advantageous in sunny rural regions where solar energy is plentiful.

II.3.3.1 Apple Preparation

- Apple selection : The best apples to dry with are fresh, ripe, and firm. The sweeter, slightly tart varieties often produce the best results. Golden Delicious-type or Fuji apples work well [II8].
- Washing and Peeling: Wash apples well to remove dirt or residues, and peeling is optional based on preference.
- Rehydration (rehumidification): apples can be briefly blanched in hot or boiling water for 2 to 5 minutes prior to drying. This step, which will soften the apples and help to facilitate more even drying, should be done [II14].

Solar drying process

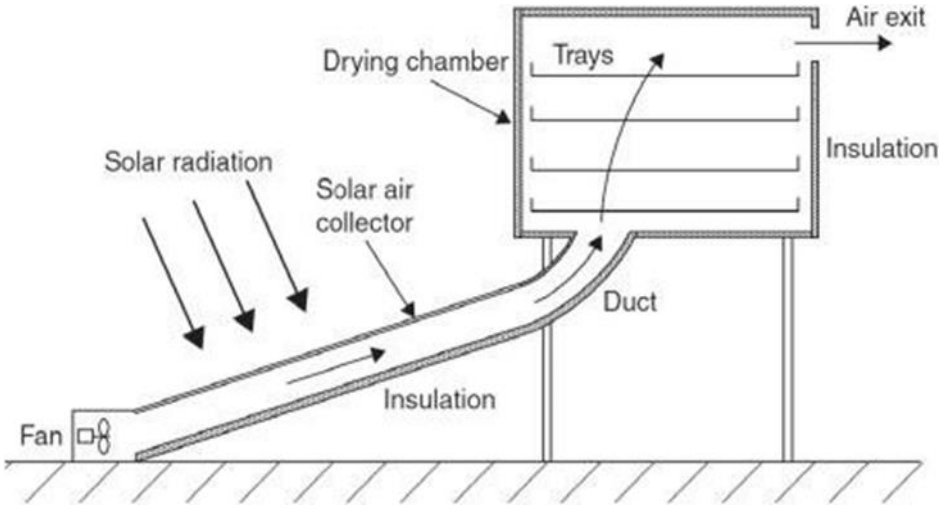

Figure II.8.Solar drying process

- Slicing : The apples are sliced thinly (0.2 to 0.4 inches or 0.5 to 1 cm thick or thinner) and cored and seeded.
- Placing : Spread the slices out evenly across trays that allow for air circulation.
- Sun-drying : The trays are set out in a sunny, clean, well-ventilated area, free from insect contamination. Using an appropriate solar dryer can help optimize drying efficiency [II15].
- Monitoring and Turning

Turning the slices regularly will help to even out the drying process and reduce the opportunity for mold growth [II16].

Drying times can take anywhere between 2 to 7 days depending on the sun and humidity level.

- Storage of Dried Apples

According to FAO (1986), once the apples are dried (pliable, slight sticky, and no visible moisture), they should be cooled and stored in an airtight container, protected from light, moisture, and heat.

When stored properly dried apples, can last for several months in good condition.

To sum up, solar drying is a sustainable and environmentally friendly and especially useful in low- energy environments. It provides a useful post-harvest preservation strategy for food security and waste reduction [II17].

Figure II.9. Storage of Dried Apples

Chapter III

Numerical Study

III.1 Mathematical Model

The current investigation employs air change per hour (ACH) as a performance metric, as specified by ANSI/ ASH-RAE in 2004. The preceding quantities are provided as follows:

$$Q = v \times A\ solar\ chimney \quad (1)$$

Q : volumetric flow rate, v: air velocity and $A_{solar\ chimney}$: cross-sectional vector area of solar chimney.

$$ACH = (Q \times 3600)/V_{room} \quad (2)$$

V_{room} indicates the volume of the room where the solar chimney is connected. The air change per hour (ACH) depends on the room size ratio to the chimney area. The value of living room volume (V_{room}) in real life is 27 m3, calculated using the dimensions of a standard living space measuring 3 m x 3 m x 3 m.

In the equation presented, the typical room volume is substituted with a realistic room volume (e.g., 27 m^3) to estimate the ventilation rate in real-life situations. The underlying assumption is that the chamber volume does not affect the volumetric flow rate calculated by the equa- tion. To more accurately represent real-life conditions, vol- umetric flow rates have been converted to equivalent air changes per hour for a room of 27 m3. It is important to note that the air change rate is calculated using Equations (1) and (2). [44]

III.1.1 System Modelling

The heat balance equations for each component of the solar chimney are the basis for the finite element of the understudied system. Set assumptions have been consid- ered for this:

- The nodal method is considered (the temperature of each layer of the solar device is considered spatially constant).
- Each solid layer’s thermo-physical characteristics are assumed to be constant.
- The lateral thermal losses have been ignored.
- The fluid duct pressure losses are neglected.

- The ground-to-solar device radiative heat transfer is disregarded.

The energy conservation concept is applied to each component to forecast the temperatures of each solar device and determine their performances. The following equation commonly expresses this principle. [44]

$$M_I C_I \frac{dT_I}{dT} = \sum_{in} Q_i \sum_{ou} Q_i \tag{3}$$

where

$M_i C_i \frac{dT_i}{dt}$ the thermal inertia of the component i.

$\sum_{in} Q_i$ total of the energy that component i received through different heat exchange modes.

- $\sum_{ou} Q_i$ is the total of the energy that component i lost through different heat exchange modes.

➢ For the glass cover

$$M_g C_g \frac{dT_g}{dt} = A_m\left[\alpha_g G + h_{r,g-sky}\left(T_{sky} - T_g\right) + h_{r,g-p}\left(T_p - T_g\right) - h_{v,g-f}\left(T_g - T_f\right) + h_{v,a}\left(T_a - T_g\right)\right] \tag{4}$$

The equivalent temperature of the sky is given by the relation [30, 31]:

$$T_{sky=}0.0552T_a^{1.5} \tag{5}$$

The following correlation can be used to determine the radiative heat transfer coefficient between the glass of a PV module and the sky [32]:

$$h_{r,sky-g=}\sigma\epsilon_g \frac{\left(T_g^2 - T_{sky}^2\right)\left(T_c^2 - T_{sky}^2\right)}{\left(T_g - T_a\right)} \tag{6}$$

The following equation gives the radiative heat transfer coefficient between two parallel flat plates [33, 34]:

$$h_{r,i-j} = \sigma \frac{\left(T_i + T_j\right)\left(T_i^2 + T_j^2\right)}{\frac{1}{\varepsilon_i} + \frac{1}{\varepsilon_j} - 1} \tag{7}$$

The convective heat coefficient due to the wind is described by the following relation [35-37]:

$$h_{v,a} = 5.7 + 3.8V_w \tag{8}$$

- For the air

$$\dot{m}_f C_f \frac{\dot{dT_f}}{dx} = 1\left[h_{v,f-p}\left(T_{p-}T_f\right) - h_{v,f-g}\left(T_f - T_g\right)\right] \tag{9}$$

The Nusselt number correlation reported by Hollands et al. (1976) is applied in the case of natural convection occurring in an inclined rectangular duct. The following Eq can be used to determine the convective heat transfer coefficient in the air space. This correlation is valid with the following criteria of rectangular duct; tilt angle $\theta \leq 70°$ and $H/L \geq 12$ [33, 38, 39, 40]:

$$h_{v,cf} = \frac{K_f}{l_{cf}} Nu = \frac{K_f}{l_{cf}}\left[1 + 1.44\left[\left(1 - \frac{1708}{Ra\cos\theta}\right) + \left(1 - 1708\frac{(sin\,1.8\theta)^{1.6}}{Ra\cos\theta}\right)\right] + \left(\left(\frac{Ra\cos\theta}{5830}\right)^{\frac{1}{3}}\right) - 1\right] \tag{10}$$

The terms with the sign (+) for this correlation denote that only positive values are considered (i.e. if negative, the 0 is used).

Ra can be expressed as the Rayleigh number, which is:

$$R_a = GrPr = \frac{g\beta L^3 \Delta T}{v_f^2} Pr = \frac{g\beta L^3 \Delta T}{v_{fa}} \tag{11}$$

where g, β, L, v_f and a are the gravity acceleration, the expansion volume coefficient, the characteristic length (l_{cf}), the kinematic viscosity, and the thermal diffusivity $\left(\frac{K_f}{\rho_f C_f}\right)$, respectively. All fluid proprieties are calculated using wall mean temperature of the rectangular cavity. $\left(\frac{T_p+T_g}{2}\right)$

In the Rayleigh number, ΔT is calculated as:

(T_g - T_f) for the exchange fluid-top glass cover, and; (T_p - T_f) for the exchange fluid-bottom glass cover.

The mass flow rate is evaluated by adopting the formula suggested by Bansal et al. (1993) and Arce et al. (2013) [41, 42]:

$$\dot{m}_f = C_d \frac{\rho_f A_o}{\sqrt{1+A_r}} \sqrt{\frac{2gL(T_f - T_r)}{T_r}} \tag{12}$$

Where

$$A_r = \frac{A_0}{2A_{in}} \tag{13}$$

A_{in} and A_o are the inlet and outlet areas of the chimney. The experimental investigation of Arce et al. [43] showed that the appropriate value for the discharge coeffi-

cient, Cd is about 0.52:

- For the absorber

$$M_p C_p \frac{dT_p}{dt} = A_m\left[\tau_g \alpha_p G + h_{r,p-g}(T_g - T_p) + h_{v,p-f}(T_f - T_p) - h_{c,p-in}(T_p - T_{in})\right] \tag{14}$$

It is easy to express the air temperature along the duct of the cheminy as:

$$T_f(x) = \left[\left(T_{f,in} - \frac{(T_t h_{v,f\_t} + T_p h_{v,f-p})}{(h_{v,f-t} + h_{v,f-p})}\right) e^{\frac{W_c(h_{v,f}+h_{v,f-p})}{\dot{m}_f C_f}} + \frac{(T_t h_{v,f-t} + T_h h_{v,f-p})}{(h_{v,f-t} + h_{v,f-p})}\right] \tag{15}$$

- For the absorber plate

$$M_p C_p \frac{dT_p}{dt} = A_c\left[h_{c,p-in}(T_{in} - T_p) - h_{v,f-p}(T_p - T_f) - h_{r,p-g}(T_p - T_g)\right] \tag{16}$$

The neighboring solar device parts create a pathway for the conductive heat transfer. The following formula describes how the heat transfer coefficient in this case is stated between two nearby components, i and j:

$$h_{c,i-j} = 1/\left(\frac{l_i}{\lambda_i} + \frac{l_j}{\lambda_j}\right) \tag{17}$$

- For the thermal insulator

$$M_{in}C_{in}\frac{dT_{in}}{dt} = A_c\left[h_{c,in-p}\left(T_p - T_{in}\right) - h_{v,a}(T_{in} - T_a)\right] \quad (18)$$

- **Heat transfer equation:**

$$k\Delta^2 T = \rho c_p\left(\frac{T\partial}{t\partial} + u.\Delta T\right) \quad (19)$$

- **Navier-stokes equation:**

$$\rho\left(\frac{u\partial}{t\partial} + (u.\nabla)u = -F + \mu\Delta^2 u + p\nabla\right) \quad (20)$$

III.2 Study one

III.2.1 Geometric Model

The two-dimensional geometric model of an indirect solar dryer was developed using **comsol multiphysics**. This model represents a longitudinal section of the system, enabling a detailed study of heat and mass transfer within its components. The design focuses on airflow and heat transfer behavior to enhance the efficiency of the drying process.

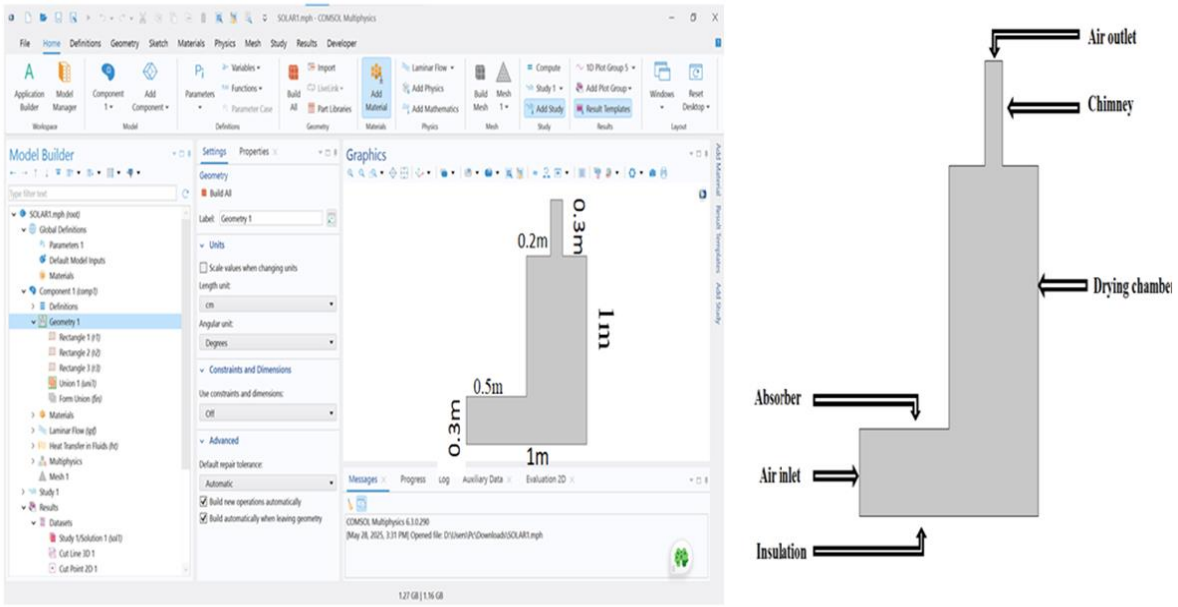

Figure III. 1.Geometric model design using comsol multiphysics.

III.2.1.1 Geometric Domain:

❖ **Drying Chamber**:

- Designed as the primary component of the system, with rectangular dimensions of 1.00 m in length and 1.60 m in height.
- Used for drying materials by facilitating the flow of hot air and ensuring uniform heat distribution.

❖ **Hot Air Inlet:**

- An inclined duct with dimensions: 0.40 m wide at the base, narrowing to 0.20 m at the outlet, with a height of 0.40 m.

- Functions to channel preheated air from the solar collector into the drying chamber, ensuring efficient heat transfer.

❖ **Moist Air Outlet (Chimney):**

- A vertical duct with dimensions: 0.80 m in height and 0.20 m in width, starting at 1.60 m and extending to 2.40 m.
- Designed to exhaust moisture-laden air while promoting natural convection.

III.2.2 Boundary conditions

The boundary conditions have been updated to enhance the accuracy of airflow and heat transfer simulation within the indirect solar dryer model. The updated conditions are as follows:

III.2.3 Laminar flow :

❖ **Reference Parameters:**

- **Reference Pressure Level**(P_{ref}) **:** Set to atmospheric pressure [atm]
- **Reference Temperature** T_{ref}**:** Set to **293.15 K**.

❖ **Hot air inlet:**

- **Temperature:** A fixed temperature representing preheated air from the solar collector.
- **Air Velocity:** Defined at **0.005 m/s**.
- **Pressure:** Set to a reference value of **0 Pa**.

❖ **Moist Air Outlet:**

- **Velocity and Pressure:** Both set to **0**, allowing unrestricted exit of moisture-laden air from the system.

❖ Walls

- **Thermal Conditions:** Walls are considered **thermally insulated**, preventing heat exchange with the external environment.
- **Flow Conditions:** A **No-Slip** condition is applied, ensuring that the air velocity at the wall surfaces is zero.

❖ Initial Values

- **Velocity Field**
  - $v_x = 0\ m/s$
  - $v_y = 0\ m/s$
- **Pressure:** The initial pressure is set to $P = 0$ pa

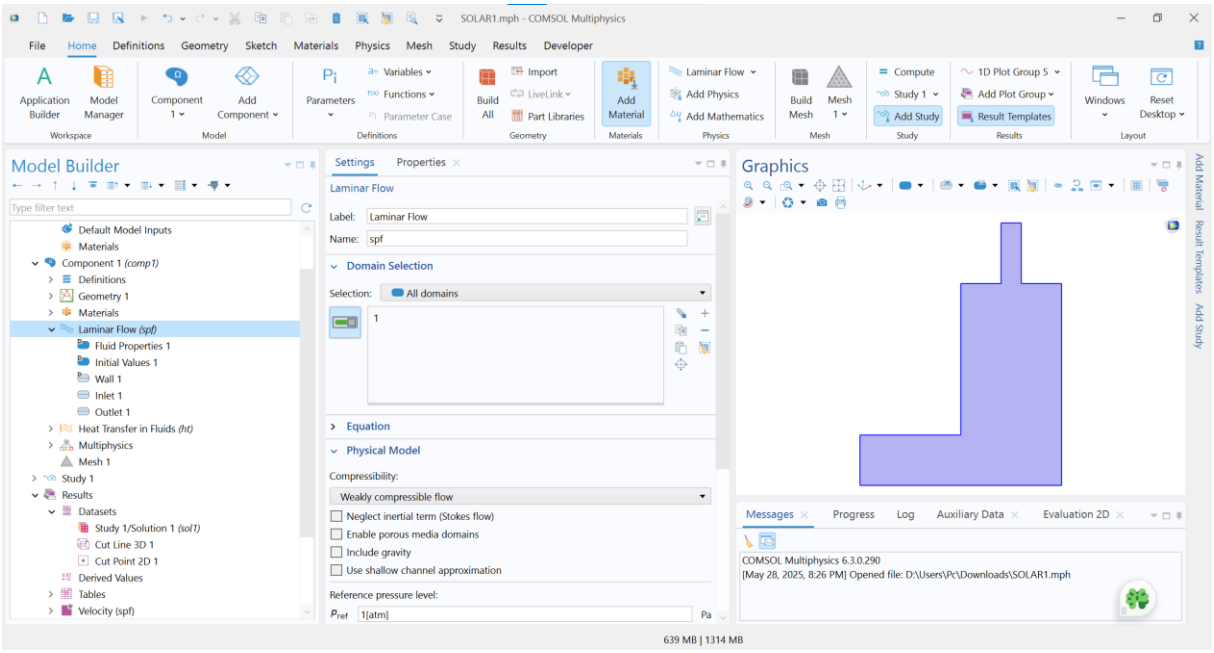

Figure III. 2.Laminar flow

III.2.4 Heat transfert in fluid

❖ Reference Parameters:

- **Domain Thickness** (dz) **:** 1m
- **Reference Temperature** (T_{ref})**:** 293.15 K

- **Initial Values:**

- **Temperature:** 293.15 K

- **Heat Flow: $100\ W/m^2$**
- **Inflow:**

- **Temperature:** 293.15 K

- **Outflow:**

- Heat transfer conditions are left unrestricted to allow for the free exit of thermal energy.

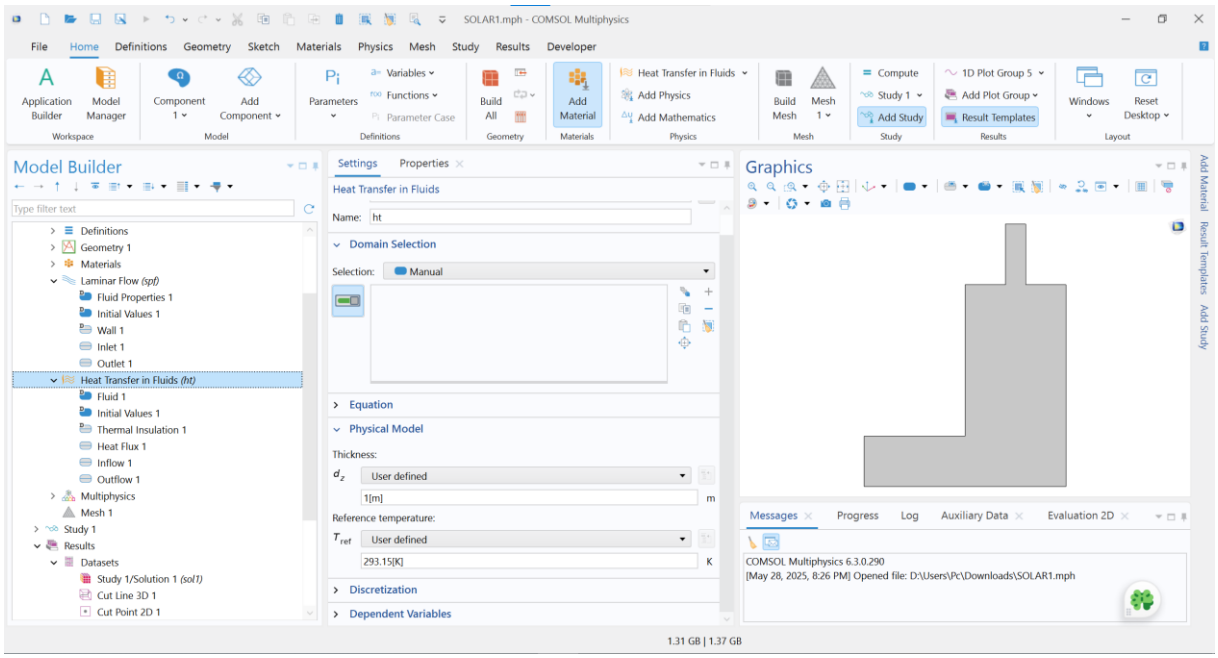

Figure III. 3.Heat transfert in fluid

III.2.5 Meshing

Study of mesh type impact on the simulation results of an indirect solar dryer in the context of simulating an indirect solar dryer using comsol multiphysics, three different mesh refinement levels were used: coarse, normal, and fine, in order to evaluate how mesh density affects the accuracy of the results and the numerical stability of the solution.

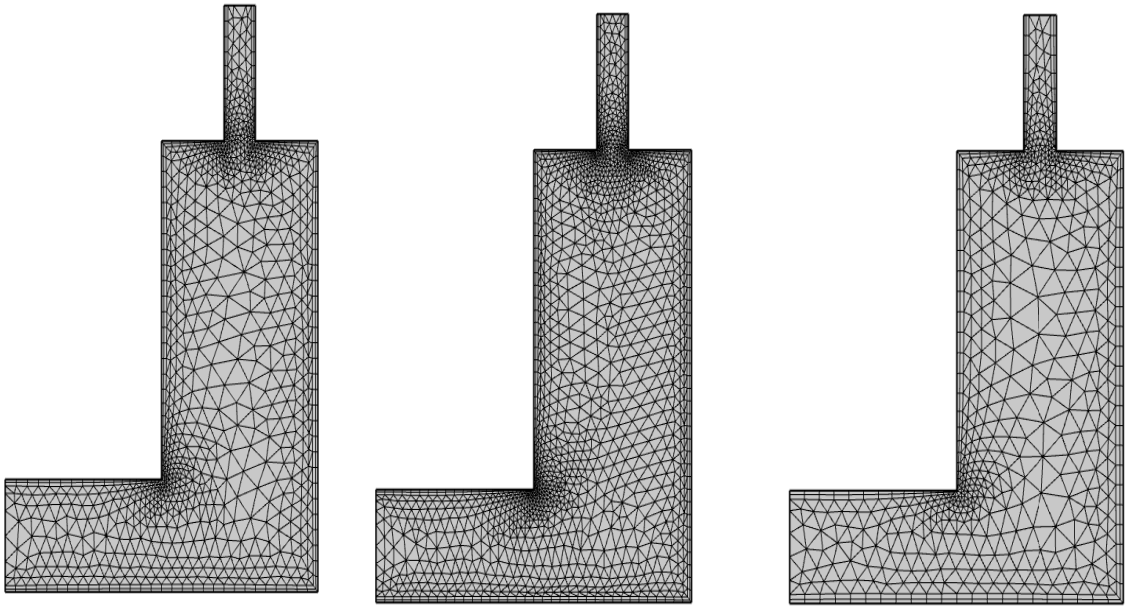

Normal mesh Fine mesh Coarse mesh

Figure III. 4.Meshing of chimney center

Table III.1. Comparative mesh statistics for the chimney center

Description	**Fine Mesh**	**Coarse Mesh**	**Normal Mesh**
Number of mesh vertices	1839	848	1237
Triangular elements	2715	1093	1704
Quadrilateral elements	347	232	298
Edge elements	213	137	172
Vertex elements	11	11	11
Total number of elements	3089	1325	2002
Minimum element quality	0.1597	0.2678	0.1547
Average element quality	0.8257	0.8146	0.8193
Element area ratio	0.006463	0.005919	0.005283
Total mesh area $[cm^2]$	6550	6550	6550

III.2.6 Results and discussion

In the context of heat transfer studies, the heat flux of 100 W/m² plays a crucial role in understanding the distribution of temperature, velocity, pressure, and isothermal contours within the studied medium. The simulation was conducted using COMSOL Multiphysics, relying on Step Stationary to solve the system in a steady-state manner, allowing for the analysis of thermal equilibrium and the distribution of physical variables without being affected by time-dependent factors.

III.2.6.1 Velocity

Figure [III.5] illustrates the air velocity magnitude distribution within the main chamber of the solar dryer in a two-dimensional plane. It can be observed that the highest air velocity occurs at the upper inlet zone, where the airflow follows a narrow vertical path, resulting in a noticeable acceleration. This behavior is consistent with the principle of mass conservation in enclosed systems, as the narrowing of the cross-sectional area leads to an increase in velocity, in accordance with the continuity equation $A_1V_1 = A_2V_2$

As the air enters the wider section of the drying chamber, the velocity gradually decreases, as indicated by the color gradient in the figure—from red (maximum velocity) to dark blue (minimum velocity). This reduction is due to flow expansion and frictional effects along the chamber walls and internal surfaces.

The simulation also reveals the presence of low-velocity or stagnant zones, particularly near the lower corners of the chamber. These areas are critical in practice, as they contribute to non-uniform distribution of hot air, resulting in uneven drying of the products. This non-uniformity in airflow is a clear indication of the need to optimize the chamber design or adjust the placement of drying materials to avoid moisture accumulation in low-flow regions.

From an engineering perspective, these findings serve as a valuable guide for redesigning the internal ventilation system or for determining optimal locations to place products with high moisture content in areas of higher airflow. Moreover, the

results offer an important foundation for further investigations involving temperature distribution and relative humidity fields.

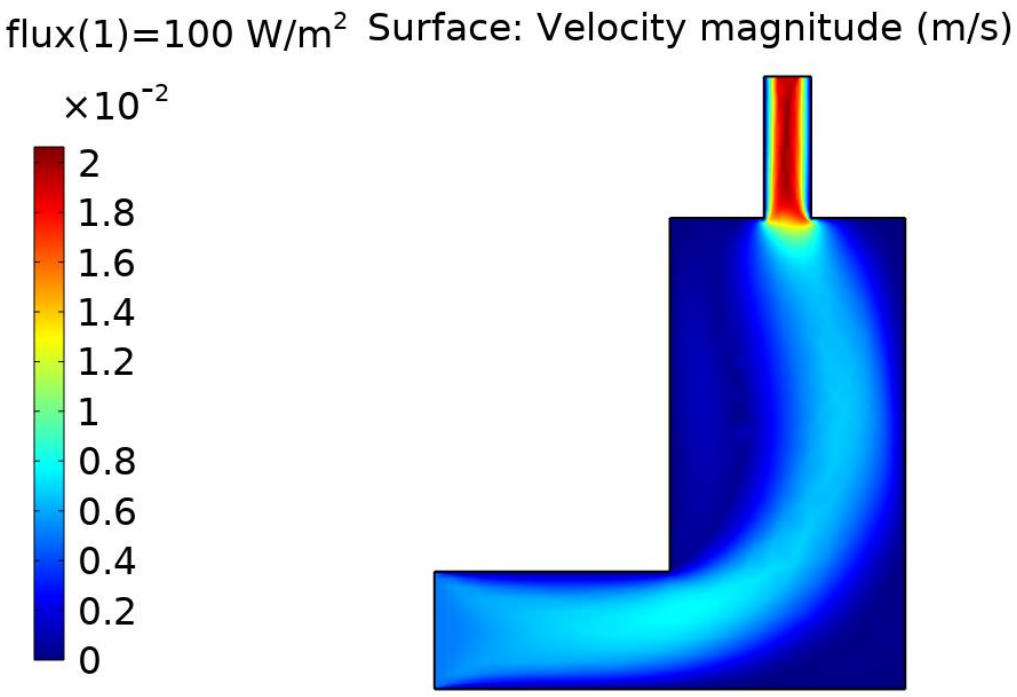

Figure III. 5.Velocity magnitude

III.2.6.2 Analysis of Pressure Distribution in the Solar Dryer

The figure [III.6] illustrates the static pressure distribution within the two-dimensional geometry of the solar drying chamber. The highest pressure values are observed near the air inlet at the top, represented by warm colors (red and orange). As the airflow progresses downward through the chamber, the pressure gradually decreases, reaching its minimum near the outlet at the bottom, as indicated by the dark blue tones.

This pressure gradient is consistent with Bernoulli's principle, where pressure decreases as the airflow velocity increases in narrow regions and increases where the flow decelerates. The gradual pressure drop within the chamber is attributed to flow resistance due to changing cross-sectional area and interaction with the internal walls, resulting in pressure losses caused by friction and dissipation of kinetic energy.

The pattern of isobaric lines in the image highlights the presence of localized recirculation zones near the outlet, indicating some degree of airflow disturbance. These regions are critical as they may contribute to moisture accumulation or uneven drying rates across the drying chamber.

From a design perspective, the pressure distribution results provide essential insights into the aerodynamic efficiency of the dryer. They also serve as a foundation for proposing structural improvements, such as adjusting the inlet angle or reshaping the internal passage to promote more stable flow and reduce significant pressure losses. These findings support the analytical approach to enhancing the thermal performance of the solar dryer by ensuring more effective airflow and minimizing variations in drying conditions inside the chamber.

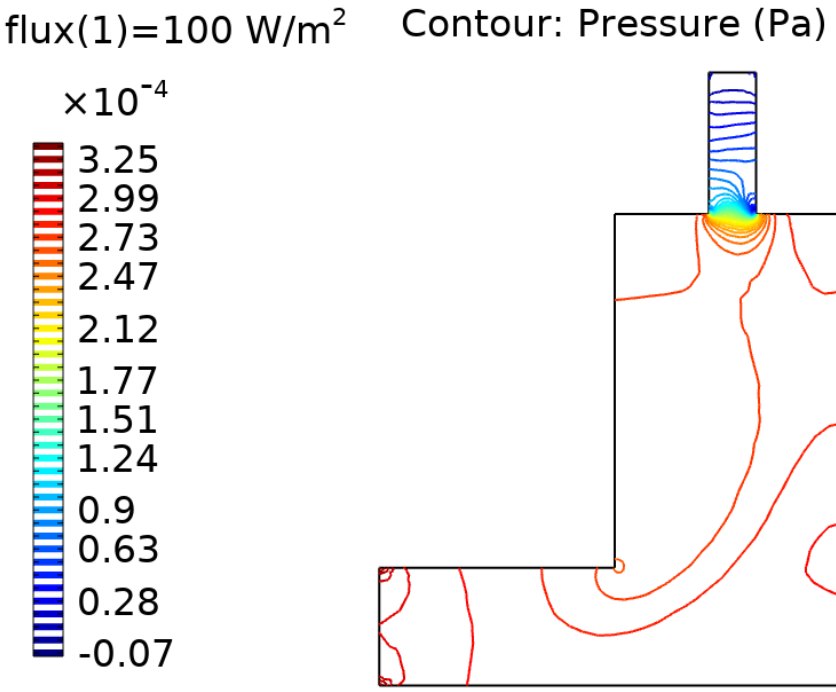

Figure III. 6.Contour pressure

III.2.6.3 Temperature Distribution within the Solar Dryer

The figure [III.7] above illustrates the surface temperature distribution (in Kelvin) within the solar drying chamber under a constant incident heat flux of 100 W/m². The thermal profile reveals a clear spatial variation in temperature, with the

highest values concentrated near the absorber plate at the bottom left region of the chamber. This zone reaches temperatures exceeding 480 K, indicated by the bright white and yellow hues. These high temperatures are consistent with the zone of direct solar irradiation, where heat absorption is maximized.

As the air is heated, it rises through the drying chamber, and the temperature gradually decreases along the vertical axis. This decrease is due to the heat loss to surrounding walls and the natural convection-driven movement of air away from the hot absorber surface. The transition from yellow to deep red shades clearly indicates this thermal gradient.

The chimney region, located at the top of the geometry, exhibits moderately high temperatures, which is a desirable feature for sustaining the buoyancy-driven flow (chimney effect) essential for maintaining continuous ventilation. The elevated air temperature in this area supports the natural convection mechanism, helping to evacuate humid air from the drying chamber.

From a thermal performance perspective, the configuration ensures effective heat transfer from the absorber to the internal air volume. However, the strong temperature gradient near the absorber also highlights the need to manage heat distribution more uniformly across the drying section to ensure consistent drying rates for the agricultural product.

This result confirms the effective conversion of solar energy into thermal energy and its subsequent transmission into the drying volume, which is critical for the drying process efficiency. The data further supports the design's capability to achieve optimal thermal conditions in the critical drying zone, thus validating the overall functionality of the indirect solar dryer under simulated thermal loads.

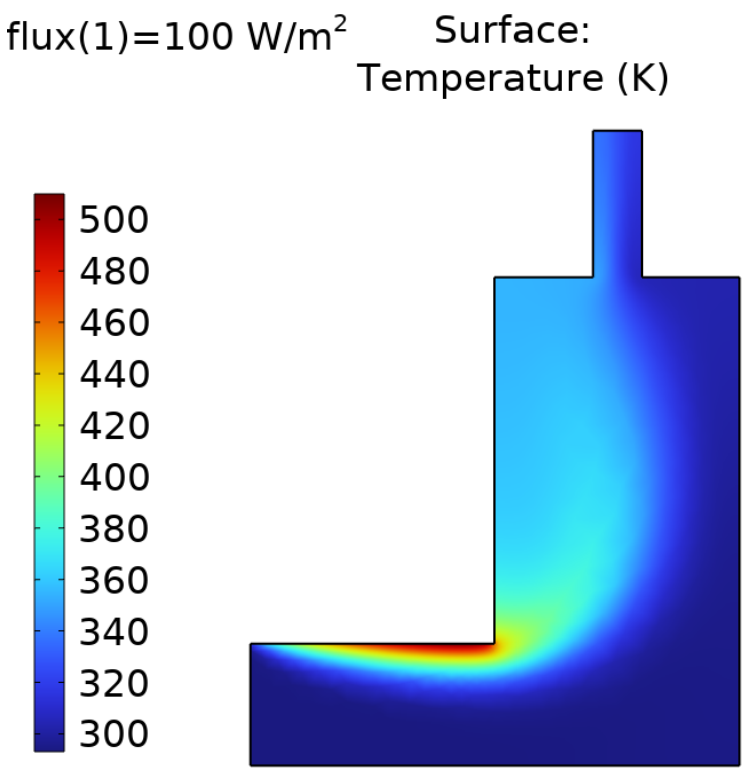

Figure III. 7.Surface temperature

III.2.6.4 Isothermal Contours Within the Solar Dryer

The figure [III.8] illustrates the distribution of isothermal contours inside the drying chamber of the solar dryer. These contours represent regions of equal temperature and serve as an effective tool for visualizing heat transfer patterns within the system. The image clearly shows a dense clustering of contours near the absorber surface (bottom-left corner of the chamber), indicating a steep temperature gradient in this region due to direct solar heat absorption.

As the air heats up and rises, the contours gradually space out vertically, reflecting a decrease in temperature due to natural convection-driven heat transfer. The geometric shape of the chamber significantly influences the distribution of these contours, as they bend and expand upward, indicating mixing between the rising hot air and the cooler surrounding air, thereby reducing temperature differences.

In the chimney region, the contours are more widely spaced but follow a smooth upward flow pattern, confirming the effectiveness of the chimney effect in drawing out

hot and humid air. This natural ventilation mechanism is essential for maintaining continuous airflow through the drying chamber.

This qualitative analysis highlights the efficiency of convective heat transfer within the system and shows that the current design promotes heat concentration in the main drying zone while ensuring the upward flow of heated air. However, the dense clustering of contours near the absorber also suggests the potential need to enhance heat distribution. This could be addressed by integrating thermal diffusers or low-speed fans to promote a more uniform temperature field.

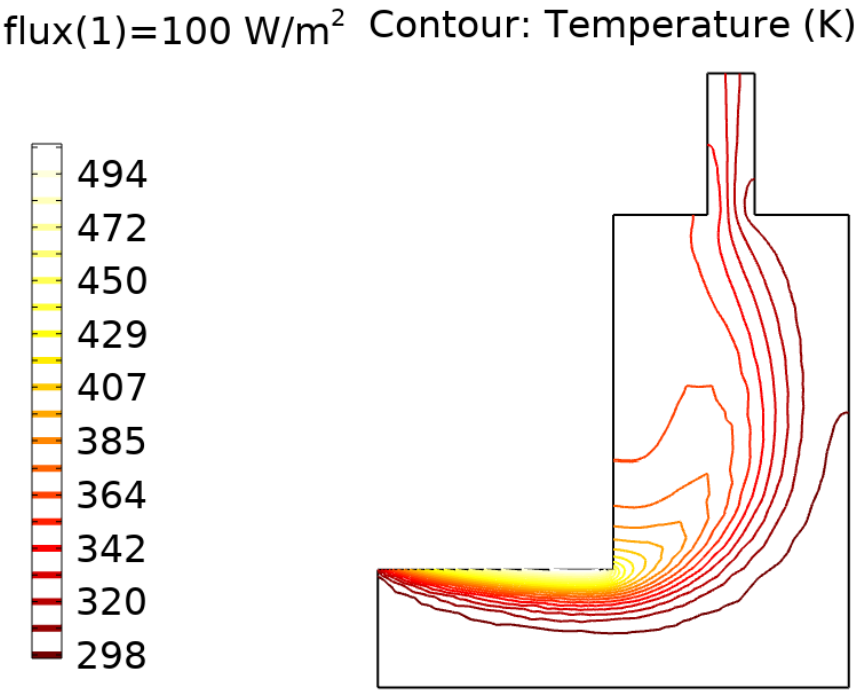

Figure III. 8.Isothermal contours

III.3 Study tow

III.3.1 Impact of changing the chimney location

After completing the first study, which analyzed the heat distribution and airflow within the solar dryer with a centrally positioned chimney, the transition to the second study (study 2) aimed to assess the impact of changing the chimney's location on the thermal and dynamic performance of the air inside the drying chamber.

At this stage, the chimney was relocated to the far right side of the geometric design to examine how this modification affects airflow patterns and thermal distribution due to natural convection.

It is important to note that all boundary conditions adopted in the first study were maintained unchanged to ensure an accurate comparison between the two studies. These conditions include the heat flux applied to the absorber surface, the ambient air temperature, the physical properties of the air, as well as the implementation of the laminar flow model and the heat transfer in fluid model.

This adjustment aims to evaluate the system's sensitivity to minor geometric modifications and analyze the effect of the chimney's location on:

- the effectiveness of the chimney effect in promoting natural ventilation.

- the temperature distribution inside the chamber.

- the stability and direction of the airflow.

- the uniformity of the drying process within the chamber.

This comparison is essential for guiding future design decisions and enhancing the efficiency of the solar dryer, particularly for agricultural applications that require safe and uniform drying of products.

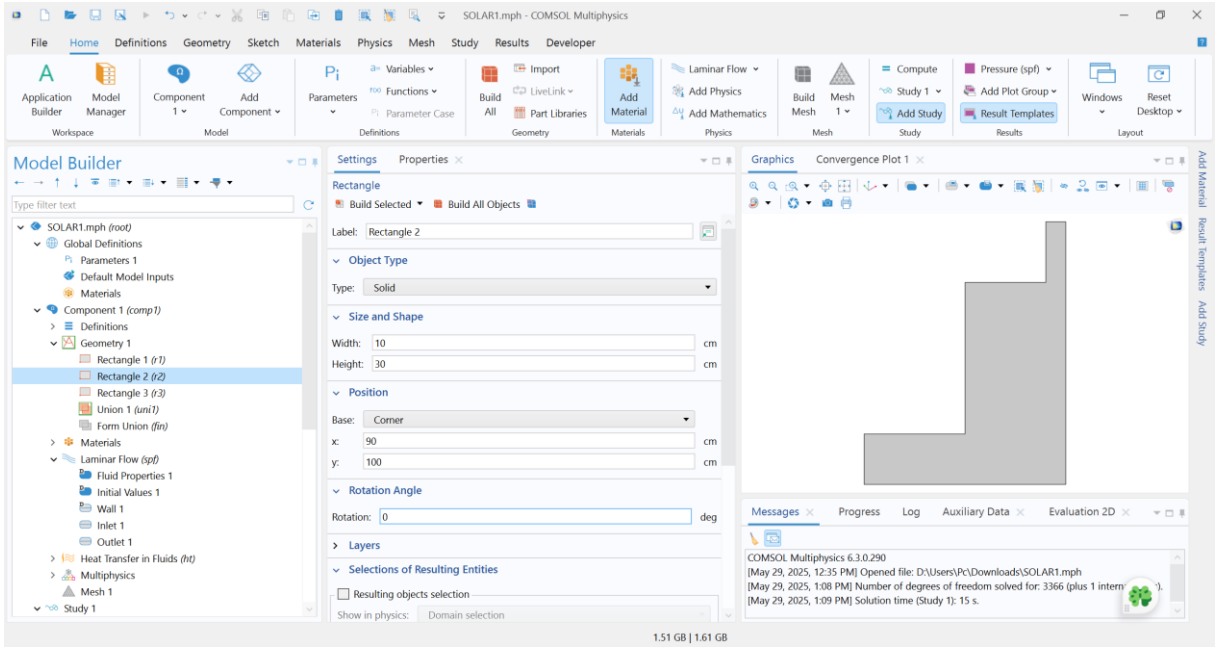

Figure III. 9.Impact of changing the chimney location(right)

III.3.2 Meshing of changing the chimney location

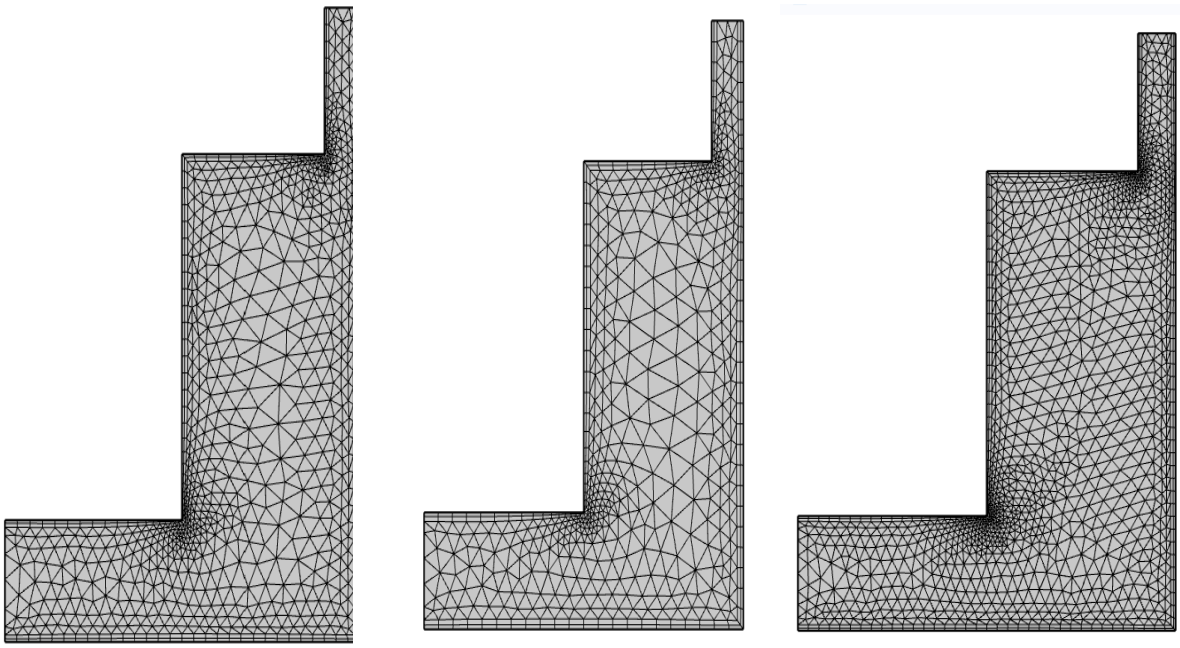

Normal mesh Coarse mesh Fine mesh

Figure III. 10.Meshing of changing the chimney location (right)

Table.III.2. Comparative mesh statistics for the chimney right

property	**Coarse mesh**	**Normal mesh**	**Fine mesh**
Number of mesh vertices	771	1122	1666
Number of triangular elements	961	1501	2411
Number of quadrilateral elements	224	288	358
Total number of elements	1185	1789	2769
Minimum element quality	0.2721	0.2515	0.2447
Average element quality	0.8111	0.795	0.7836
Total mesh area [cm^2]	6550	6550	6550
Smallest element area[cm^2]	0.006571	0.004626	0.006678

III.3.3 Results and discussion

III.3.3.1 Surface velocity magnitude (m/s)

This figure [III.11] illustrates the velocity distribution of air within the solar dryer chamber. The color scale represents the magnitude of velocity in meters per second. The highest airflow speeds are observed near the upper right region of the chamber, close to the outlet chimney. This pattern is a clear indication of the chimney effect, where hot air naturally rises due to thermal buoyancy.

The airflow accelerates upward, reaching a maximum velocity of approximately , consistent with natural convection behavior in enclosures heated from below. These results demonstrate the system's ability to sustain air movement passively without the need for mechanical fans, highlighting the energy efficiency of the design.

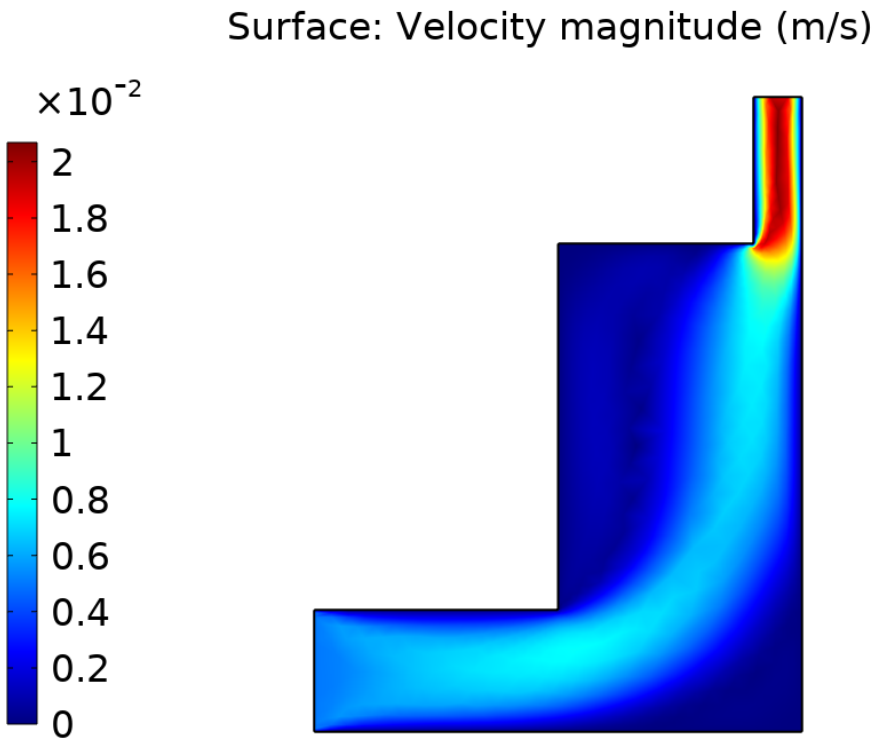

Figure III. 11.Surface velocity magnitude (m/s).

III.3.3.2 Contour pressure (Pa)

This plot presents the pressure distribution within the drying chamber, depicted using contour lines. The pressure ranges from approximately to , with the highest values occurring near the upper outlet.

Although the pressure differences are minimal, they are sufficient to drive natural convection. The pressure gradient from the bottom to the top promotes upward airflow, supporting the passive ventilation mechanism. This pressure pattern confirms the system's capability to generate effective air movement solely through thermal effects, reinforcing the solar dryer's low-energy nature.

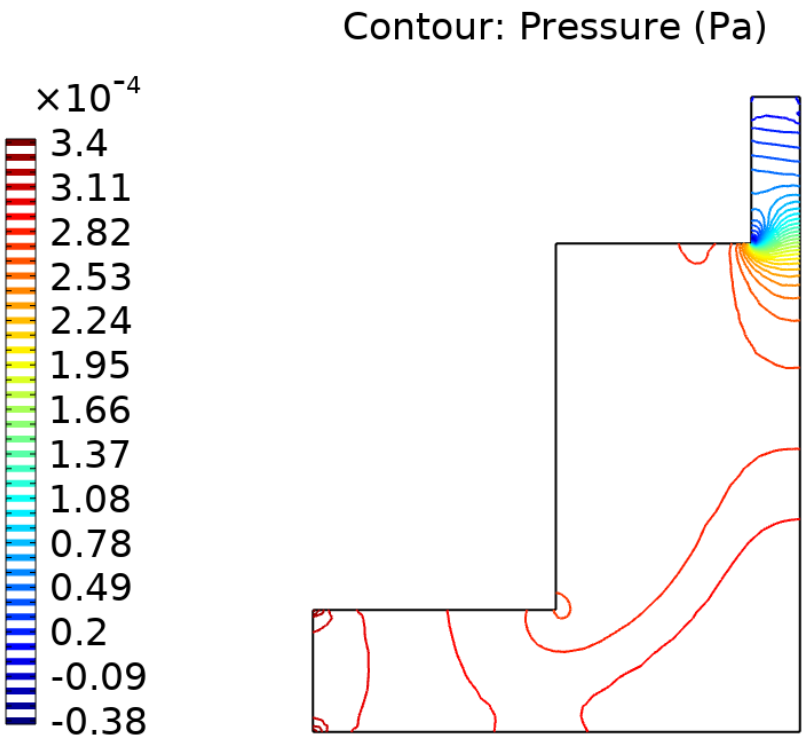

Figure III. 12.Contour pressure (Pa)

III.3.3.3 Surface Temperature (K)

The temperature distribution on the inner surfaces of the chamber is shown in this figure, with values expressed in Kelvin. The highest temperatures are concentrated in the lower left region, near the absorber plate, reaching up to500 K.

This area corresponds to the location of direct solar heat input, emphasizing effective energy absorption and heat generation.

A temperature gradient is evident as heat propagates upward, diminishing due to wall losses and vertical convection. The clear stratification of temperature indicates a strong natural convective current, essential for promoting air circulation and effective drying.

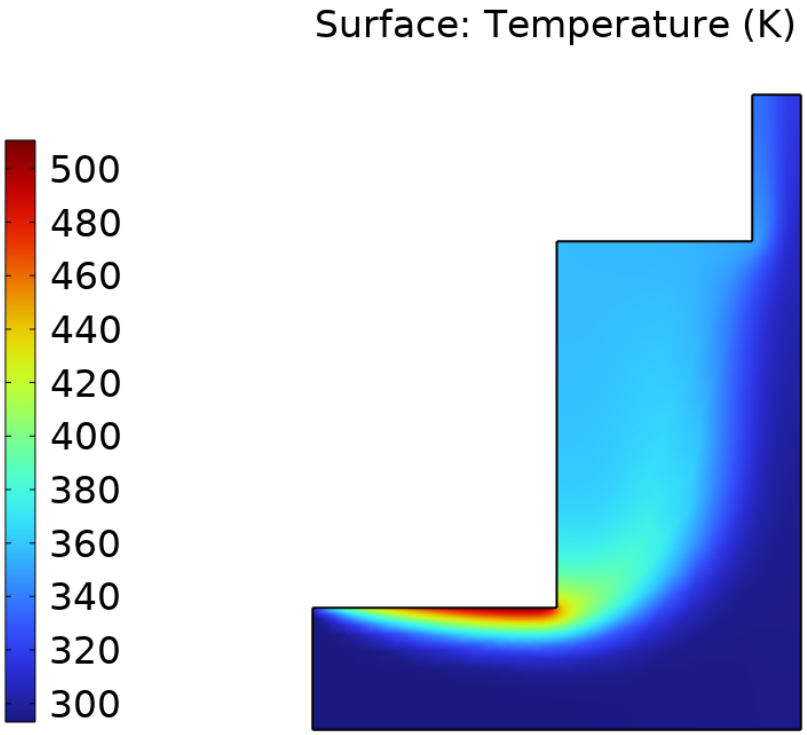

Figure III. 13.Surface Temperature (K)

III.3.3.4 Contour temperature (K)

This figure [III.14] displays temperature contour lines within the drying chamber, providing a detailed view of thermal stratification. The contours indicate that heat is primarily concentrated at the bottom and gradually dissipates toward the top.

Air temperatures near the absorber exceed 480 K, while the upper regions show reduced values around 320–350 K, reflecting the progressive cooling of the rising air. This thermal pattern not only confirms the efficiency of heat transfer but also highlights the need for uniform heat distribution to ensure consistent drying performance across different vertical sections

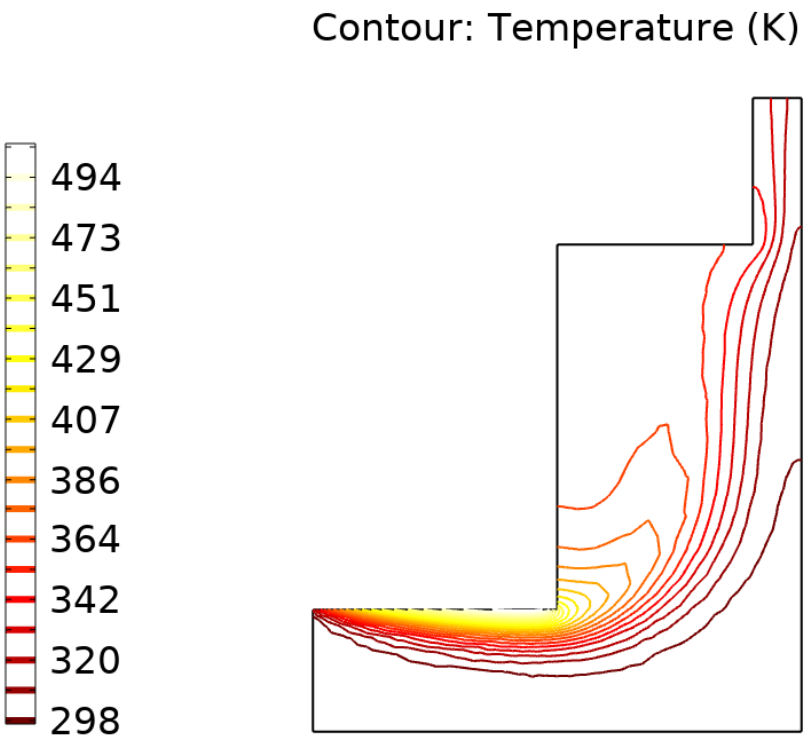

Figure III. 14.Contour temperature (K)

III.4 Study Three

III.4.1 impact of changing the chimney location

The chimney location was shifted to the far left of the geometric design to study the impact of this modification on airflow patterns and thermal distribution resulting from natural convection.

It is important to note that all boundary conditions adopted in the first study were preserved without any changes to ensure an accurate comparison between the two studies. These conditions include the heat flux applied to the absorber surface, the ambient air temperature, the physical properties of the air, as well as the implementation of the Laminar Flow model and the Heat Transfer in Fluid model.

This adjustment aims to analyze the system's sensitivity to minor geometric modifications by examining how the chimney's location affects:

- The effectiveness of the Chimney Effect in promoting natural ventilation.

- The temperature distribution inside the chamber.

- The stability and direction of the airflow.

- The uniformity of the drying process within the chamber

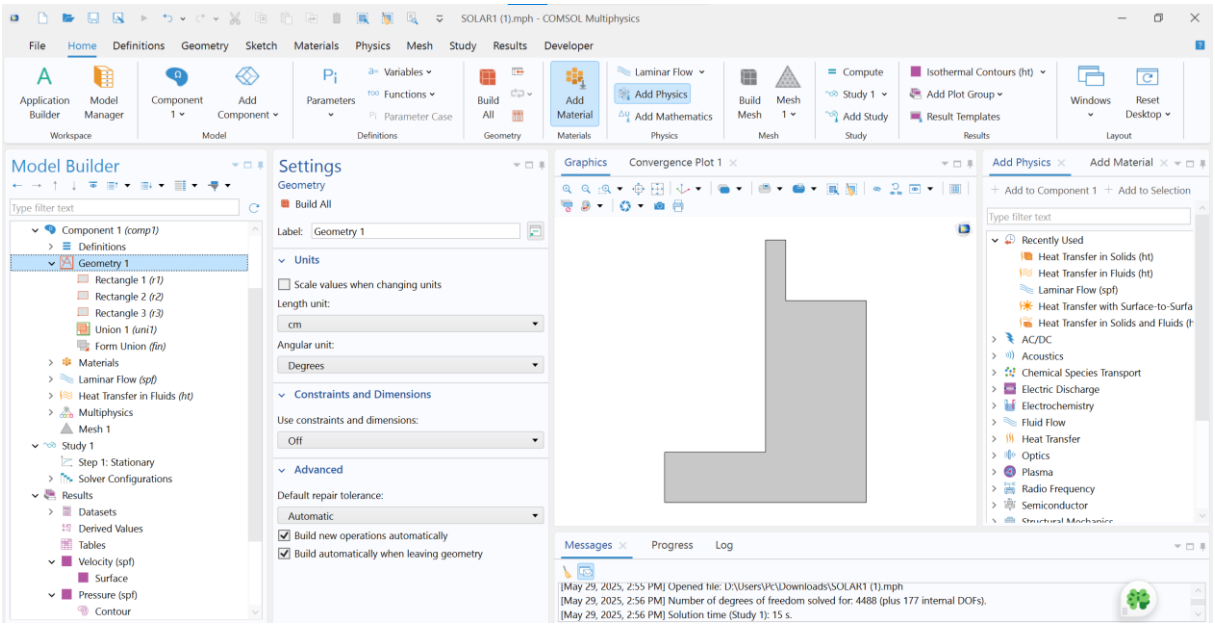

Figure III. 15.impact of changing the chimney location (left)

III.4.2 Meshing of changing the chimney location

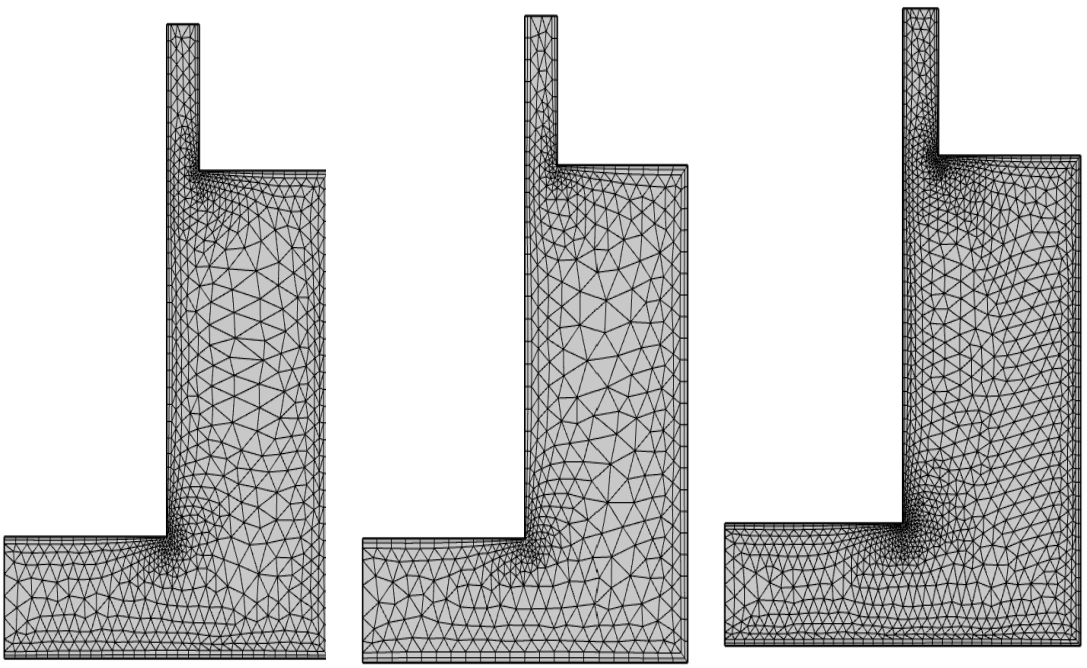

Normal mesh Coarse mesh Fine mesh

Figure III. 16.Meshing of changing the chimney location (left)

Table.III.3. Comparative mesh statistics for the chimney left

property	**Fine mesh**	**Normal mesh**	**Coarse mesh**
Mesh vertices	1680	1139	781
Triangles	2439	1535	981
Quads	358	288	224
Number of elements	2797	1823	1205
Minimum element quality	0.25	0.2524	0.2785
Average element quality	0.7844	0.7904	0.8136
Element area ratio	0.006596	0.004771	0.006731
Mesh area [cm^2]	6550	6550	6550

III.4.3 Results and discussion

III.4.3.1 Surface velocity magnitude (m/s)

This figure [III.17] displays the surface distribution of airflow velocity throughout the drying chamber. The highest velocity magnitudes, approximately , are located in the upper exit zone (chimney), confirming the existence of strong upward flow caused by buoyancy forces. The base of the chamber exhibits lower velocities, indicating that air gradually accelerates as it heats and rises. This velocity profile supports the self-sustaining ventilation mechanism and ensures continuous renewal of air, which is vital for removing evaporated moisture during the drying process.

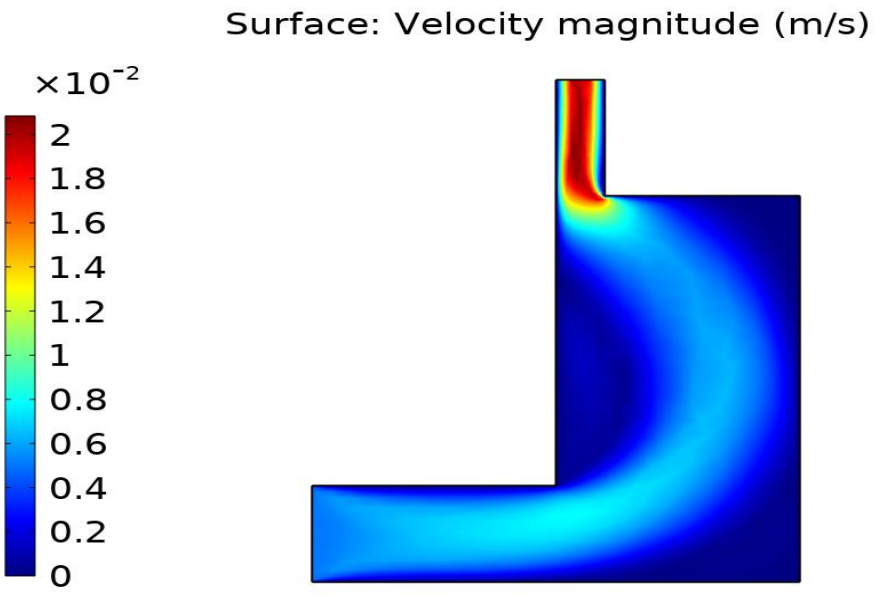

Figure III. 17.Surface velocity magnitude (m/s)

III.4.3.2 Contour Pressure (Pa)

The pressure distribution within the solar dryer is visualized using contour lines. The data reveals a maximum pressure of approximately near the upper exit region, and a minimum around near the bottom zone. This vertical pressure differential is crucial for inducing natural convection inside the dryer. The results confirm the presence of a buoyancy-driven flow, which supports the passive ventilation mechanism essential for effective moisture removal without external energy input.

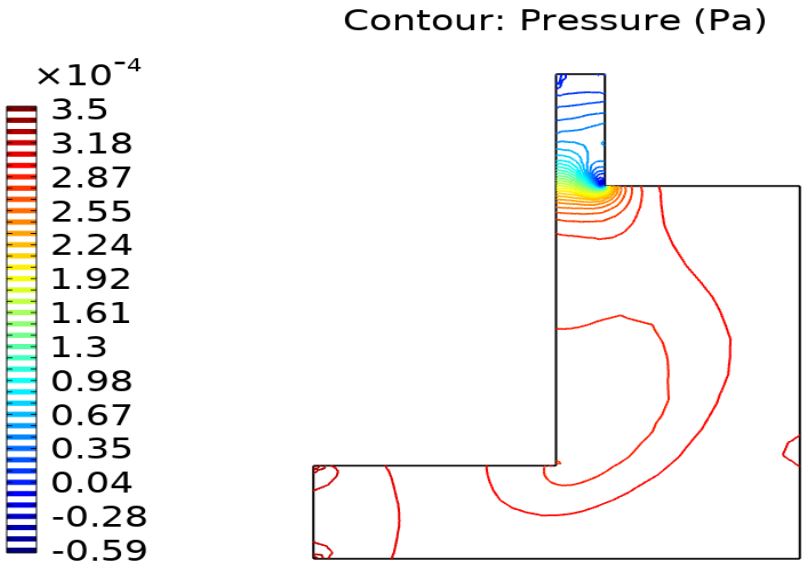

Figure III. 18.Contour pressure (Pa)

III.4.3.3 Surface temperature (K)

The surface temperature distribution indicates a strong concentration of thermal energy near the absorber area at the bottom of the chamber, with temperatures peaking around 500 K. The color scale clearly reflects the diminishing heat intensity with height, as the air loses energy due to convective transport and heat exchange with the surrounding structure. This surface visualization affirms that the system achieves efficient thermal energy capture and transmission into the drying air volume, essential for optimizing drying kinetics.

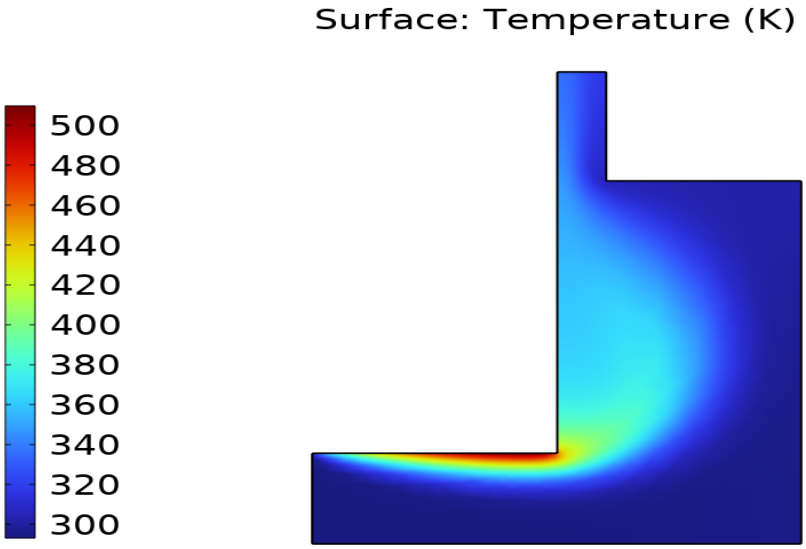

Figure III. 19.Surface temperature (K)

III.4.3.4 Contour Temperature (K)

This contour map of temperature reveals a clear gradient from the absorber plate upward through the chamber. Maximum temperatures are recorded close to the heat source, where values approach 494 K, gradually decreasing as the air rises. The thermal contours curve smoothly upward, reflecting a stable natural convection process. The temperature stratification confirms that the heated air moves effectively from the hot region to the exhaust, which is critical for promoting consistent drying performance across the drying zone.

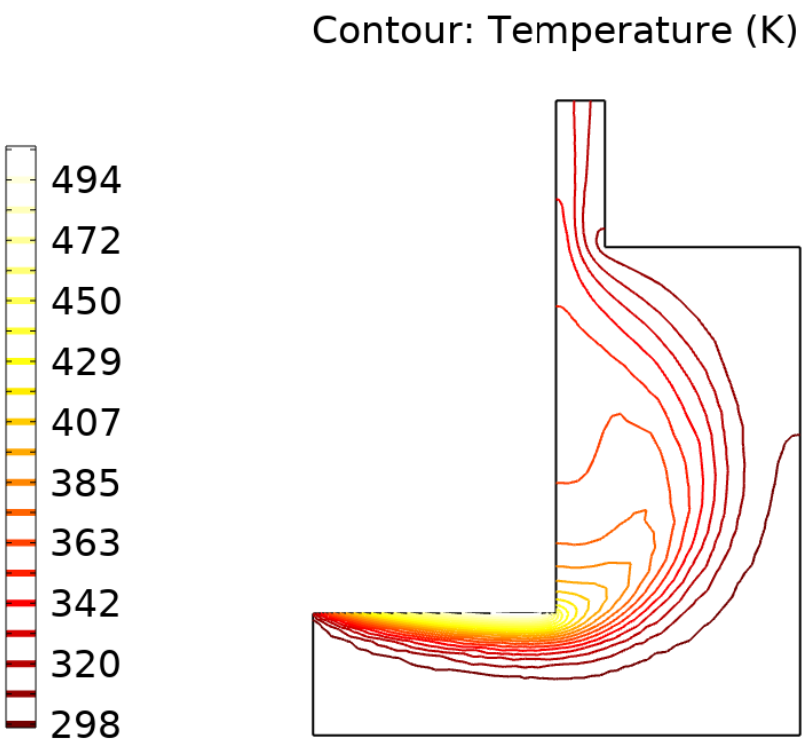

Figure III. 20.Contour Temperature (K)

III.5 Analysis of Results Based on Graphs

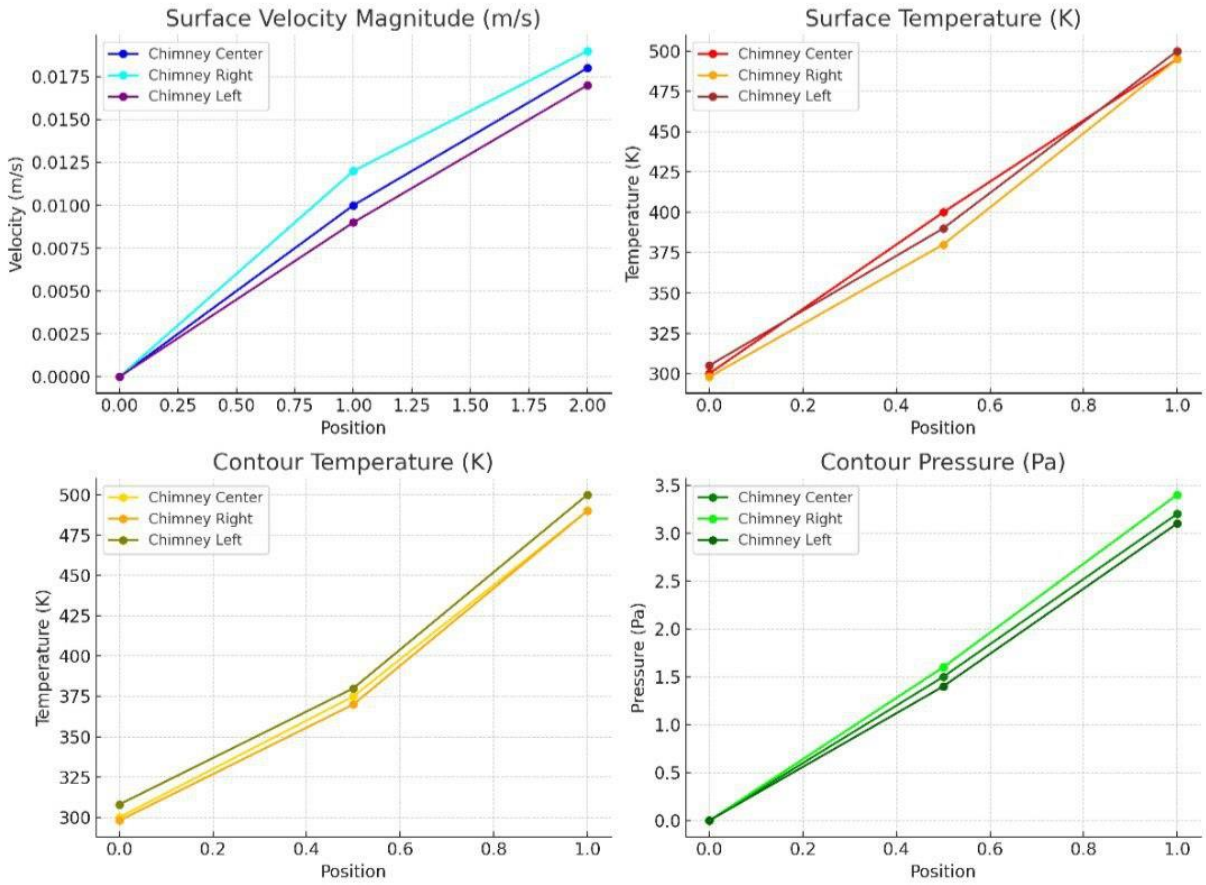

Figure III. 21. Impact of Chimney Location Changes Based on Graphs

III.5.1 Surface Velocity Magnitude (m/s):

- **Chimney Center:** The velocity increases progressively along the chamber, reaching its maximum near the outlet.
- **Chimney Right:** Velocity starts slightly lower at the inlet but rises sharply near the chimney, indicating flow redirection.
- **Chimney Left:** The velocity pattern is similar but slightly lower, possibly due to asymmetric flow behavior.

Interpretation: The chimney's position affects the velocity distribution. Center placement ensures balanced flow, while side positions cause directional acceleration towards the chimney.

III.5.2 Surface Temperature (K):

- **Chimney Center:** Temperature rises steadily, showing uniform heat distribution.
- **Chimney Right:** Initial temperatures are lower but increase near the outlet, indicating localized heating.
- **Chimney Left:** Follows a similar pattern, but with slightly lower peak values.

Interpretation: Central chimney placement promotes even thermal distribution, while lateral positions concentrate heat near the chimney, reducing uniformity.

III.5.3 Contour Temperature (K):

- **Chimney Center:** Displays a gradual and consistent thermal gradient.
- **Chimney Right and Left:** Show higher thermal accumulation near the chimney, especially in the outlet region.

Interpretation: Heat transfer is more stable with a centrally placed chimney. Lateral positions lead to uneven thermal behavior and possible hot spots near the outlet.

III.5.4 Contour Pressure (Pa):

- **Chimney Center**: Pressure distribution follows a linear gradient.
- **Chimney Right and Left:** Slight deviations with higher pressure peaks near the chimney suggest altered flow resistance.

Interpretation: Chimney location modifies the pressure field, affecting flow uniformity. Centered placement yields smoother gradients, while side placements cause asymmetric pressure zones.

III.6 Study four

III.6.1 Effect of the incidence angle of the absorber

In this section, we will study the impact of the absorber's incidence angle on the relationship between temperature, velocity,pressure,isothermal countours.

To achieve this, we have selected three angles

$$\boldsymbol{\theta = 0° \; and \; \theta = 30° \; and \; \theta = 45°}$$

It is important to note that all boundary conditions used in the first study were kept unchanged in laminar flow and heat transfer in fluid to ensure an accurate comparison between the studies.

First angle $\boldsymbol{\theta = 30°}$

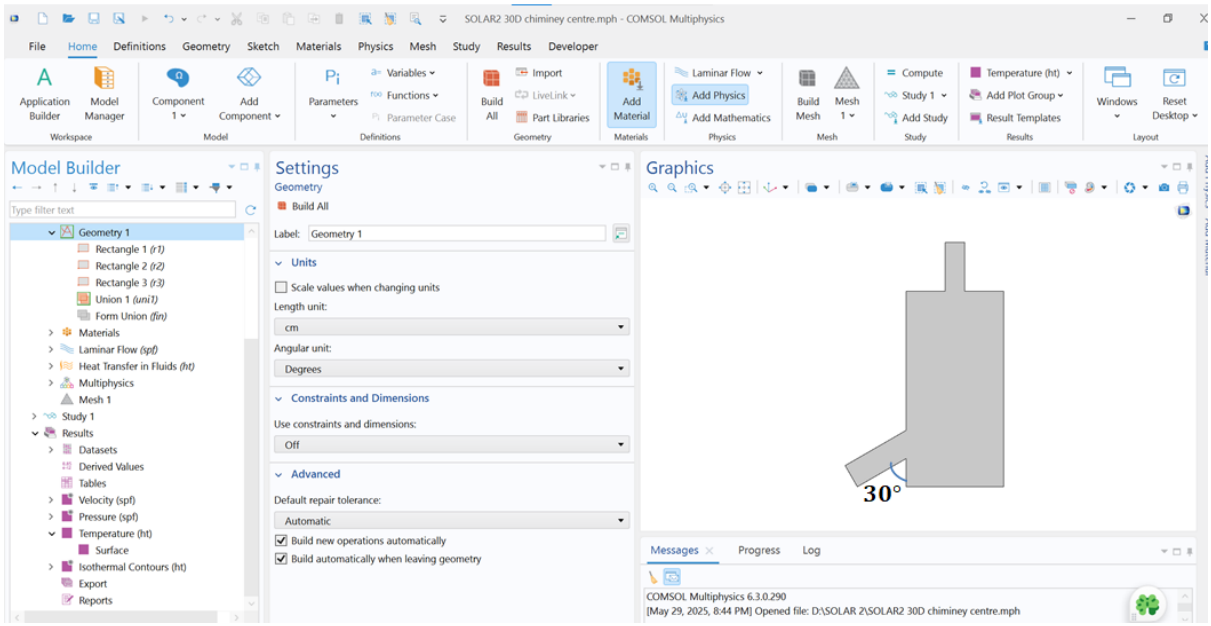

Figure III. 22.Effect of the initial incidence angle (θ = 30°)

III.6.2 Meshing

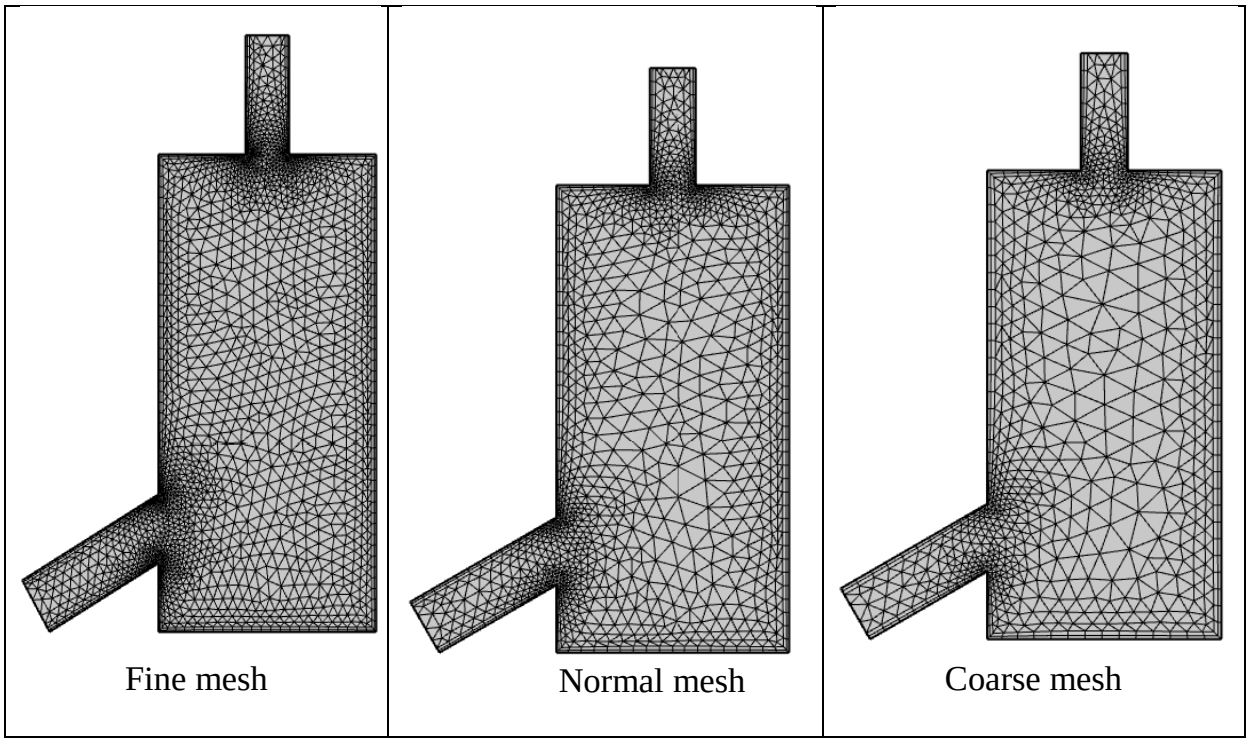

Figure III. 23.Mesh generation for the first angle (θ = 30°)

Table III.4. Comparison of mesh characteristics for the first angle (θ = 30°)

Description	**Fine mesh**	**Normal mesh**	**Coarse mesh**
Number of mesh vertices	2332	1502	1054
Triangular elements	3547	2128	1414
Quadrilateral elements	436	340	268
Edge elements	243	194	156
Vertex elements	12	12	12
Total number of elements	3983	2468	1682
Minimum element quality	0.2427	0.2573	0.2638
Average element quality	0.7976	0.7938	0.8033
Element area ratio	0.00709	0.003977	0.005438
Total mesh area $[cm^2]$	22620	22620	22620

III.6.3 Results and discussion

III.6.3.1 Surface velocity magnitude (m/s)

This figure shows the distribution of the velocity magnitude across the domain. The highest velocity is observed at the inlet region, especially at the nozzle or duct entrance, where the flow is injected. As the flow progresses inside the cavity, the velocity decreases significantly due to viscous effects and geometric constraints. The recirculation zones are clearly visible in the lower corners, indicating regions of low momentum and possible heat accumulation.

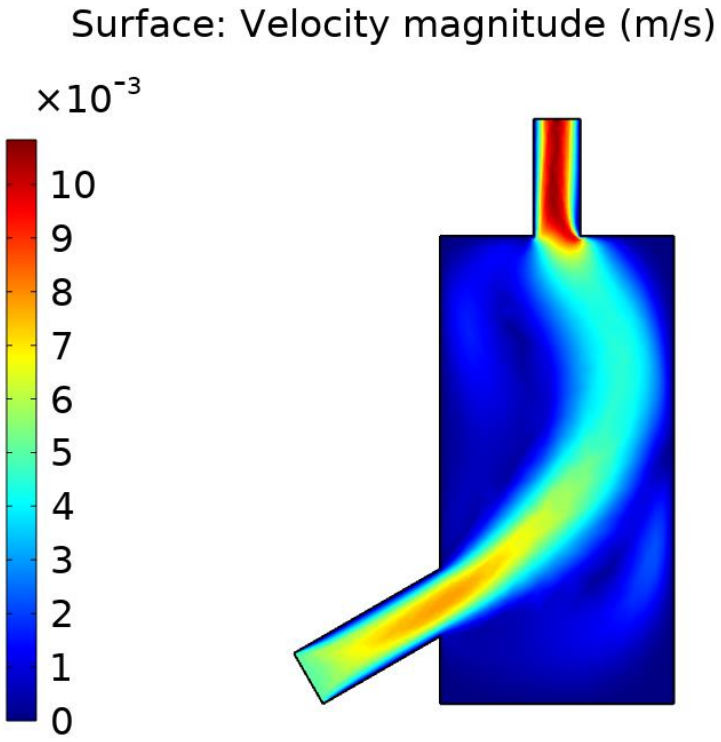

Figure III. 24.Surface velocity magnitude (m/s)

III.6.3.2 Contour Pressure (Pa)

The pressure contours reveal a high-pressure region near the inlet, gradually dropping toward the outlet. This pressure gradient drives the flow inside the chamber. Slight pressure variations inside the cavity indicate the influence of recirculation and stagnation points, which are critical for analyzing flow stability and mixing behavior.

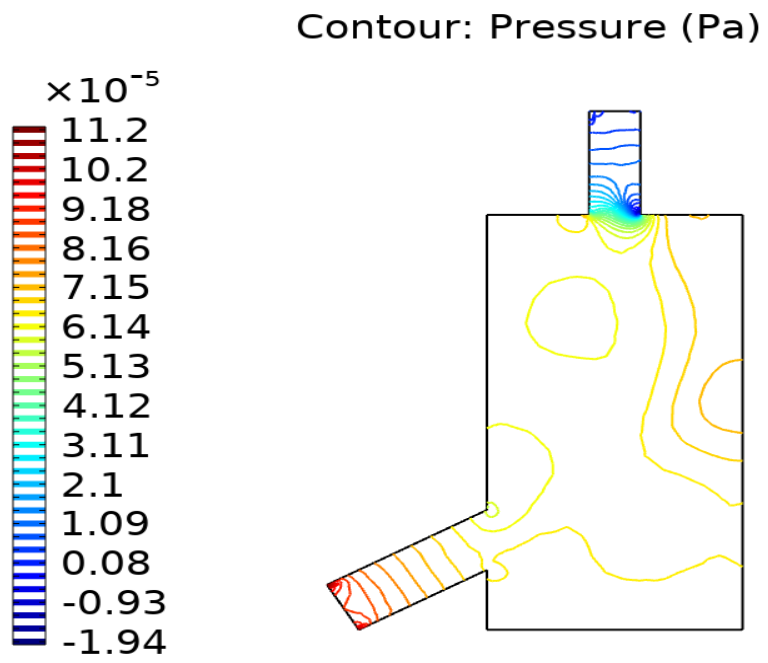

Figure III. 25.Contour Pressure (Pa)

III.6.3.3 Surface temperature (K)

The temperature field demonstrates a strong thermal gradient between the heated inlet and the rest of the domain. Maximum temperatures are concentrated around the duct entrance where hot air enters, gradually decreasing as it spreads throughout the chamber. The flow induces thermal stratification, with higher temperatures near the bottom and lower temperatures toward the upper outlet.

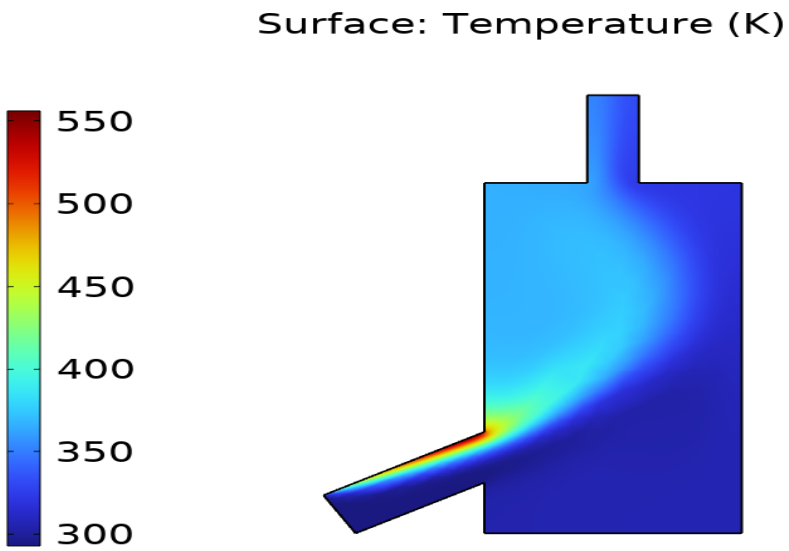

Figure III. 26.Surface temperature (K)

III.6.3.4 Contour Temperature (K)

The temperature contours provide more detail on heat distribution and stratification. The isothermal lines illustrate the flow of heat within the chamber, with a clear thermal boundary layer forming along the flow path. The temperature drop from the hot inlet to the surroundings is smooth, indicating good mixing and heat transfer efficiency, especially in zones with strong velocity gradients.

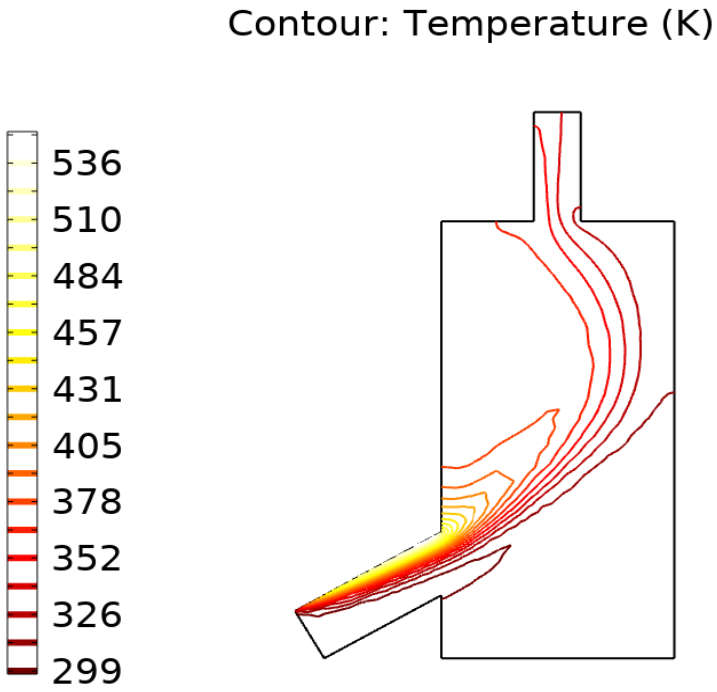

Figure III. 27.Contour Temperature (K)

III.7 Study five

Second angle $\theta = 45°$

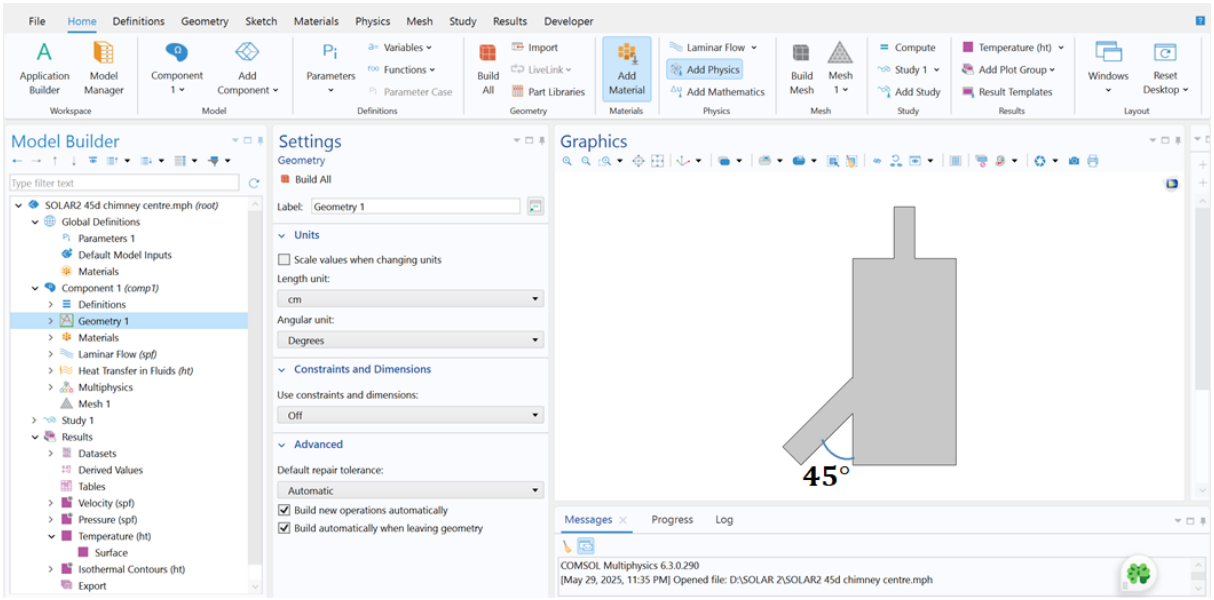

Figure III. 28.Effect of the incidence second angle θ=45°

III.7.1 Meshing

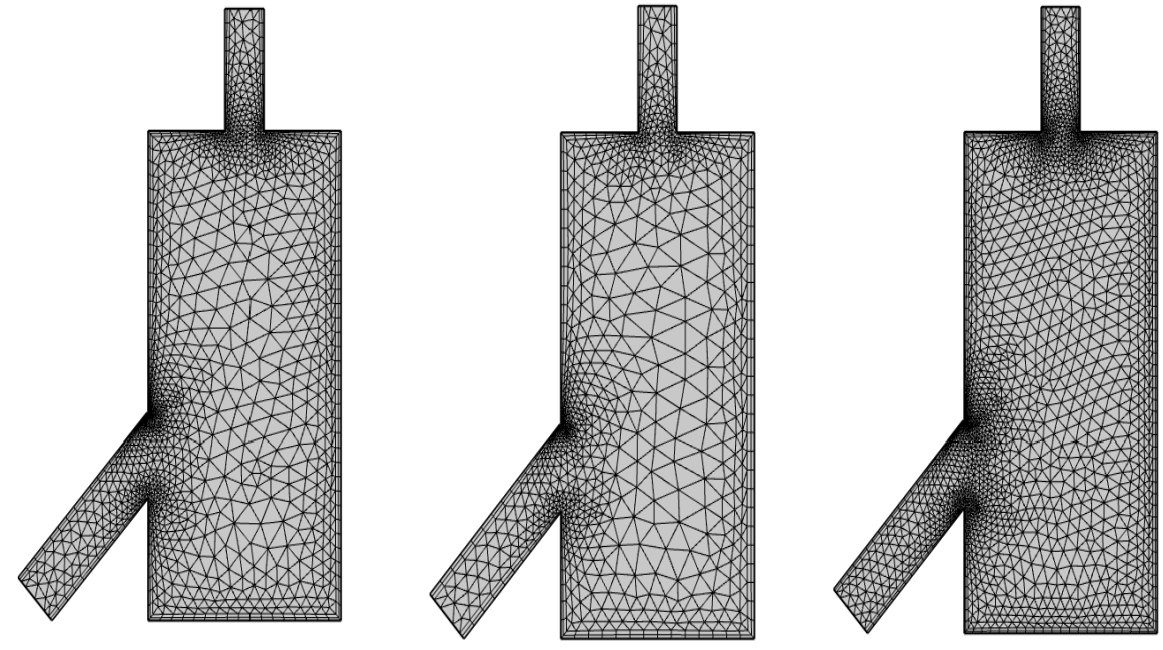

Normal mesh Coarse mesh Fine mesh

Figure III. 29.Mesh generation for the first angle (θ = 45°)

Table III.5. Comparison of mesh characteristics for the first angle (θ = 45°)

Description	**Normal mesh**	**Fine mesh**	**Coarse mesh**
Number of mesh vertices	1662	2456	1212
Triangular elements	2384	3750	1655
Quadrilateral elements	366	454	298
Edge elements	206	256	171
Vertex elements	13	13	13
Total number of elements	2750	4204	1953
Minimum element quality	0.2382	0.2208	0.2581
Average element quality	0.7894	0.7992	0.7842
Element area ratio	0.001086	0.002128	4.626e-4
Total mesh area $[cm^2]$	23080	23080	23080

III.7.2 Results and discussion

III.7.2.1 Surface velocity magnitude(m/s)

This figure shows the distribution of velocity across the domain. The highest velocities are observed at the inlet region, particularly at the nozzle or duct entrance where the flow is injected. As the flow progresses inside the cavity, the velocity decreases significantly due to viscous effects and geometric constraints. Recirculation zones are clearly visible in the lower corners, indicating regions of low momentum and potential heat accumulation.

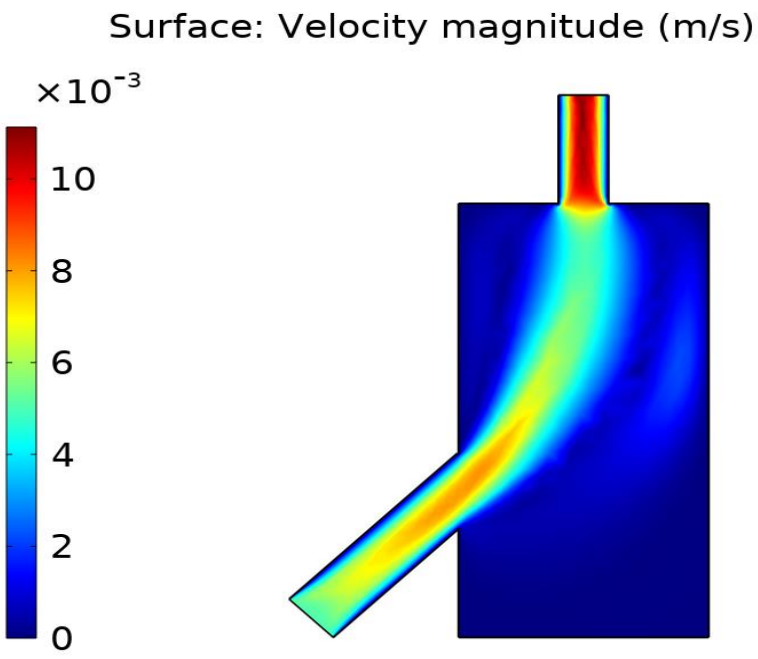

Figure III. 30.Surface velocity magnitude(m/s)

III.7.2.2 Contour Pressure (Pa)

The pressure contours indicate a high-pressure region near the inlet, which gradually decreases toward the outlet. This pressure gradient acts as the driving force for the flow within the chamber. Minor pressure variations inside the cavity highlight the effects of recirculation and stagnation points, which are crucial for analyzing flow stability and mixing behavior.

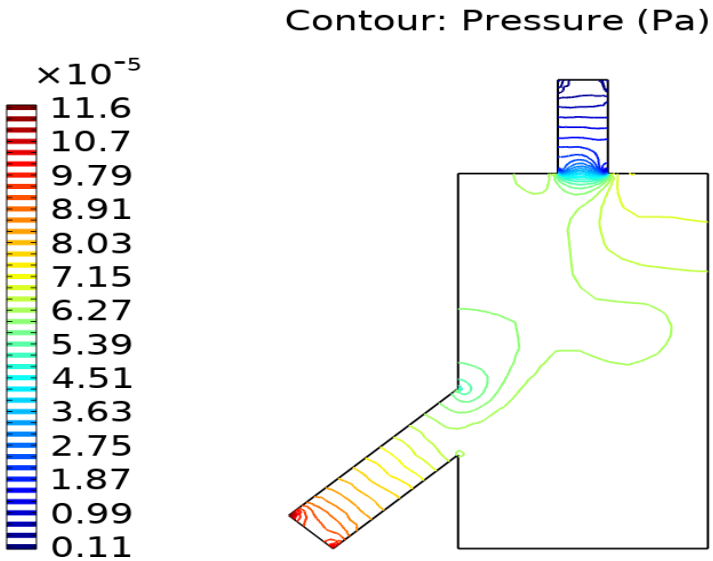

Figure III. 31.Contour Pressure (Pa)

III.7.2.3 Surface Temperature (K)

The temperature field reveals a strong thermal gradient between the heated inlet and the rest of the domain. The maximum temperatures are concentrated around the duct entrance where the hot air is introduced, gradually decreasing as the heat spreads throughout the chamber. The flow induces thermal stratification, with higher temperatures near the bottom and lower temperatures toward the upper outlet.

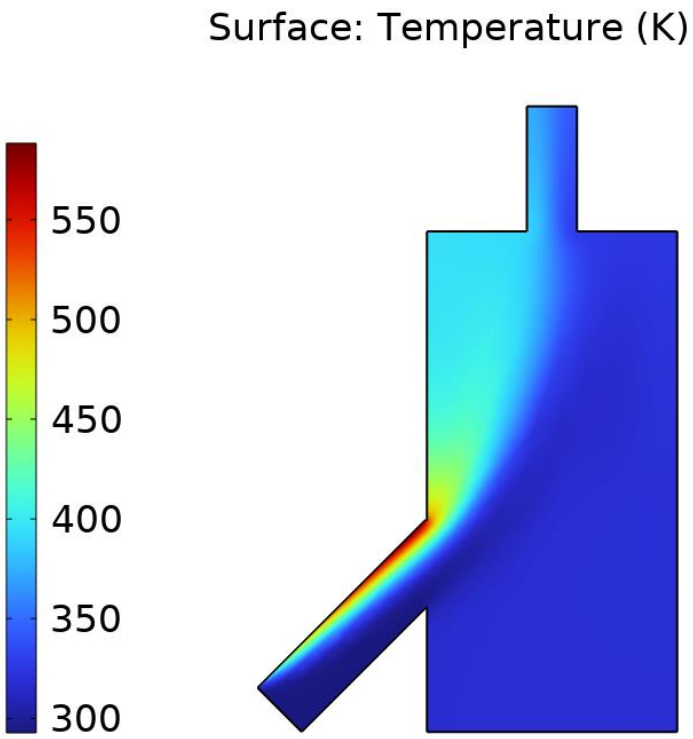

Figure III. 32.Surface Temperature (K)

III.7.2.4 Contour temperature (K)

The temperature contours provide more detailed insights into heat distribution and stratification. The isothermal lines illustrate the heat flow within the chamber, with a clear thermal boundary layer forming along the flow path. The temperature drop from the hot inlet to the surrounding regions is smooth, indicating effective mixing and efficient heat transfer, especially in zones with strong velocity gradients.

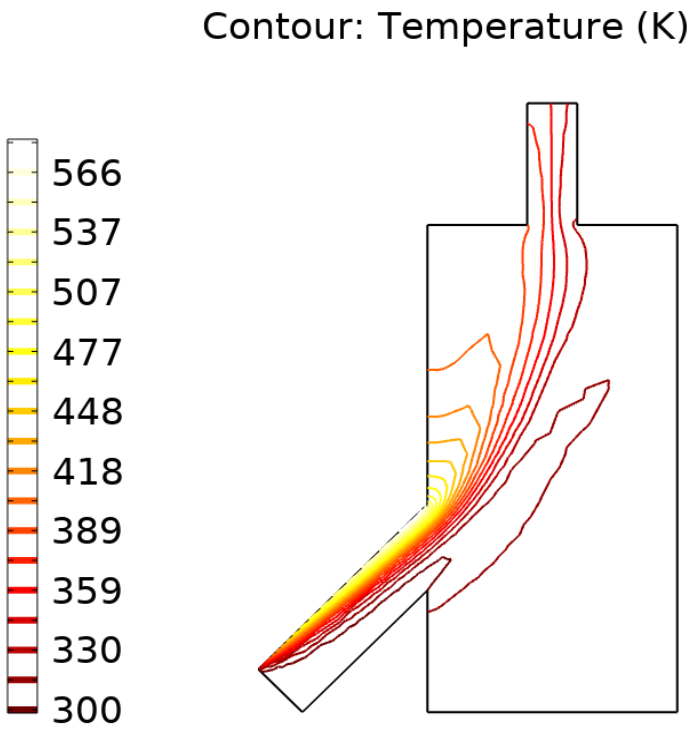

Figure III. 33.Contour temperature (K)

III.8 Analysis of Results Based on Graphs

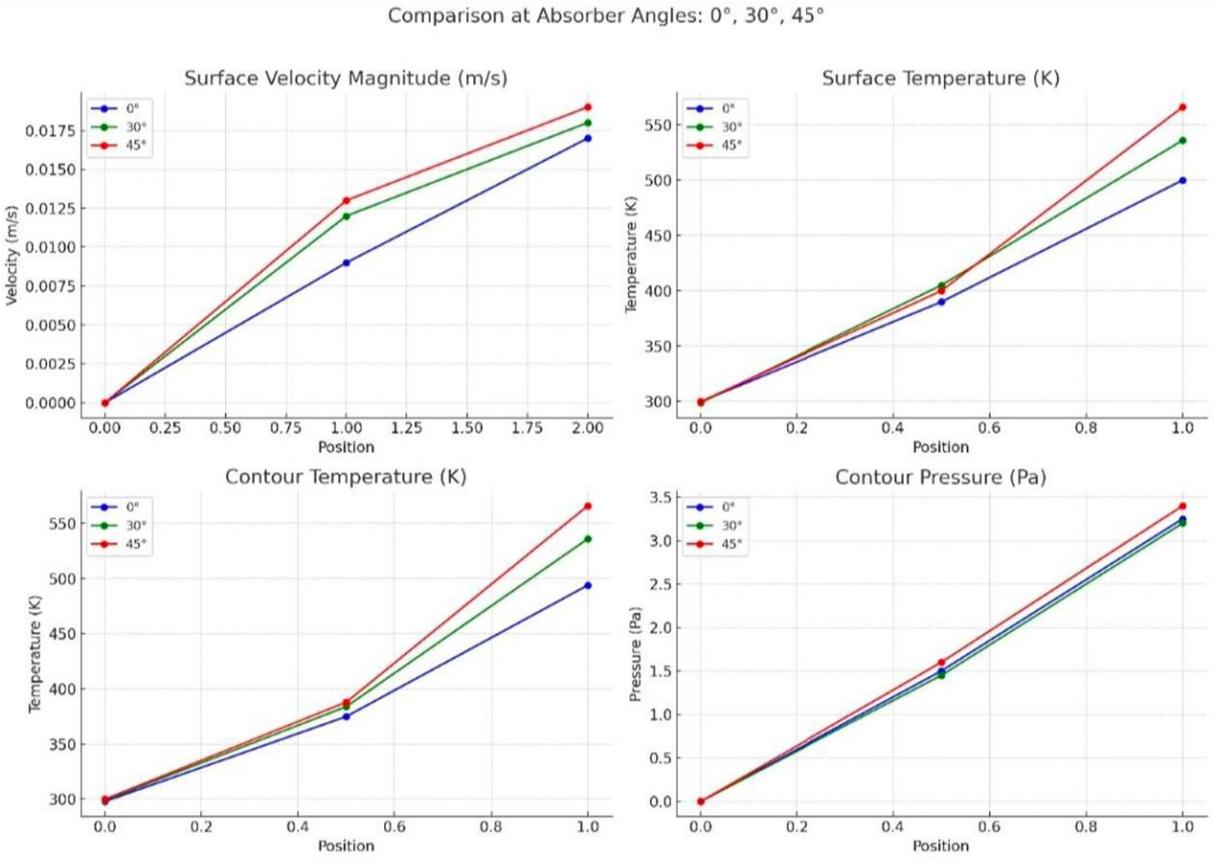

Figure III. 34. Effect of Angle Variation Based on Graphs

III.8.1 Surface Velocity Magnitude (m/s)

- Angle 0°:

Lowest velocity value.

The flow is relatively straight, with weak guidance into the chamber.

There is poor air mixing and limited acceleration.

- Angle 30°:

The velocity begins to increase, indicating improved air entry and better curved flow formation.

The 30° inclined duct helps enhance airflow toward the hot zone.

- Angle 45°:

Highest velocity value.

The increased duct angle accelerates the airflow and reduces losses at the chamber inlet.

The flow enters in a slanted and streamlined manner, enhancing mixing.

III.8.2 Surface Temperature (K)

- Angle 0°:

Low surface temperature (~300 K to 440 K).

This reflects inefficient heat entry and poor surface heat distribution.

- Angle 30°:

Clear improvement in surface temperature (~300 K to 480 K).

Better thermal distribution and higher heat absorption.

- Angle 45°:

Highest surface temperature (~500 K).

Faster airflow at this angle enhances heat transfer to the surfaces.

III.8.3 Contour Temperature (K)

- Angle 0°:

Low and bottom-concentrated heat distribution.

Significant weakness in heat spread.

- Angle 30°:

Noticeable improvement, with higher temperature along the flow path.

Indicates the formation of a thermal layer with moving air.

- Angle 45°:

Excellent thermal distribution covering most of the space.

A balance is achieved between flow and heat within the system.

III.8.4 Contour Pressure (Pa)

- Angle 0°:

Relatively low pressure (~2.7×10^{-4} Pa).

Low resistance due to straight inlet flow.

- Angle 30°:

Pressure increases (~6×10^{-5} Pa).

Indicates changes in flow behavior and curvature.

- Angle 45°:

Highest pressure (~1.2×10^{-5} Pa).

Stronger flow creates higher resistance.

III.9 Study six

III.9.1 Effect of changing the heat flux value on the results

In this section, we will study the effect of varying the heat flux value on the relationship between temperature, velocity, pressure, and isothermal contours. The selected flux values are 150, 200, 250, and 300 W/m², noting that the 100 W/m² case was already examined in the initial study.

It is important to emphasize that all boundary conditions used in the first study were kept unchanged in both the Laminar Flow and Heat Transfer in Fluids interfaces to ensure an accurate and consistent comparison between the simulations.

III.9.1.1 Surface velocity magnitude(m/s)

- **Flux(2) = 150 W/m²**

At this heat flux, the velocity magnitude distribution indicates moderate flow intensity. The velocity is higher near the inlet, gradually decreasing as the flow moves toward the cavity's interior. The flow is relatively stable with less noticeable recirculation zones due to the lower thermal driving forces.

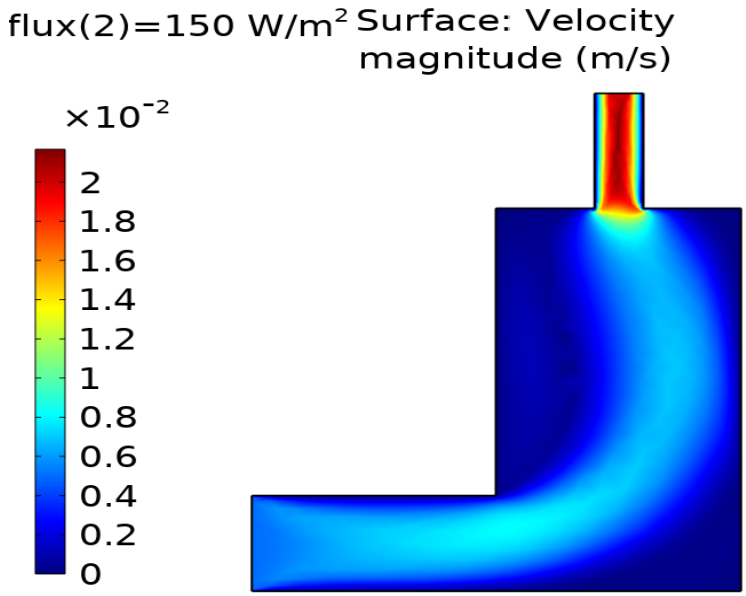

Figure III. 35.Flux(2) = 150 W/m² Surface velocity magnitude (m/s)

❖ **Flux(3) = 200 W/m²**

With an increased heat flux, the flow becomes more intense. The velocity magnitude near the inlet rises slightly, and the contours expand further into the cavity, reflecting enhanced thermal gradients. Recirculation zones begin to form more prominently, indicating a stronger influence of thermal buoyancy on the flow behavior

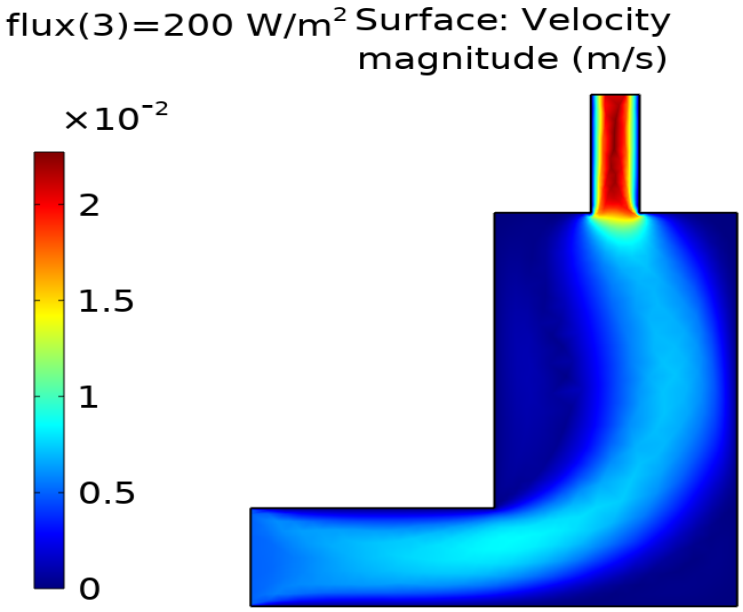

Figure III. 36.Flux(2) = 200 W/m² Surface velocity magnitude (m/s)

❖ **Flux(4) = 250 W/m²**

At this level, the velocity magnitude continues to increase. The higher heat flux drives stronger buoyant forces, amplifying the flow intensity. Recirculation zones grow further, with noticeable mixing patterns. The thermal effects are now more dominant, causing a clear distinction in flow dynamics.

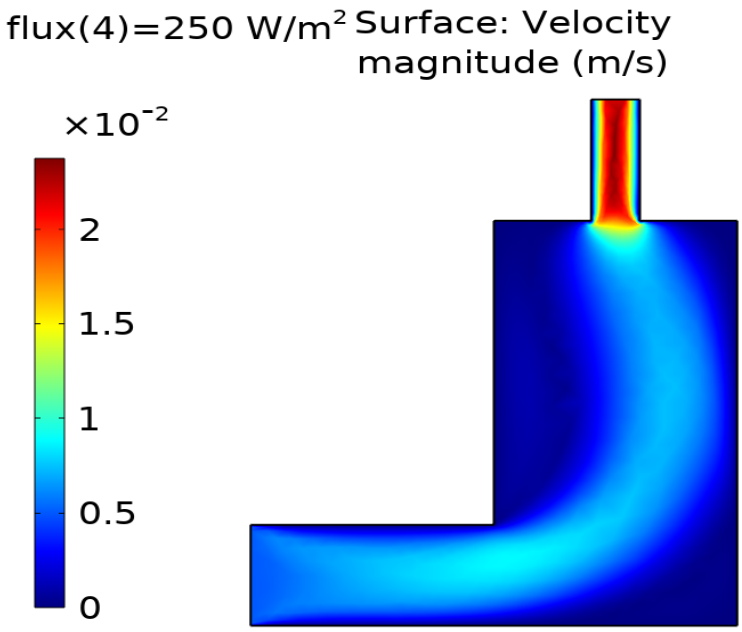

Figure III. 37.Flux(4) = 250W/m² Surface velocity magnitude (m/s)

❖ **Flux(5) = 300 W/m²**

With the highest flux value, the velocity magnitude is at its maximum near the inlet. The entire flow field becomes more dynamic, with larger and more vigorous recirculation zones. This signifies that the system is reaching its thermal-driven flow limits, where buoyancy forces dominate the overall flow pattern.

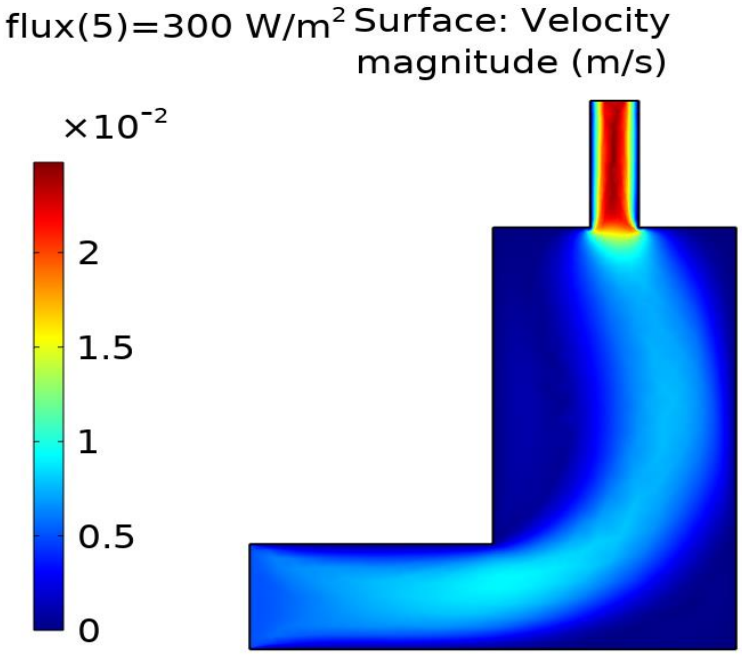

Figure III. 38.Flux(5) = 300W/m² Surface velocity magnitude (m/s)

III.9.1.2 Contour Pressure (Pa)

❖ **Flux(2) = 150 W/m²**

The pressure distribution shows regions of high pressure near the inlet, where the airflow is more active. The pressure gradually decreases throughout the cavity due to kinetic energy losses and flow diffusion. Minor pressure variations are observed, reflecting the relatively weak thermal forces at this flux level.

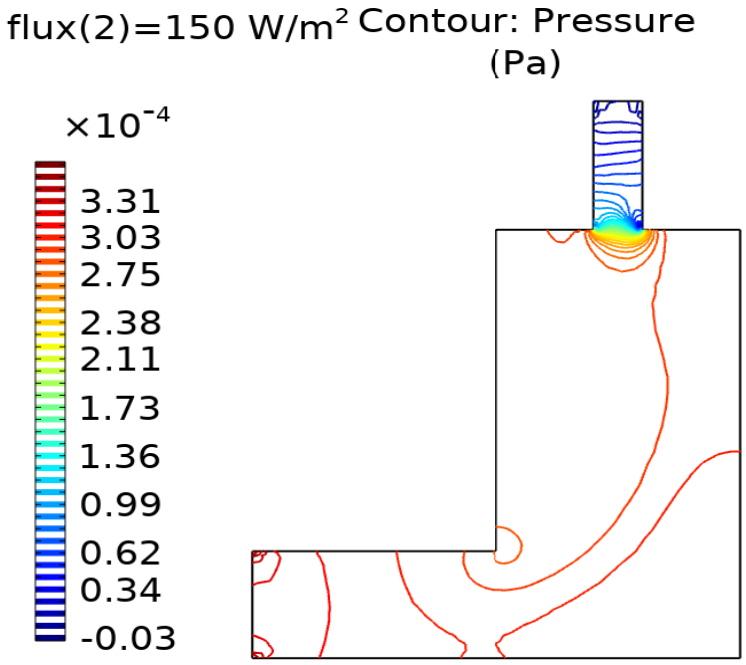

Figure III. 39.Flux(2) = 150W/m² Contour Pressure (Pa)

❖ **Flux(3) = 200 W/m²**

With an increase in heat flux, the pressure gradients become more prominent. High-pressure regions near the inlet become more pronounced, indicating stronger thermal effects. Slight variations in pressure within the cavity reflect enhanced flow mixing and thermal interactions.

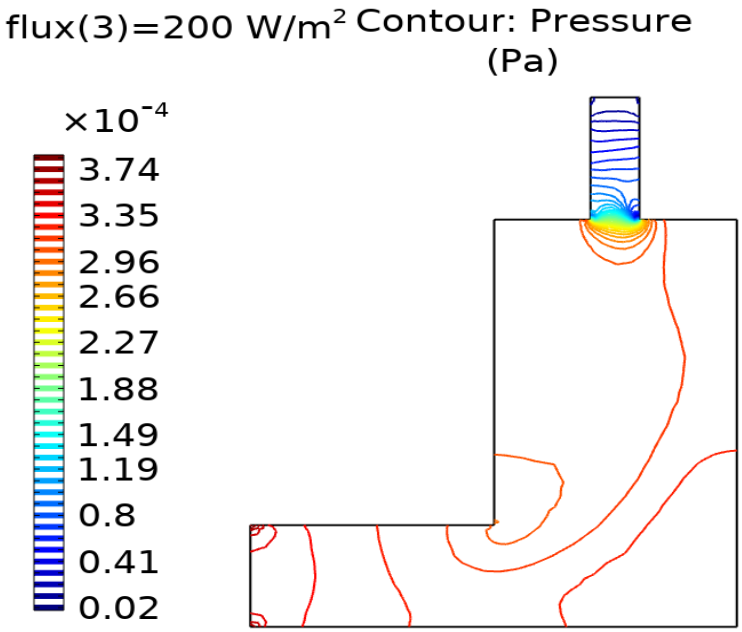

Figure III. 40.Flux(3) = 200W/m² Contour Pressure (Pa)

❖ **Flux(4) = 250 W/m²**

At this heat flux, the pressure distribution becomes more dynamic. The stronger thermal gradients result in higher pressure near the inlet, with a gradual decrease further into the cavity. This highlights the increased influence of buoyancy forces on the flow dynamics.

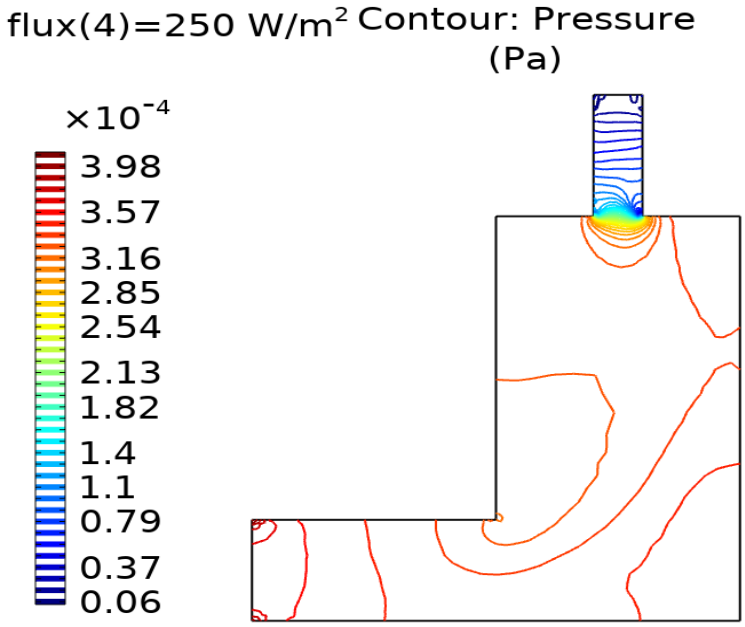

Figure III. 41.Flux(4) = 250 W/m² Contour Pressure (Pa)

❖ **Flux(5) = 300 W/m²**

At the highest heat flux, the pressure near the inlet reaches its maximum, indicating significant thermal influence. Notable pressure variations within the cavity suggest a more turbulent flow and effective mixing driven by the intensified thermal forces.

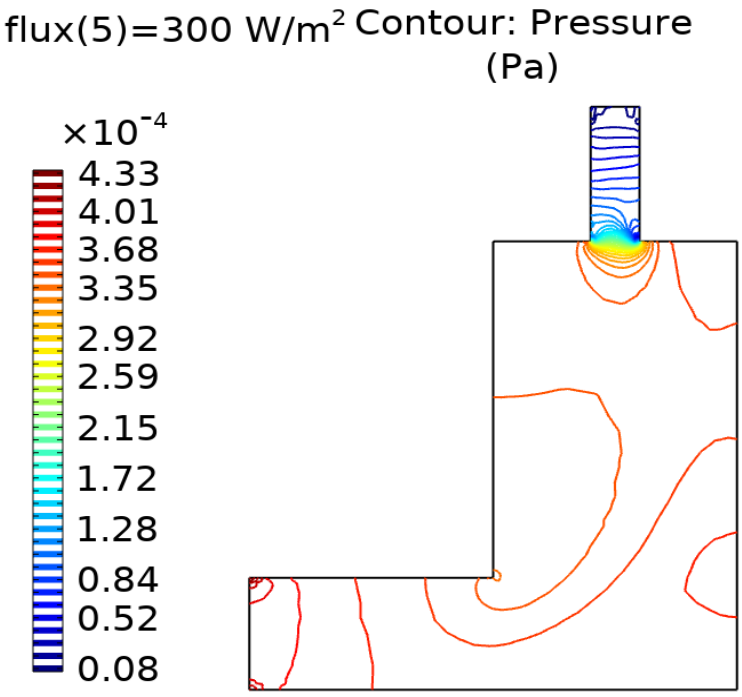

Figure III. 42.Flux(5) = 300W/m² Contour Pressure (Pa)

III.9.1.3 Surface Temperature (K)

❖ **Flux(2) = 150 W/m²**

The temperature distribution shows a moderate heat transfer at this stage, with heat concentrated near the upper surface exposed to radiation. The heat gradually diffuses into the internal cavity, but the overall heating effect remains limited due to the low heat flux intensity. Most inner regions stay at relatively low temperatures.

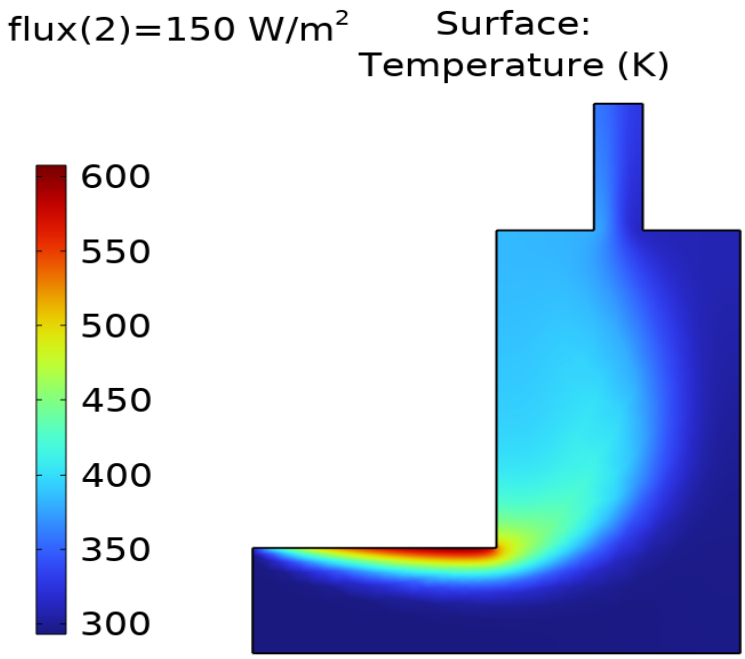

Figure III. 43.Flux(2) = 150 W/m² Surface Temperature (K)

❖ **Flux(3) = 200 W/m²**

As the heat flux increases, hotter regions become more distinct and widespread, especially near the heat source. More effective heat transfer is observed towards the interior, with a noticeable rise in temperature across wider areas. This indicates improved thermal conduction and a stronger radiative effect within the system.

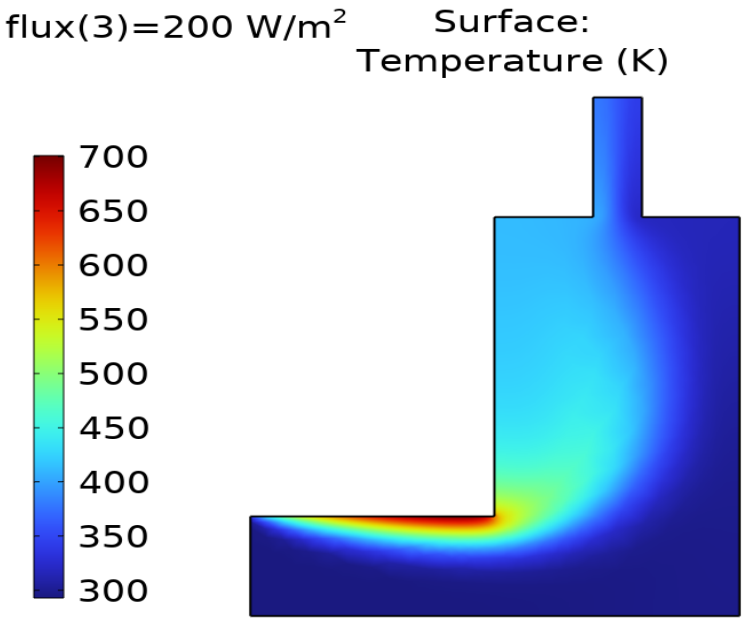

Figure III. 44.Flux(3) = 200 W/m² Surface temperature (K)

❖ **Flux(4) = 250 W/m²**

At this flux level, high-temperature regions expand and penetrate deeper into the cavity. The influence of radiation becomes more pronounced, resulting in a more uniform thermal distribution. The middle and lower zones of the dryer experience a clear temperature increase, enhancing drying conditions.

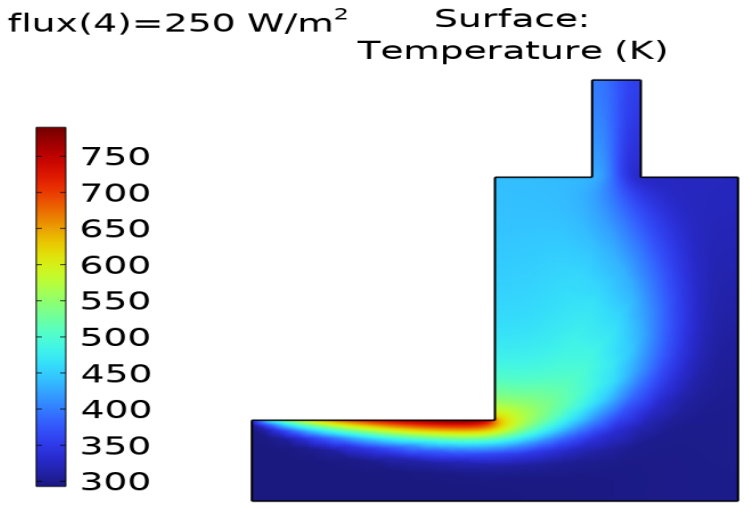

Figure III. 45.Flux(4) = 250 W/m² Surface Temperature (K)

❖ **Flux(5) = 300 W/m²**

At the highest heat flux, the heating effect reaches its peak, with elevated temperatures observed throughout most of the cavity. Strong thermal gradients are present, indicating highly effective heat transfer. The radiative effect spreads across the entire system, significantly improving drying performance and energy utilization.

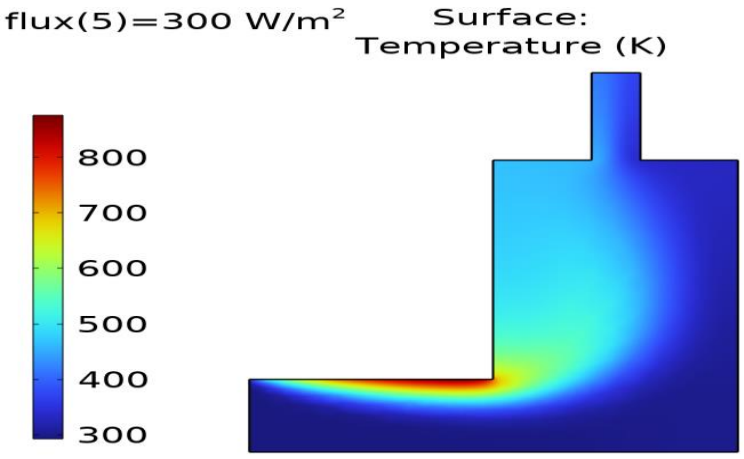

Figure III. 46.Flux(5) = 300 W/m² Surface Temperature (K)

III.9.1.4 Contour temperature (K)

❖ **Flux(2) = 150 W/m²**

The isothermal contours are mostly concentrated near the lower heated surface, with tight and closely spaced lines indicating a sharp temperature gradient. The heat does not penetrate deeply into the cavity, reflecting limited thermal diffusion and weaker buoyancy forces.

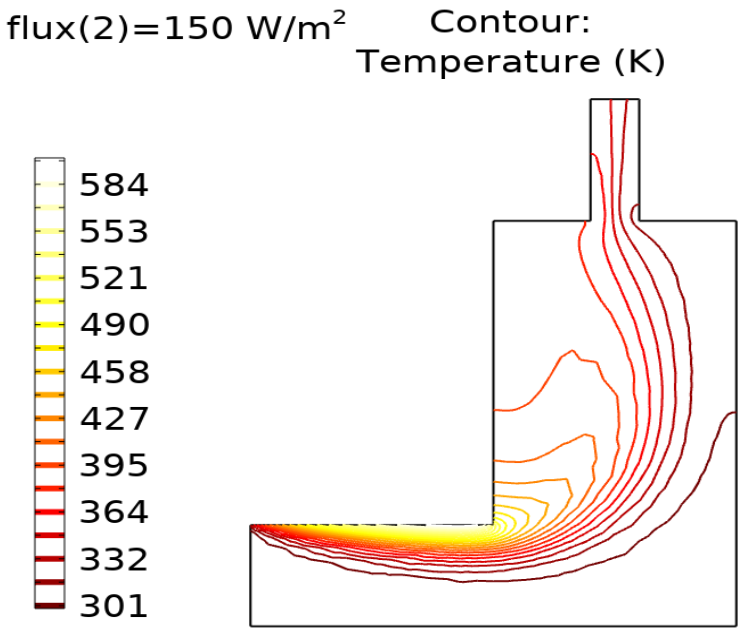

Figure III. 47.Flux(2) = 150 W/m² contour temperature (K)

❖ **Flux(3) = 200 W/m²**

As the heat flux increases, the contours become more extended and begin to curve upwards, illustrating enhanced thermal penetration. The thermal boundary layer becomes thicker, and the internal heat distribution becomes more apparent, indicating more effective convective flow.

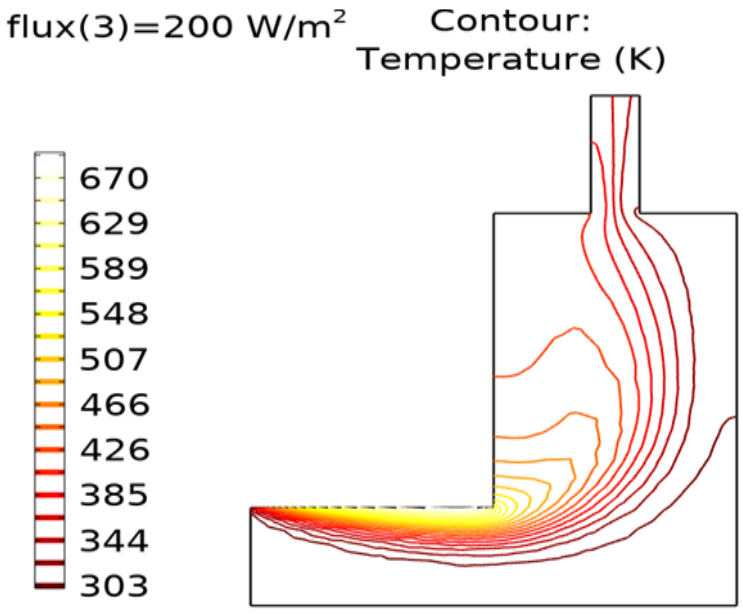

Figure III. 48.Flux(3) = 200 W/m² contour temperature (K)

❖ **Flux(4) = 250 W/m²**

At this level, the isothermal lines are more spread out and reach higher regions of the cavity. The contours show a smoother temperature gradient and stronger vertical motion of heated air. This implies a more dominant natural convection process and improved mixing of hot and cold air masses.

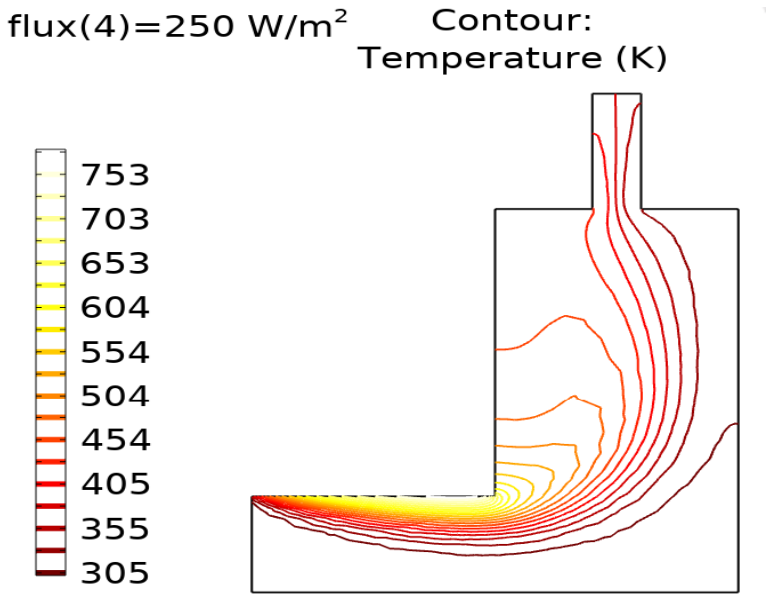

Figure III. 49.Flux(4) = 250 W/m² contour temperature (K)

❖ **Flux(5) = 300 W/m²**

The contours at the highest flux value demonstrate the most significant temperature spread and curvature, reaching the upper outlet. The cavity experiences intense heat transfer, and the spacing between the contours indicates efficient energy distribution. Strong buoyancy-driven circulation is evident, enhancing thermal performance throughout the cavity.

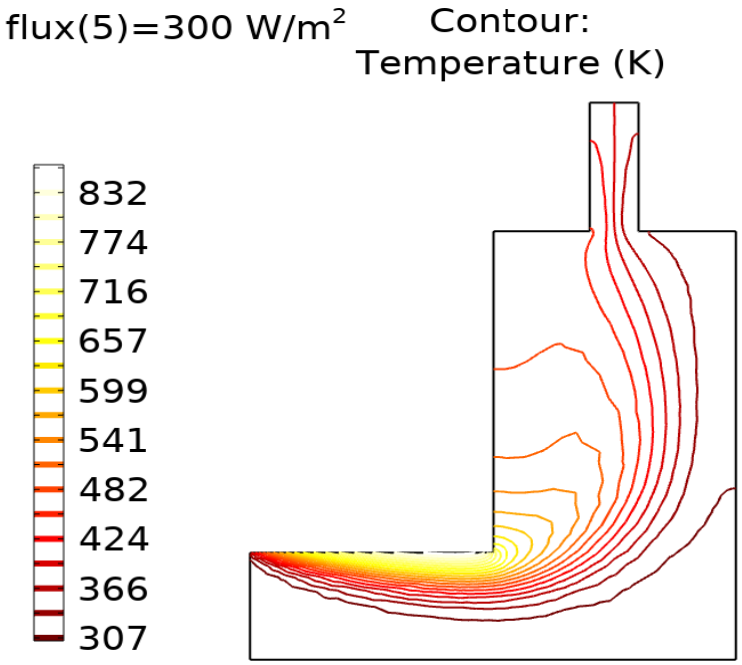

Figure III. 50.Flux(4) = 300 W/m² contour temperature (K)

III.10 Analysis of Results Based on Graphs

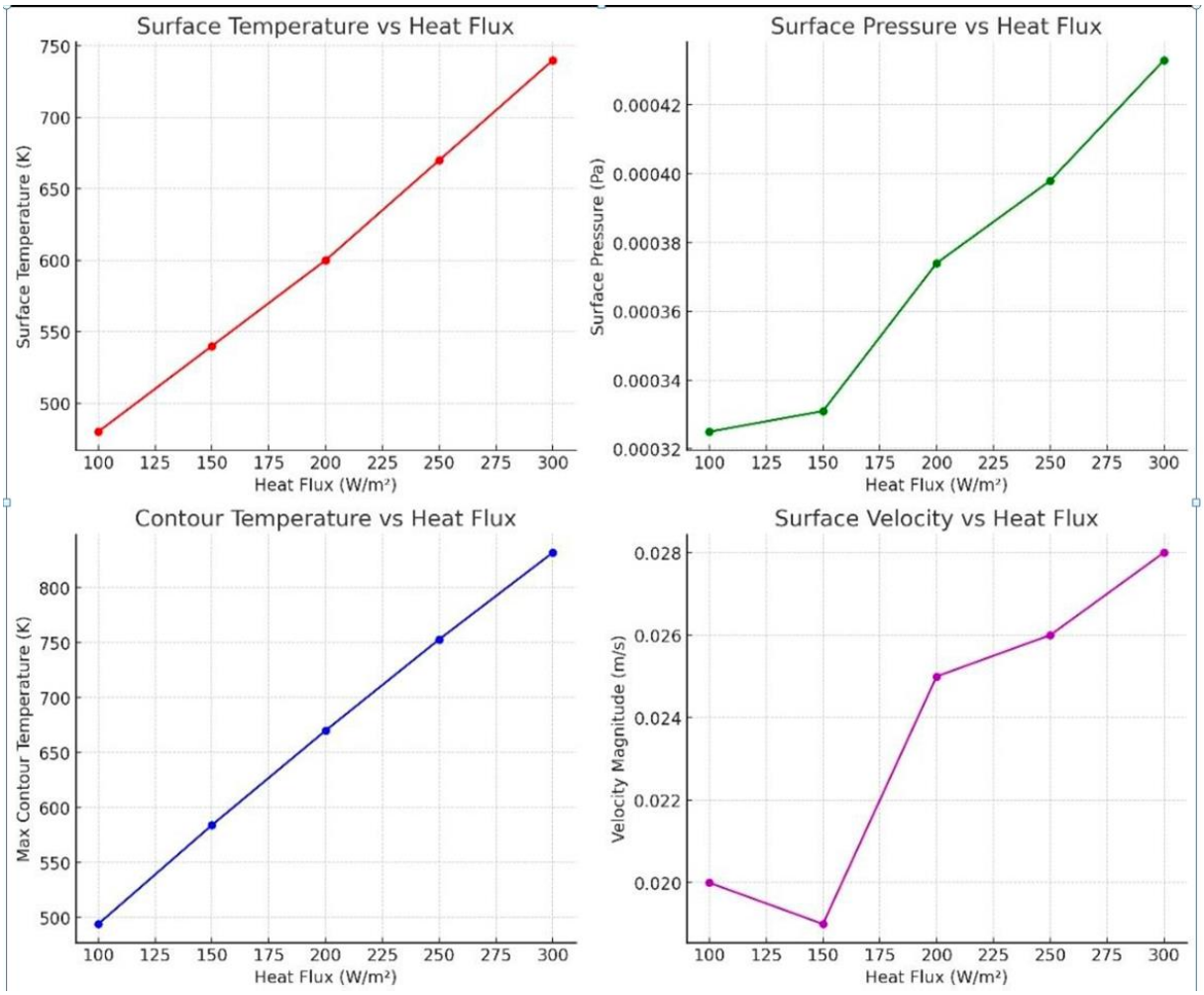

Figure III. 50.Effect of Heat Flow Variation Based on Graphs

III.10.1 Surface Temperature vs Heat Flux

- Observation: The surface temperature clearly increases as the heat flux increases.
- Interpretation: When the heat flux applied to the surface increases, more thermal energy is supplied, which raises the surface temperature of the body.
- Behavior: Approximately linear, with a tendency to rise faster at higher heat flux values.

III.10.2 Surface Pressure vs Heat Flux

- Observation: The surface pressure increases proportionally with the heat flux, but the rise is relatively slight.

- Interpretation: As temperature increases, the gas expands and its pressure rises. However, since this is likely a nanoscale or low-pressure system (possibly plasma), the pressure increase remains small.
- Behavior: Slowly increasing curve.

III.10.3 Max Contour Temperature vs Heat Flux

- Observation: The maximum temperature within the domain (not just on the surface) increases with the heat flux, at a nearly consistent rate.
- Interpretation: More heat flux means more overall heating in the thermal field, causing the maximum internal temperature to rise accordingly.
- Behavior: Nearly linear relationship.

III.10.4 Surface Velocity Magnitude vs Heat Flux

- Observation: Surface velocity increases as the heat flux increases, though there is a slight drop at 150 W/m^2.
- Interpretation: Higher temperatures result in differences in density and pressure, which enhance buoyancy and natural convection forces—leading to increased fluid flow. The slight dip at 150 W/m^2 may indicate a transitional behavior in flow dynamics.
- Behavior: Generally increasing after a small dip—indicating a transitional thermal flow behavior.

General Conclusion

1. Performance and Design Analysis

This study analyzed the performance of an indirect solar dryer using numerical simulations to enhance system efficiency and optimize heat and airflow distribution within the dryer. The focus was on critical design and analytical factors, including chimney location, absorber plate angle, and varying heat flux levels.

Key Findings

- **Effect of Chimney Location**

Results showed that positioning the chimney at the center of the design achieves optimal performance in terms of pressure and airflow distribution.

Other locations (left or right) resulted in uneven airflow and reduced natural ventilation efficiency.

Absorber Plate Angle

An angle of 45° was found to be the most suitable for improving heat transfer and thermal flow.

Smaller angles (30° or less) did not achieve the same level of efficiency, while angles larger than 45° caused irregular airflow.

- **Heat Flux Levels:**

Higher heat flux levels (300 W/m²) improved drying efficiency but caused excessive temperature rises.

Moderate heat flux levels (150-200 W/m²) provided a good balance between drying efficiency and system stability.

- **Computational Mesh (Meshing):**

Using a fine mesh improved result accuracy but required longer computational times.
A medium mesh was the optimal choice for balancing accuracy and computational speed.

- **Heat and Airflow Distribution Analysis:**

Uniform distribution of heat and airflow within the system enhances drying efficiency and reduces risks associated with uneven temperature distribution.

2. Recommendations

Optimal Design: Positioning the chimney at the center of the system with a 45° absorber plate angle ensures high efficiency.

Heat Flux Levels: Selecting moderate heat flux levels ensures system stability and reduces energy consumption.

Accurate Modeling: Using medium-density meshes achieves a balance between result accuracy and computational time.

Improved Natural Ventilation: Emphasize designs that support natural ventilation to avoid reliance on additional energy sources.

3. Overall Conclusion

This study concludes that improving the engineering design and optimizing operational parameters significantly enhance the efficiency of the indirect solar dryer while ensuring high-quality dried products. The findings highlight the importance of numerical simulations as a tool for analyzing and designing thermal drying systems in the future.

References

[1] Burade, P. N., Dongre, R. M., Thomas, S., Tamgadge, S., & Mandavgade, D. N. K. (2017). Application of solar in food dryer - A literature review. [Journal Name], 2.

[2] Moussaoui, H., Bahammou, Y., Tagnamas, Z., Kouhila, M., Lamharrar, A., & Idlimam, A. (2021). Application of solar drying on the apple peels using an indirect hybrid solar-electrical forced convection dryer. Renewable Energy, 168, 131–140. https://doi.org/10.1016/j.renene.2020.12.046

[3] Keey, R. B. (2011). Drying. In Thermopedia. Begell House Inc. https://doi.org/10.1615/AtoZ.d.drying

[4] Drying vs. Dehydration. Retrieved May 15, 2025, from [Online Source].

[5] Kamarulzaman, A., Hasanuzzaman, M., & Rahim, N. A. (2021). Global advancement of solar drying technologies and its future prospects: A review. Solar Energy, 221, 559–582. https://doi.org/10.1016/j.solener.2021.04.056

[6] Lungten, & Dorji, J. (2023). Direct Solar Dryer. Research Project, Lund University in collaboration with Jigme Namgyel Engineering College.

[7] Ijsrst, I. J. of S. R. in S. and T. (2025). Importance of Solar Energy Technologies for Development of Rural Area in India. Retrieved May 23, 2025, from https://www.academia.edu/34606936/Importance_of_Solar_Energy_Technologies_for_Development_of_Rural_Area_in_India

[8]https://www.academia.edu/download/34606936/Importance_of_Solar_Energy_Technologies_for_Development_of_Rural_Area_in_India.pdf

[9] Figure I 9. (a) Dryer with area enhancing panels (Jitjack et al. 2016). Retrieved May 23, 2025, from https://www.researchgate.net/figure/a-Dryer-with-area-enhancing-panels-Jitjack-et-al-2016-b-Dryer-with-heat-exchanger_fig9_343661545

[10] Indirect natural convection solar dryer with chimney and storage material. Retrieved May 23, 2025, from https://www.researchgate.net/figure/ndirect-natural-convection-solar-dryer-with-chimney-and-storage-material_fig9_286417592

[11] Karami, H., et al. (2021). Thermodynamic Evaluation of the Forced Convective Hybrid-Solar Dryer during Drying Process of Rosemary (Rosmarinus officinalis L.) Leaves. Energies, 14(18), Article 18. https://doi.org/10.3390/en14185835

[12] Figure I.10. Working principle of open sun drying (Sharma et al. 2009). Retrieved May 23, 2025, from https://www.researchgate.net/figure/Working-principle-of-open-sun-drying-Sharma-et-al-2009_fig7_264510127

[13] Solar Dryer - an overview | ScienceDirect Topics. Retrieved May 23, 2025, from https://www.sciencedirect.com/topics/engineering/solar-dryer

[14] Velmurugan, E., & Edwin Geo, W. (2015). Solar Drying Technologies: A review. International Research Journal of Engineering Science (IRJES), 4(4), 29–35.

[15] Mugi, V. R., Gilago, M. C., & Chandramohan, V. P. (2023). Thermal performance of indirect solar dryer and drying kinetics of guava without and with thermal energy storage. International Journal of Environmental Science and Technology, 20(12), 13619–13634. https://doi.org/10.1007/s13762-022-04713-8

[16] Working principle of indirect solar drying system in a passive solar... Retrieved May 23, 2025, from [Online Source].

[17] Chouicha, S. (2010). Experimental Study of Solar Drying of Moist Dates and Its Impact on Quality. [Publisher].

[18] Solar Dryer Final Thesis | PDF | Solar Energy | Solar Power. Retrieved from Scribd.

[19] Mennouche, D. (2006). Valorization of Agro-Food Products and Medicinal Plants Through Solar Drying Processes. Master's Thesis.

[20] Kouhila, M., Belghit, A., & Boutaleb, B. C. (2000). Experimental Study of Convective Drying of Sage in a Solar Dryer with an Electric Auxiliary System. [Journal Name].

[21] Memoire Online - Contribution to the study of the conservation of dates of the Deglet-Nour variety: Adsorption and desorption isotherm - Med Assad Allah MATALLAH. Retrieved from [Online Source].

[22] Touati. (2008). Theoretical and Experimental Study of Solar Drying of Green Mint Leaves (Mentha Viridis). Doctoral Thesis.

[23] Benzita, H. (2011). Experimental Determination and Simulation of Sorption Curves of an Agro-Food Product for Convective Solar Drying. Master's Thesis.

[24] Randriamorasota, J. A. (1985). Research on a New Industrial Product: Modular Multipurpose Indirect Solar Dryer. Doctoral Thesis.

[25] Boughali, S. (2010). Study and Optimization of Solar Drying of Agro-Food Products in Arid and Desert Areas. Doctoral Thesis.

[26] Model analysis of sorption isotherms. Retrieved from ResearchGate.

[27] Alkadri Plants. (2025). Le pommier et ses variétés. Retrieved May 17, 2025, from [Online Source].

[28] Zaoui, M., & Mellas, M. R. (2021). Suivi de la qualité physicochimique de la confiture de la pomme. Université Saad Dahleb Blida.
[29] Barkat, D., & Djebil, K. (2018). Caractérisation chimique de différents extraits de pommes locales et leur valorisation en phytothérapie. Université Saad Dahleb Blida.
[30] Djellouat, Z., & Ben Brahim, F. Z. (2020). Incidence du stade de maturation des fruits sur l'effet biofongicide des composés phénoliques extraits éthanoliques des pelures de pommier. Université Saad Dahleb Blida.
[31] Birali, J. M. (2023-2024). Cours de technologie post-récolte 2024 : Fruits et légumes. Université Catholique de Bukavu.
[32] Organisation des Nations Unies pour l'alimentation et l'agriculture (FAO). (2025). Facteurs liés au système post-récolte. Retrieved May 17, 2025, from [Online Source].
[33] Maghreb, A. (2023). Stockage des fruits : quelles sont les bonnes pratiques. Agriculture du Maghreb.
[34] Kader, A. A. (2002). Postharvest technology of horticultural crops (3rd ed.). University of California, Agriculture and Natural Resources.
[35] Thompson, J. F., Mitchell, F. G., Rumsey, T. R., Kasmire, R. F., & Crisosto, C. H. (2002). Commercial cooling of fruits, vegetables, and flowers. University of California, Division of Agriculture and Natural Resources.
[36] Artés, F., Gómez, P., & Artés-Hernández, F. (2006). Modified atmosphere packaging of fruits and vegetables. Stewart Postharvest Review, 2(5), 1–13.
[37] Yahia, E. M. (2011). Apple postharvest preservation and storage. In Postharvest biology and technology of tropical and subtropical fruits (Vol. 1, pp. 263–299). Woodhead Publishing.
[38] Saltveit, M. E. (2004). Respiration and quality. In The Commercial Storage of Fruits, Vegetables, and Florist and Nursery Stocks. USDA.
[39] Abano, E. E., & Sam-Amoah, L. K. (2011). Effects of different pre-treatments on drying characteristics of banana slices. Journal of Engineering and Applied Sciences, 6(3), 121–129.
[40] Doymaz, İ. (2010). Evaluation of some thin-layer drying models of persimmon slices. Energy Conversion and Management, 51(2), 301–307.
[41] Esper, A., & Muhlbauer, W. (1996). Solar drying—An effective means of food preservation. Renewable Energy, 7(2), 119–127.

[42] Müller, J., & Sauerborn, J. (1997). Drying of medicinal plants. University of Hohenheim.

[43] Abano, E. E., & Al-Mohsin, M. (2014). Solar drying of fruits and vegetables: Retention of nutritional components. International Journal of Engineering Research and Applications, 4(7), 19–25.

[44] Oussama, B., Abdelmadjid, D., Noureddine, H., Slimani, M. E.-A., & Abdessamia, H. (2024). An experimental investigation of an inclined solar chimney integrated into residential buildings with different materials construction for natural ventilation in a hot-arid climate. *Journal of Thermal Engineering*. Advance online publication.